PUBLICATIONS OF THE ASTRONOMICAL SOCIETY OF THE PACIFIC, 112:1008–1080, 2000 August

Near-Infrared Galaxy Morphology Atlas

T. H. JARRETT

Infrared Processing and Analysis Center, MS 100-22, California Institute of Technology,
Jet Propulsion Laboratory, Pasadena, CA 91125; jarrett@ipac.caltech.edu

Received 2000 March 9; accepted 2000 April 18

ABSTRACT. We present a representative sample of near-infrared (1–2 μm) images spanning the Hubble galaxy morphology classification sequence. The images come from the Two Micron All-Sky Survey, with a range in brightness of 7 mag $< K_s <$ 13.5 mag, and the morphological classifications from the NASA/IPAC Extragalactic Database. We differentiate between elliptical, normal, and barred spirals, compact, dwarf, peculiar, and active galactic nucleus/Seyfert-type galaxies. This image atlas serves as a qualitative guide to the appearance of galaxies at wavelengths that penetrate the obscuring veil of dust, as well as provides a window to the older population of stars that dominate the observed light at 2 μm, including large-scale bar features. We show that central surface brightness and integrated flux may be used to discriminate spheroid and early-type spirals from late-type spirals. The optical and near-infrared properties are compared.

1. INTRODUCTION

For well over a century astronomers have differentiated or classified galaxies based on their visual appearance (of course, in the time of Herschel, the true nature of galaxies was yet to be deciphered, but nonetheless these "nebulae" exhibited repeating characteristic patterns). The science of galaxy "morphology" matured with the work of Hubble (1926, 1936), whose famous "Hubble sequence" remains today a standard technique by which to study galaxies. This sequence of normal spiral and elliptical galaxies was further expanded and delineated into subclasses by de Vaucouleurs in his classic 1959 paper, also described in the *Hubble Atlas* (Sandage 1961; see also Sandage 1975). More recent reviews are given in Buta (1992), Roberts & Haynes (1994), and van den Bergh (1998). Even though the morphology/classification scheme has grown into a rather large and complex set of designations, the basic observables are simple: relative size and brightness of the nucleus with respect to the disk or outer envelope (quantified as the bulge-to-disk ratio), the shape of the disk (e.g., arms, bars, rings, or asymmetries), and other factors, such as the surface brightness, color, and the presence of dust.

The Hubble sequence, at first glance, appears to be simply a qualitative "road map" giving convenient names to the wide variety of galaxies observed in the universe. But as Sandage (1986) points out, the sequence does in fact separate galaxies into physically related classes, representing an "evolutionary" sequence. For example, the mean disk age of spirals progresses along the sequence (early to late type), as does the present star formation rate (e.g., late-type galaxies are forming stars at a much higher rate than early-type galaxies; see also Ferrini & Galli 1988). Hubble & Humason (1931) understood that the morphological sequence was correlated to the galaxy density environment: galaxy *clusters* contain more lenticular and elliptical galaxies than the typical field density.

Morphological segregation appears to be a property of large clusters, including those of Virgo and Coma. Further, the luminosity functions of spirals are different from those of elliptical-type galaxies (see Binggeli, Sandage, & Tammann 1988). Although the origin and formation of elliptical galaxies is still largely not understood, more recent work has pointed to a scenario in which elliptical galaxies may be the creation of spiral galaxy mergers in the dense cores of galaxy clusters (e.g., Dressler 1980; Postman & Geller 1984; but also see Mamon 1992; Whitmore, Gilmore, & Jones 1993; Julian, Kooiman, & Sanders 1997). There is evidence that widely separated morphological types (in the Hubble sequence) have systematically different mean colors (e.g., $B-V$), presumably from different populations of stars, both old and newly formed, that dominate the light (e.g., Holmberg 1958; de Vaucouleurs 1977; Giovanelli & Haynes 1983; see the review by Roberts & Haynes 1994; Buta et al. 1994; Odewahn et al. 1996). Another class of galaxy, the dwarf spheroidal, also appears to be associated with the dense environments of clusters, although their origin, evolution, age, and sustained existence (from the disruptive gravitational tidal forces) remains a mystery (see Sandage 1990; also discussed by Impey & Bothun 1997).

Spheroidal galaxies have the simplest morphology,

exhibiting a smooth triaxial (in two dimensions, elliptical) distribution. Disk galaxies, on the other hand, have a variety of morphological features, comprising the bulk of the Hubble Sequence. Spiral galaxies, for example, may exhibit large-scale "ringlike" or "barred" features, both delineated in the revised sequence of de Vaucouleurs (1959). Finally, there are galaxies that defy classification; they do not fit neatly into any category of the Hubble sequence other than generic "irregular," "peculiar," or otherwise "unknown" classifications. These galaxies are relatively few in number, implying either a short-lived transition phase (evolution into something more recognizable) or that their formation requires unusual circumstances (e.g., galaxy-galaxy interactions). A galaxy of this "type" does *not* fall under the broad definition of a "normal" galaxy. In this paper we present results for what are mostly "normal" spiral and elliptical galaxies, as based on luminosity, color, and symmetry. For comparison, we include galaxies that are not "normal," including active, irregular, and peculiar types. Morphologies are generally derived from optical images, primarily because of the superior resolution, sensitivity, and areal coverage gained from photographic and CCD detectors. At these wavelengths, the light of a spiral galaxy disk is dominated by intrinsically bright and massive young stars, providing a clear contrast between the core/bulge (whose light is dominated by the older stellar population) and disk/spiral-arm components. Elliptical galaxies, mostly devoid of gas and dust (with very little star formation) and other discriminating features, are instead classified by their spheroidal shape.

The spiral "evolution" is clearly separated into early-type ("Sa"), intermediate-type ("Sb"), late-type ("Sc"), and very late type ("Sd") classifications. Some spirals clearly show a "bar" feature, while others appear to be intermediary between "normal" and "barred" spirals. It may be that most if not all spirals contain some form of a linear "bar," but this issue remains controversial (see Roberts & Haynes 1994). Although this issue remains unresolved, the near-infrared images presented in this paper include these three closely related types (normal, barred, intermediary) for comparison.

Galaxies may be "classified" using alternative wavelength imagery, but the contrast between morphological classes is not as clearly defined as that seen in the optical. Nonetheless, these alternative-λ data can provide vital supplementary information toward more reliable classification and, in particular, for those systems with significant dust absorption (e.g., barred galaxies). In the near-infrared (NIR), for example, ~ 2 μm, the emitted light from galaxies is dominated by the older population of stars—which represents the major integrated *mass* component. Moreover, this light is mainly free of the obscuring effects of dust, a particularly vexing problem in late-type spirals, rendering an optically thin view of the galaxies. It is possible to construct a large database of morphologically ordered galaxies, as seen in the NIR window, using data coming from modern large areal coverage surveys.

The Two Micron All-Sky Survey (2MASS; see Skrutskie et al. 1997) is now publicly releasing catalog and imaging data that covers a large fraction of the sky at J (1.2 μm), H (1.6 μm), and K_s (2.2 μm) bands. Galaxies as faint as $J = 15.0$ and $K_s = 13.5$ mag, or 1.7 mJy and 3.1 mJy, respectively, will comprise a complete and reliable extended source catalog (Jarrett et al. 1997, 2000). 2MASS provides a large enough data set to construct an infrared version of the Hubble sequence. However, as we show in § 5, the sensitivity and resolution ($\sim 2''$) of the NIR image data is not adequate to derive independent subclassifications with the exquisite fidelity that optical imaging allows. Consequently, we utilized optically derived classifications coming from previously identified galaxies in the NASA/IPAC Extragalactic Database (NED) to separate our infrared galaxy images into a Hubble sequence of elliptical, spiral, and other types. The "atlas" presented here functions as a "first step" toward deriving a classification sequence based solely upon infrared imaging or, most promising, in combination with optical imaging. A true infrared/optical "sequence" would have the advantage of being minimally affected from dust extinction—particularly important for understanding bar features—and would be more representative of the stellar populations that dominate the system mass.

The basic data are introduced in § 2. A definition and brief review of the Hubble types is given in § 3. In § 4 we present an "atlas" of galaxy images, coming from 2MASS, separated according to the previously derived optical-λ Hubble type. A "composite" infrared Hubble sequence is first presented showing the seven categories of galaxies types: elliptical, spiral, compact, dwarf, irregular/peculiar, and active galactic nucleus (AGN)/Seyfert, with the main atlas images to follow. Irregular, peculiar and active galaxies are not easily classified, but we include them here for completeness. Spirals are further delineated into subclasses, including normal and barred versions, while ellipticals are separated according to their ellipticity or spheroidal flattening. In § 5 we consider some of the basic image parameters, including surface brightness, flux, and color, to evaluate the degree with which the different Hubble types separate at NIR wavelengths. Finally, a comparison with optical properties is given.

2. DATA AND ATLAS IMAGE PARAMETERS

The NIR data come from the 2MASS Second Incremental Release, covering over 47% of the sky, including the northern and southern hemispheres. 2MASS extended sources (e.g., galaxies) are identified and characterized with a "pipeline" software package called GALWORKS, devel-

oped specifically for 2MASS images. The 2MASS Extended Source Catalog includes the coordinate positions, integrated brightness, radial and azimuthal parametric measurements, and images. An overview and description of the algorithms and GALWORKS can be found in Jarrett et al. (2000). For a more general overview of the 2MASS "pipeline" reduction and resultant data products, see the 2MASS Explanatory Supplement.[1]

2.1. Galaxy Size and Photometry

The morphology atlas presented in this paper is sorted by the optically derived morphological type *and* the 2.2 μm integrated flux. 2MASS computes a variety of integrated flux measurements for a given extended source. In this study we use the integrated flux based on the elliptical aperture best fit to the K_s-band isophote corresponding to 20.0 mag arcsec^{-2} surface brightness (roughly equivalent to 1 σ of the rms background noise in the K_s-band image). We show in § 5.4 that the equivalent surface brightness in the B band is $\sim$24 mag arcsec^{-2} for early types and $\sim$23 mag arcsec^{-2} for late types; hence, for late-type spirals the 2MASS images are sensitive to only the brighter morphological features. The same "fiducial" aperture (position, size, and orientation) is applied to each band, allowing cross-comparison between bands. It is this aperture diameter, D_{20}, that represents the *size* of a galaxy. The elliptical orientation (position angle and axis ratio) of the galaxy is determined from the K_s (2.2 μm) image at roughly the isophote corresponding to 3 times the background rms "noise" or 3 σ.

2.2. Extended Source Atlas Images

Each extended source in the 2MASS database includes a small image data cube, representing the J, H, and K_s "postage stamp" images (planes 1, 2, and 3, respectively), extracted from the full resolution 8.5 × 17′ images which comprise a 2MASS "scan" or "tile." The size of the cube is dynamically selected, scaled according to the measured *size* of the extended source (see above), with minimum and maximum limits of 21″ and 101″ pixels, where each pixel is 1″ in width. For the largest galaxies (typically $K_s < 9$ mag in brightness) the image size is not large enough and the outer parts of the galaxy are clipped, resulting in an underestimated total flux; galaxies larger than $\sim$1′ in diameter have integrated fluxes that are systematically too small (some examples can be found in the images presented in this paper). Note that the $J-K_s$ color is only minimally affected since the flux loss occurs nearly equally for all bands.

2.3. Galaxy Images

We have elected to present the galaxy "postage stamp" images as gray-scale halftones of the K_s (2.2 μm) image, overlaid with contours corresponding to the J (1.3 μm) image (Fig. 20). The gray scale ranges from a minimum value of 1 σ of the background noise to a maximum value corresponding to the peak pixel value for the galaxy (but no smaller than 5 σ). We then take the base-10 logarithm of the 2.2 μm image, which enhances the contrast in the low signal-to-noise ratio (S/N) galaxy emission. The J-band contours correspond to the 1%, 2%, 4%, 8%, 16%, and 32% 1.3 μm peak intensity levels. The typical surface brightness of the lowest contour is 20.4 mag arcsec^{-2} in J ($1\ \sigma \approx 21.6$ mag arcsec^{-2}). A caption accompanies each image, including the catalog or NED name, morphological or Hubble type, 2MASS name, K_s mag, and $J-K_s$ color. The 2MASS name maps into the J2000 equatorial position of the source (Jhhmmss.s ± ddmmss). The angular size of the image is noted in the lower right-hand corner of the image, ranging from 21″ to 101″.

3. MORPHOLOGICAL TYPES

We employ the revised system of de Vaucouleurs (1959), with brief descriptions of the basic categories and classes given below. We will combine some subclasses for convenience. Galaxy morphology and name or designation are taken from NED, a large heterogeneous set derived from predominantly visual-λ catalogs and surveys. The bulk of NED's types are from the *Third Reference Catalogue of Bright Galaxies* (de Vaucouleurs et al. 1991, hereafter RC3), with a smaller number coming from Sandage (1961) and Buta (1995).

3.1. Elliptical Types

Elliptical galaxies are characterized by a bright nucleus and a featureless envelope (i.e., lacking a disk). They are, more precisely, spheroidal in shape. They typically have a characteristic $r^{1/4}$ surface brightness profile and usually are redder in $B-V$ color than spirals (indicative of older more evolved stars). These are further subclassified according to their ellipticity: $E(n)$, where $n = 10(1 - b/a)$, where b/a is the axis ratio. Hence, classifications progress from E0 to E7.

[1] The 2MASS Explanatory Supplement (by R. M. Cutri et al. 2000) is an Internet on-line hyperdocument: http://www.ipac.caltech.edu/2mass/releases/docs.html.

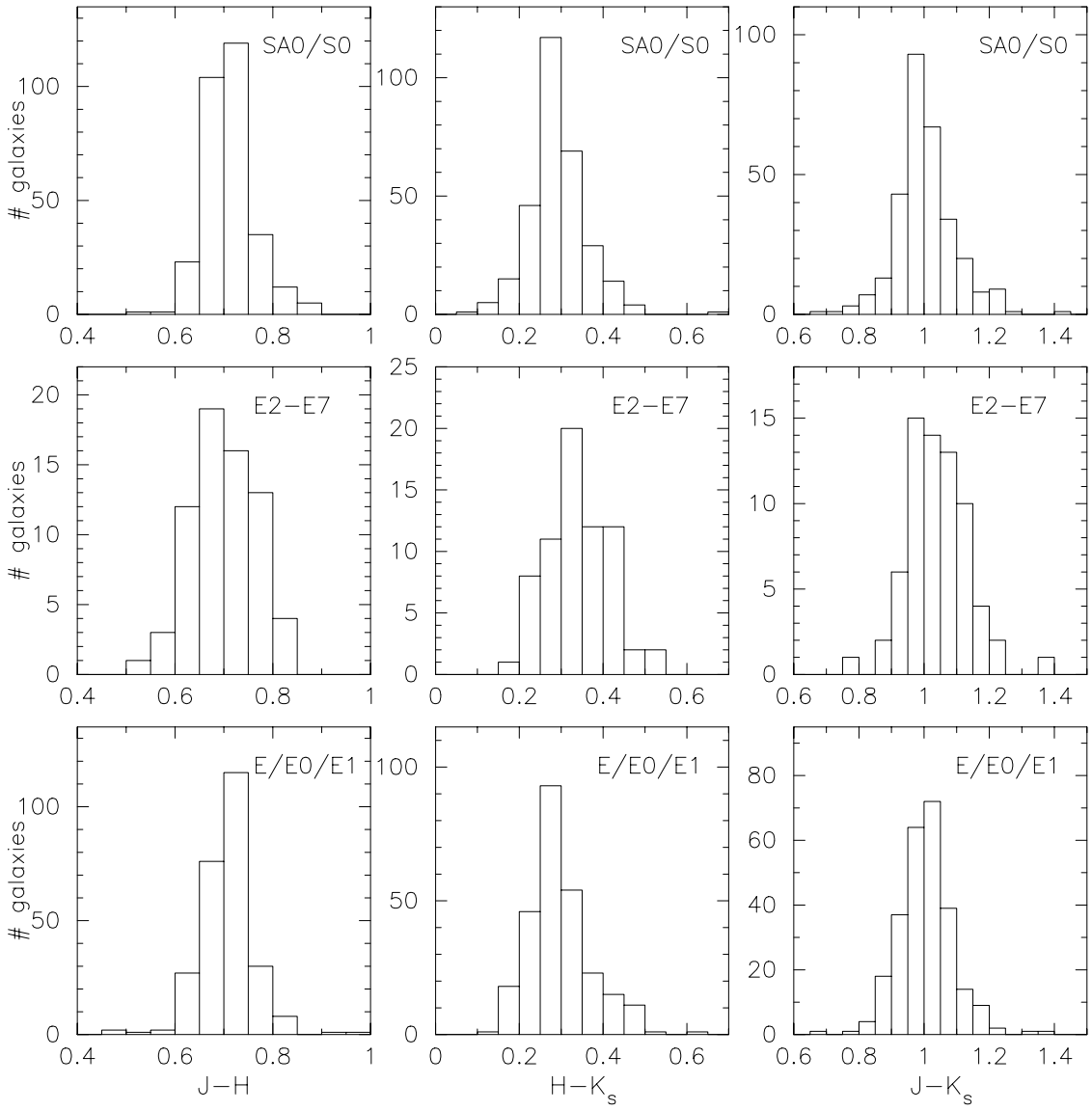

FIG. 1.—Near-infrared color distribution for elliptical- and lenticular-type galaxies. Three different color combinations are shown: $J-H$ (*left column*), $H-K_s$ (*middle column*), and $J-K_s$ (*right column*).

3.2. Lenticular Types

Lenticular galaxies, S0 and SA0, are probably some kind of "transition" class between an elliptical and spiral galaxy, although this relationship is not well understood. They have a bright nucleus and a smooth envelope and disk, resembling a "lens" shape or profile. In general they do not have delineated arms, although some lenticulars do have dust lanes. It is not clear whether lenticulars represent an evolution from the ellipticals or the reverse, an evolution from the spiral class (see Roberts & Haynes 1994; see also van den Bergh 1994 for a different perspective). Qualitatively, they represent an "early" type in comparison to most other spiral types.

3.3. Spiral Types

Normal spiral galaxies range from early type (Sa), intermediate (Sb), late type (Sc), and very late type (Sd). Qualitatively early-type spirals have prominent cores, while late-type spirals have prominent disks.

Barred spirals exhibit a large-scale linear "bar" feature crossing the nucleus. The bar-to-disk/arm association may be closed, forming a ring (or "r" type), or may be open, forming a spiral (or "s" type) shape. Early-type galaxies, SB0 and SBa, tend to have closed structures, while late-type galaxies, SBb and SBc, tend to have more open spiral structures. A "transition" class between normal and barred spirals is designated as SAB. It should be emphasized that

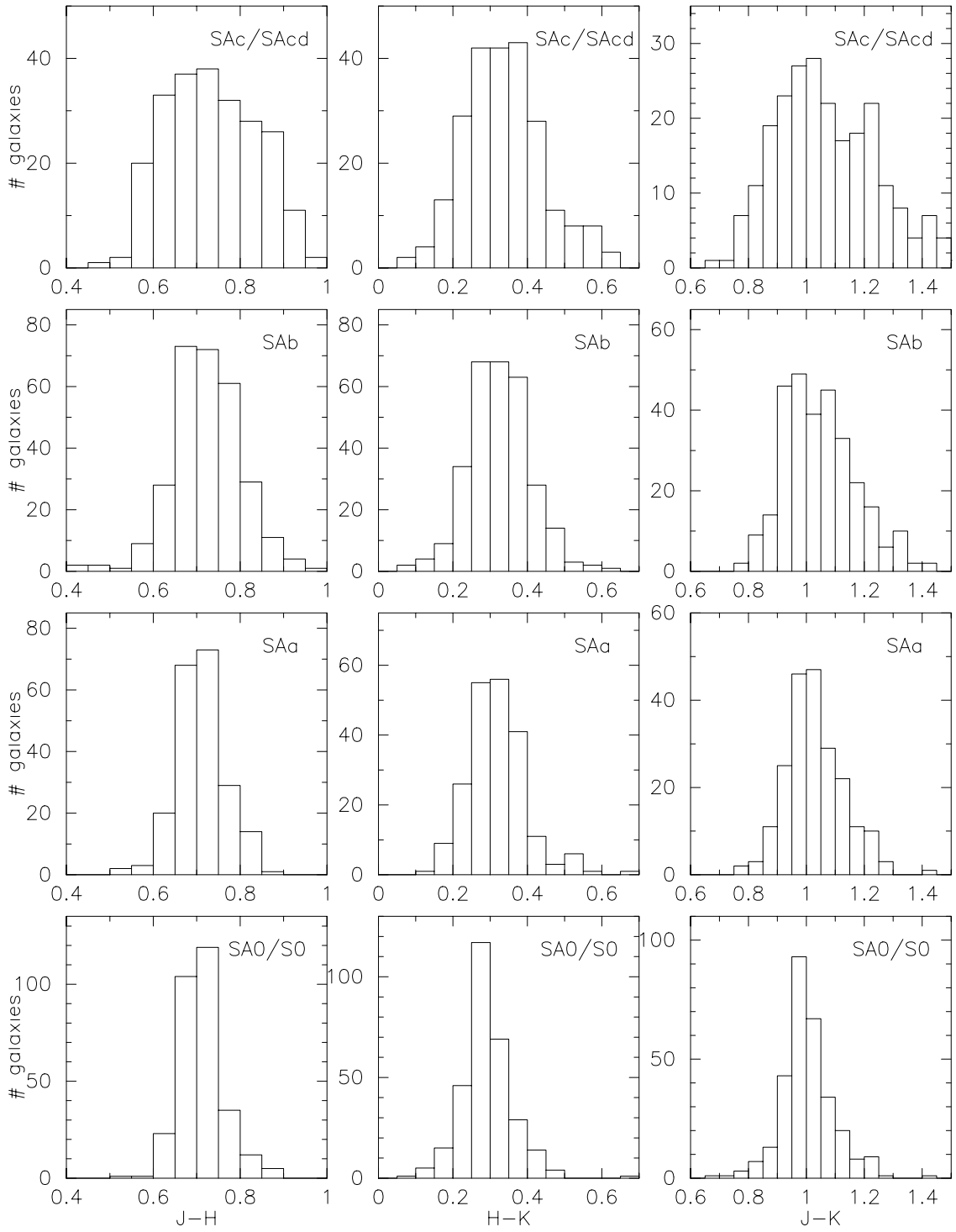

FIG. 2.—Near-infrared color distribution for normal spiral galaxies, starting with lenticulars (*bottom row*) and sequentially later types moving upward: SAa (*second row*), SAb (*third row*), and SAc/SAd (*top row*).

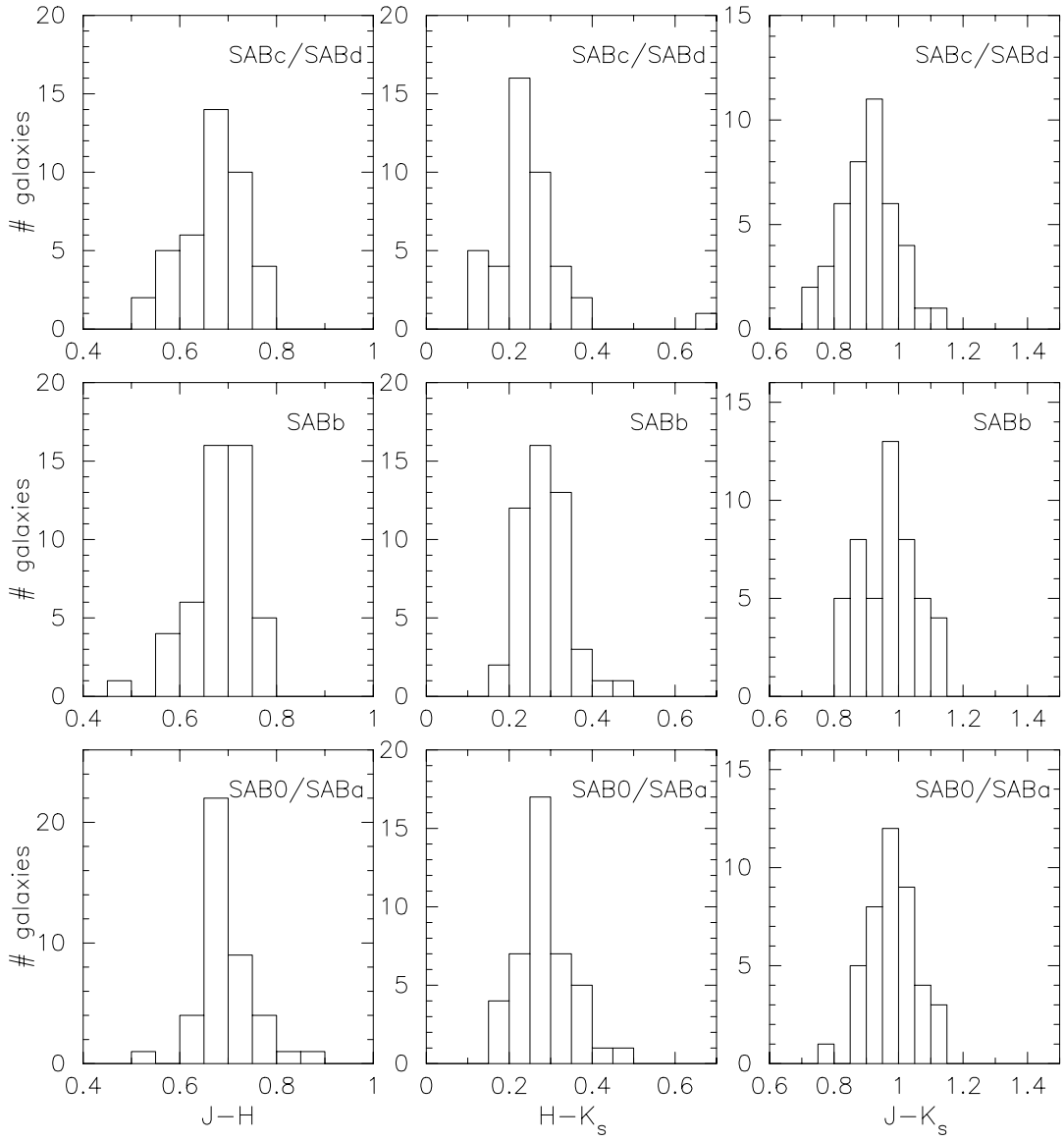

FIG. 3.—Near-infrared color distribution for normal-barred transition spiral galaxies, starting with early-type SAB0/SABa (*bottom row*), next with SABb (*middle row*), and finally SABc/SABd (*top row*).

aside from the bar itself, there is little (if any) difference in optical properties between SA and SB galaxies of similar age and evolution.

3.4. Other Types

Compact galaxies are not obviously elliptical or spiral. They include the "blue compact dwarf" (BCD) galaxy (see Sandage & Binggeli 1984; Hoffman et al. 1989). As their name implies, their cores are much more prominent than their envelopes. They are almost exclusively round in shape. Compact galaxies will not usually be *resolved* with 2MASS and, hence, will only be sporadically included in the *extended* source catalog.

Dwarf galaxies include spheroidal/spiral (dS) and elliptical (dE) versions (see Sandage & Binggeli 1984). They tend to have a low surface brightness (LSB), with weak or absent central cores (e.g., Kormendy 1977). They may also be compact, with a high surface brightness in the core, or they may be "irregular" with asymmetric profiles (see below). See Sandage (1990) for a comprehensive look at Virgo & Fornax dwarf galaxies.

Seyfert, LINER, and AGN-type galaxies exhibit strong emission lines in their cores (e.g., Osterbrock 1993). These

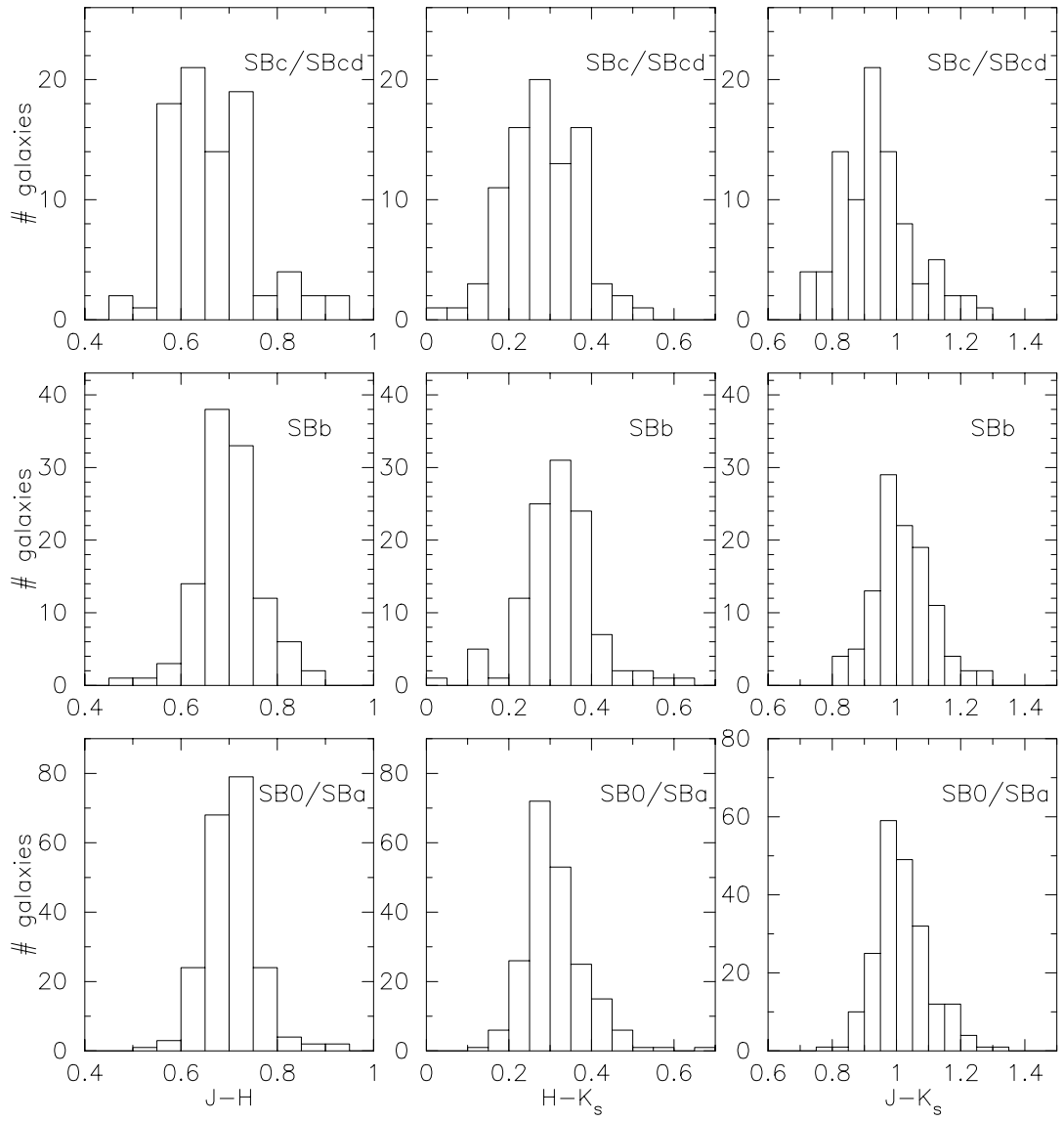

FIG. 4.—Near-infrared color distribution for barred spiral galaxies, starting with early-type SB0/SBa (*bottom row*), next with SBb (*middle row*), and finally SBc/SBd (*top row*).

galaxies may be spirals, peculiar (e.g., interacting pairs) or part of starbursts or very dusty galaxies, and many are associated with quasars. They tend to have red colors in the near-infrared. They also tend to be distant ($z > 0.3$), making them difficult to detect and resolve with 2MASS.

Finally, irregular galaxies (Irr) may include dwarfs (although we make a distinction, see above), peculiar (Pec), interacting, merger, and "magellanic cloud" (SBm; Im) versions (e.g., de Vaucouleurs & Freeman 1972). Irregulars are usually barred, IB, and "s"-shaped, I(s). In general, galaxies that are not classified as elliptical or spiral type may be lumped into this disparate group, even though some may be physically unrelated.

4. NEAR-INFRARED MORPHOLOGY ATLAS

The NIR images are presented in "plates" of 16 images each (see Table 1 and Fig. 20), comprising 864 total galaxies. The sequence order is ellipticals, spirals, compacts, dwarfs, peculiars, and AGN/Seyferts. A handful of the elliptical and spiral galaxy types includes LINER or Seyfert features (although qualitatively they are indistinguishable from their "normal" cousins). The order within the plate is given by the integrated K_s flux of the galaxy (denoted with the K_s mag in the figure legend), ranging between 7 and 13.5 mag (300 and 2 mJy, respectively). The size (in arcseconds) for each image is noted in the lower right-hand corner of the

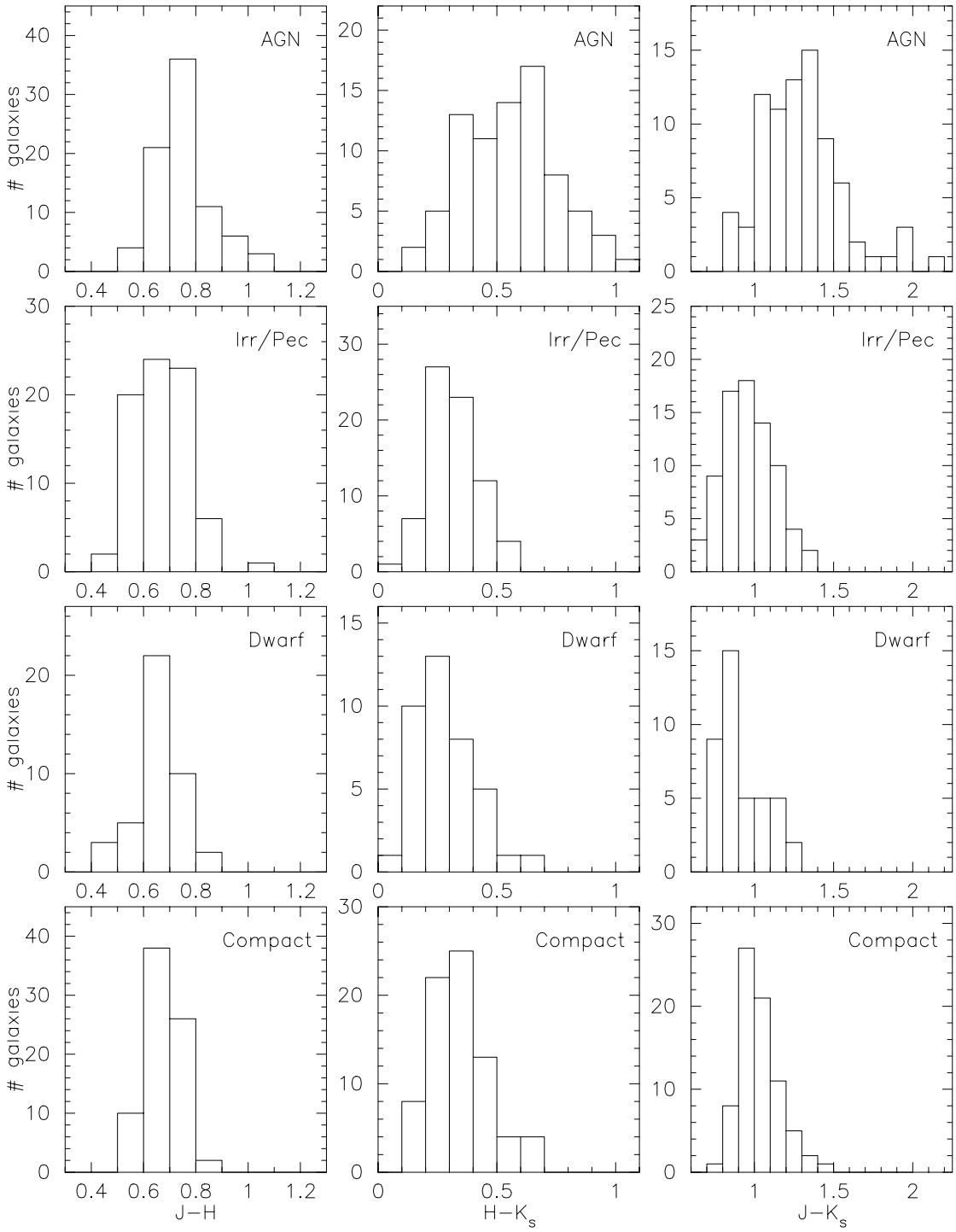

FIG. 5.—Near-infrared color distribution for compact (*bottom row*), dwarf (*second row*), irregular/peculiar (*third row*), and AGN/Seyfert (*top row*) types of galaxies.

TABLE 1

NEAR-INFRARED MORPHOLOGY ATLAS PLATES

Figure	Category	Types	K_s Magnitude Range
19.....	Composite	All	10–11
20*a*	Elliptical	E0	7.4–12.6
20*b*	Elliptical	E1	7.2–12.8
20*c*	Elliptical	E2	7.8–12.0
20*d*	Elliptical	E3	8.2–12.5
20*e*	Elliptical	E4	9.8–13.4
20*f*, 20*g*	Elliptical	E5, E6, E7	7.9–13.3
20*h*–20*k*	Lenticular	S0, SA0	7.8–13.0
20*l*–20*o*	Spiral	Sa, SAa	7.6–13.4
20*p*–20*s*	Spiral	Sb, SAb	7.9–13.1
20*t*–20*w*	Spiral	Sc, SAc, Sd, SAd	7.1–13.8
20*x*, 20*y*.....	Normal-barred spiral	SAB0, SABa	7.5–11.0
20*z*, 20*aa*.....	Normal-barred spiral	SABb	7.5–11.3
20*ab*, 20*ac*	Normal-barred spiral	SABc, SABd	8.1–11.5
20*ad*–20*ag*	Barred spiral	SB0, SBa	7.1–13.0
20*ah*–20*aj*.....	Barred spiral	SBb	7.8–12.3
20*ak*–20*am*.....	Barred spiral	SBc, SBd	8.0–14.3
20*an*–20*aq*	Compact	C, BCD	10.9–13.0
20*ar*–20*at*	Dwarf	D, dE, dS	10.9–14.4
20*au*–20*ax*	Irregular/peculiar	Irr, IA, IB, Im, Sm, Pec	8.6–13.5
20*ay*–20*bb*	AGN/Seyfert	AGN, Seyfert	10.1–13.5

gray-scale image. The atlas does not represent a complete sample, nor does it represent a flux-limited sample (although we do avoid sources fainter than S/N $\sim$ 10, or $K_s \sim 13.5$ mag). However, the atlas does represent a mostly unbiased sample of 2MASS galaxies that have cataloged morphological classifications—it is biased only in the sense that the NED is biased. Figure 19 represents a composite near-infrared sequence, directly analogous to the Hubble

TABLE 2

OPTICAL VERSUS NEAR-INFRARED DIAMETERS AND COLORS

Type	D_{20}/D_{25}	D_{20}/A_e	$B_T - K_s$	$\mu_e - \mu_{Ke}$	$K_{b/a} \times R_{25}$
E.....	0.767(0.187)	1.977(0.709)	3.926(0.413)	4.672(0.278)	0.987(0.121)
SA0.....	0.746(0.162)	2.367(1.061)	3.974(0.346)	4.689(0.370)	1.029(0.205)
SAa.....	0.713(0.159)	2.131(0.671)	3.870(0.427)	4.674(0.640)	1.068(0.195)
SAb.....	0.632(0.158)	1.870(0.547)	3.758(0.467)	4.550(0.644)	1.054(0.269)
SAcd	0.561(0.169)	1.591(0.495)	3.144(0.513)	4.123(0.484)	1.060(0.284)
SAB0.....	0.767(0.146)	2.609(0.969)	3.962(0.371)	4.686(0.342)	0.977(0.151)
SABa.....	0.688(0.210)	2.020(0.656)	3.774(0.526)	4.464(0.654)	1.032(0.237)
SABb.....	0.650(0.146)	1.705(0.587)	3.467(0.445)	4.423(0.472)	1.008(0.342)
SABcd.....	0.610(0.163)	1.322(0.518)	3.099(0.606)	4.052(0.462)	0.955(0.260)
SB0.....	0.757(0.149)	2.444(0.876)	3.854(0.304)	4.711(0.273)	0.997(0.221)
SBa.....	0.759(0.165)	2.063(0.751)	3.800(0.321)	4.753(0.457)	0.815(0.400)
SBb.....	0.692(0.163)	1.937(0.511)	3.445(0.545)	4.403(0.506)	0.980(0.393)
SBcd.....	0.674(0.238)	1.469(0.556)	2.860(0.635)	3.824(0.389)	0.841(0.371)
IRR/Pec.....	0.590(0.183)	1.984(0.737)	2.945(0.799)	3.465(0.818)	1.080(0.292)

NOTE.—D_{20} is the K-band elliptical isophotal diameter corresponding to 20 mag arcsec^{-2} surface brightness. D_{25} is the RC3 optical radius (25 B mag arcsec^{-2}). A_e is the RC3 optical apparent diameter of the "effective" aperture (i.e., the half-light radius). B_T is the RC3 total B magnitude (derived from D_{25}) and K_s is the 2MASS isophotal mag (at 20 mag arcsec^{-2}). The mean surface brightness (mag arcsec^{-2}) corresponding to the effective aperture (the half-light radius) is μ_e from the RC3 and μ_{Ke} from 2MASS using the same RC3 aperture. The K-band 2MASS minor-to-major axis ratio is $K_{b/a}$, and the RC3 major-to-minor isophotal axis is R_{25}. Each bin has between 50 and 100 sources. The rms uncertainties are given in parentheses.

sequence, including the elliptical sequence (E0–E6) and the spiral sequence (S0, Sa, Sb, Sc, Sd), delineated between barred, transition, and nonbarred types.

5. CHARACTERISTICS OF THE INFRARED ATLAS

In order to make sense of the Hubble sequence with NIR imaging, we investigate the key basic image parameters that 2MASS derives, including the integrated flux, central surface brightness, axial ratio, and colors. As we show below, just a few simple image parameters coming from the survey can be used to delineate early-type spirals and ellipticals from disk-dominated galaxies. These measurements are only a subset of what can be potentially derived from the image data, although they do represent the most important measurements extracted by 2MASS. There are undoubtedly other parameters (and their corresponding phase space) which may prove to be even more powerful at discriminating between spiral types as well as between normal, transition, and barred spirals. More sophisticated methods, for example, the implementation of supervised neural networks and the addition of image information coming from visual-based surveys (e.g., using the POSS II), are a promising avenue toward effective morphological classification.

The integrated flux is represented by the K_s-band fiducial 20 mag arcsec^{-2} elliptical isophote aperture (see § 2.1), which approximates the "total" flux of the galaxy. In actuality, this measure underestimates the total flux between 10% and 20%, depending on the radial distribution (i.e., Hubble type). The surface brightness is computed from the peak-pixel flux (which we call the "peak" surface brightness) and from the mean of the pixels located inward of 5″ from the nucleus (which we call the "core" or "bulge" surface brightness). The surface brightness is coupled to the galaxy size. One must be careful how to interpret this nonoptimized mean surface brightness (see § 5.4 for a discussion of the half-light radius). The axial ratio corresponds to the minor-to-major axis ratio computed from the K_s image at the 3 σ contour (roughly 18.8 mag arcsec^{-2}; see Jarrett et al. 2000). The infrared colors correspond to $J-H$, $H-K_s$, and $J-K_s$. In § 5.4 we compare the optical and NIR size and photometry of galaxies.

5.1. Colors

The infrared color distribution is shown in Figures 1–5, corresponding to ellipticals (Fig. 1), normal spirals (Fig. 2), normal-barred transition spirals (Fig. 3), barred spirals (Fig. 4), and other types: compact, dwarf, irregular/peculiar, and AGN/Seyfert (Fig. 5). Early to late types are ordered from bottom to top. For the ensemble average, ellipticals are slightly, ~few percent, redder in color than lenticulars (Fig. 1). For normal and transition spirals the color differences are not statistically significant (Figs. 2 and 3). Note, however, there is a clear increase, by a factor of ~2, in the dispersion going from early type (S0) to late type (Sc). This early- to late-type dispersion gradient is undoubtedly the same phenomenon seen at visual wavelengths: the effects of star formation, a younger population of stars, and an increase in extinction all lead to an increase in the color dispersion for late-type galaxies. The trend is even apparent between lenticulars and their close-cousin early-type Sa galaxies. Barred spirals (Fig. 4) also show little color difference between Hubble types and between nonbarred spirals, except for the addition of a "blue" tail for late types. A population of relatively blue barred spirals is consistent

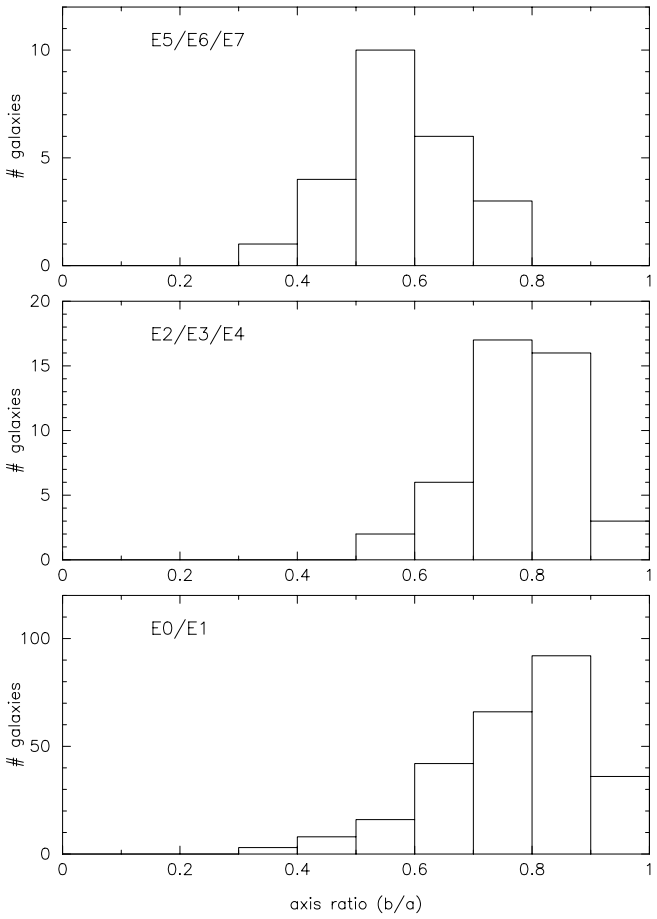

FIG. 6.—Axis ratio distribution for elliptical galaxies. The axis ratio, or the ratio between the minor-to-major axis, is derived from the combined $J+H+K_s$ image (referred to as the "super" co-add; see Jarrett et al. 2000) and corresponds to the best-fit ellipse to the 3 σ isophote for each galaxy (this is typically at a surface brightness of ~20.3, 19.4, and 18.8 mag arcsec^{-2} at 1.3, 1.6, and 2.2 μm, respectively).

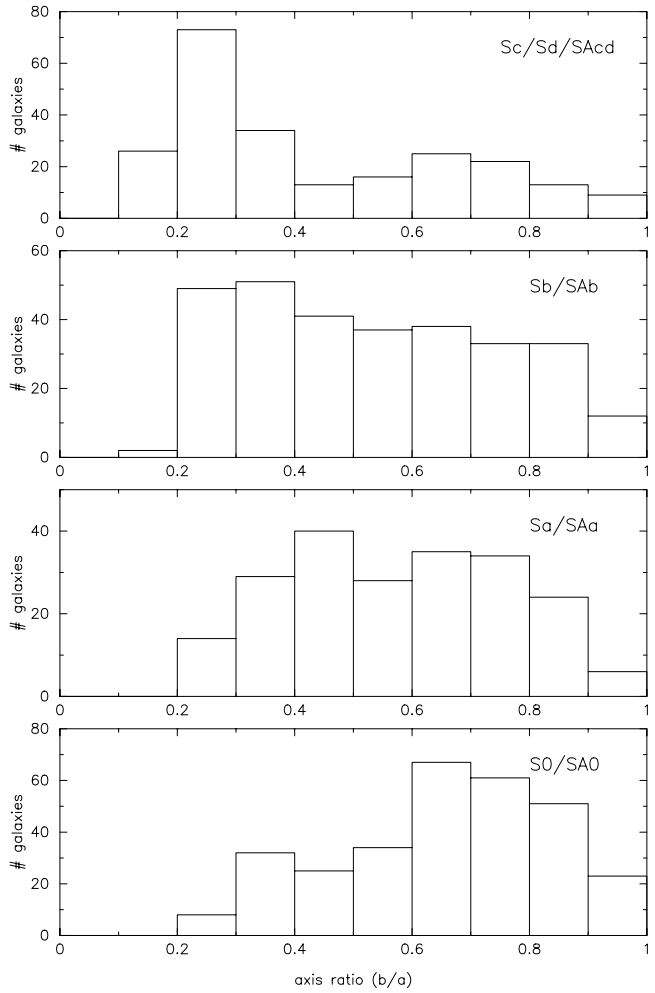

FIG. 7.—Axis ratio distribution for normal spiral galaxies. See Fig. 6 legend for details.

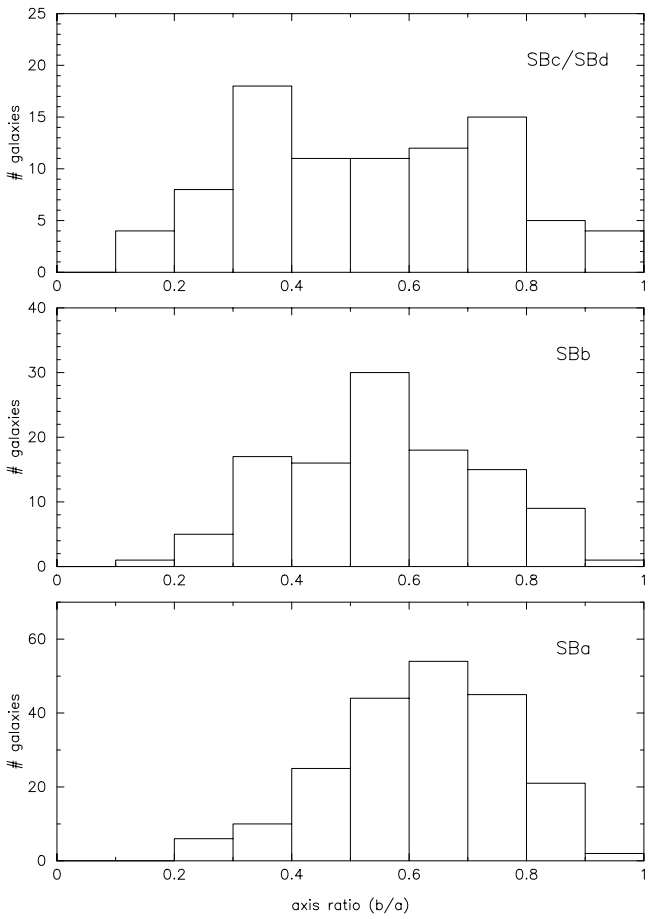

FIG. 8.—Axis ratio distribution for barred spiral galaxies. See Fig. 6 legend for details.

with a younger (and bluer) population of stars associated with star formation induced by large-scale bar structures. All told, the NIR colors in comparison to optical colors (e.g., Odewahn & Aldering 1995; Odewahn et al. 1996) show only small contrast between morphological types.

These statistical trends are not powerful enough to reliably place *individual* galaxies on the Hubble sequence—color can only be used statistically or with an ensemble of galaxies to distinguish between early and late type. On the other hand, AGN and Seyfert-type galaxies (Fig. 5) exhibit a prominent "red" bias as both $H-K_s$ and $J-K_s$ colors are typically $\sim$0.3–0.4 mag redder than, for example, compact galaxies. Active galaxies are known to be intrinsically red in color, partially due to severe dust extinction, in addition to cosmic reddening due to the expansion of the universe (i.e., their "K-correction" is significant). Extremely red, $J-K > 1.3$, 2MASS *extended* objects are good candidates for active galaxies.

5.2. Axis Ratios

The minor-to-major, b/a, axis ratio distribution is shown in Figures 6–8, corresponding to ellipticals, normal spirals, and barred spirals, respectively. We do not show figures for small angular sized galaxies (e.g., compact & AGN) due to the uncertainty in the axis ratio estimate. For ellipticals (Fig. 6), the axis ratio represents the degree of flattening in the spheroids (from circular E0 to elongated E7; see § 3.1). Not surprisingly, the near-infrared axis ratios are consistent with the Hubble classifications, where the axis ratios for E0–E1 peak at 0.85, while for E2–E4 they peak at 0.75, and for E5–E6 they peak at 0.55. Some intrinsic scatter is to be expected due to the triaxial nature of spheroids.

For spirals (Figs. 7 and 8) there is significant trend from early to late types: the b/a distribution shifts from a peak of $\sim$0.7–0.8 (i.e., the orientation is closer to face-on) for early types to a more edge-on orientation, $\sim$0.2, for late types. This trend is probably related to a discrepancy in detection completeness. Face-on spirals are harder to detect and

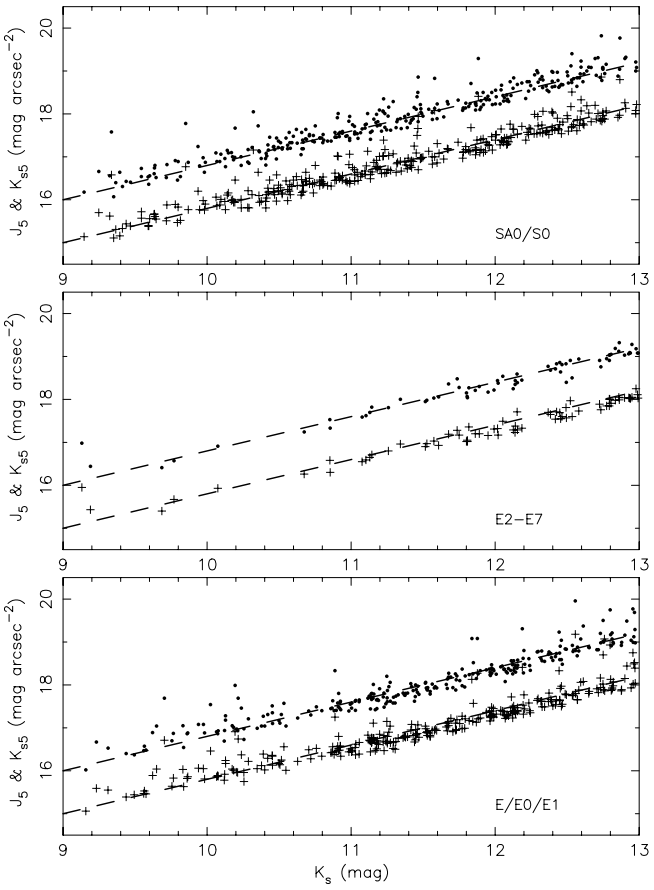

FIG. 9.—Near-infrared central surface brightness as a function of the K_s integrated flux for elliptical and lenticular galaxies. The 1.3 and 2.2 μm mean (radius $\leq 5''$) surface brightness is labeled as J_5 and K_{s5}, respectively. The J-band surface brightness (in mag arcsec^{-2}) is denoted with filled circle symbols and the K_s band with cross symbols. The J-band points generally lie above (i.e., fainter) the K_s-band points. A line (*dashed lines*) has been fitted to the points corresponding to the lenticular or SA0/S0–type galaxies (see eq. [1]). For comparison, the same lines are drawn for the later type galaxies.

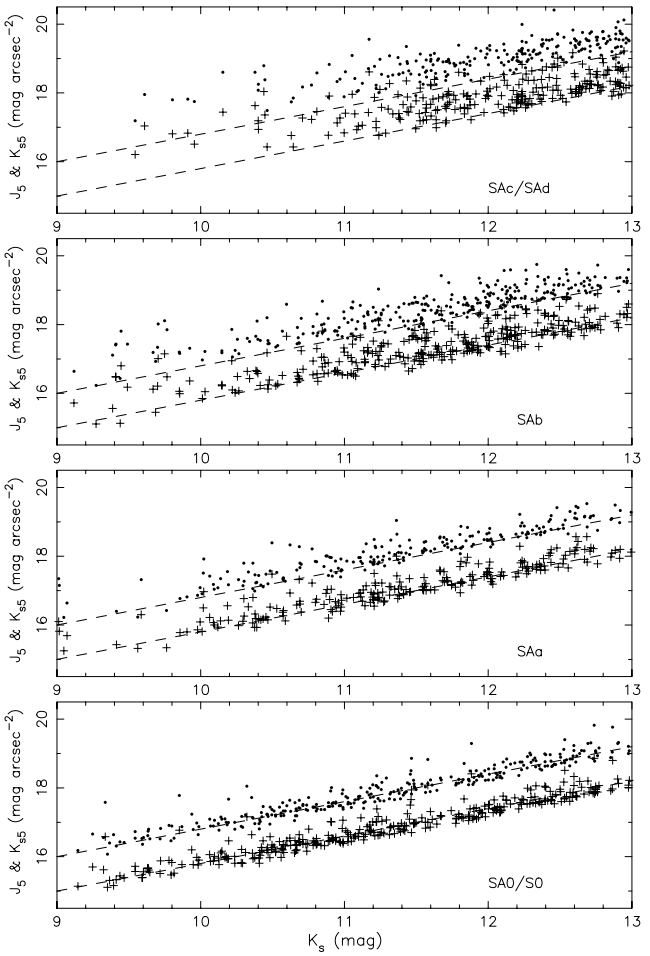

FIG. 10.—Near-infrared central surface brightness as a function of the K_s integrated flux for normal spiral galaxies. See Fig. 9 legend for details.

resolve due to their lower surface brightness, which is exaggerated for late types due to their small bulge-to-disk ratios (see below). We should caution, however, that our NED galaxy sample was not selected to minimize biases or other statistical effects. There are a number of effects that potentially complicate the axis ratio distribution (see Odewahn, Burstein, & Windhorst 1997). It is beyond the scope of this paper to accurately assess the completeness of different morphological types in the 2MASS catalog.

We are able to compare the 2MASS K-band axis ratios with those in the RC3, as given by the R_{25} parameter (ratio of the major-to-minor 25 B mag arcsec^{-2} isophotal diameters). We find good agreement ($\sim 10\%$) for early types and increasingly poorer agreement ($>20\%$) for late-types (see § 5.4 and Table 2). Interestingly, the 2MASS axis ratios are systematically larger (i.e., more face-on) than those of RC3 for normal spirals, while for barred spirals the trend is reversed: the NIR axis ratios are considerably more elongated than their optical counterparts. This result is consistent with the NIR being more sensitive to the (rounder) bulge component *and* the (linear) barred components of spirals.

The near-infrared is most sensitive to older (redder) populations of stars, which are generally not the dominant stellar source of light coming from late-type spirals (nor of many dwarf or LSB-type galaxies). The inclination is strongly correlated with surface brightness such that *blue* low surface brightness galaxies (e.g., Sc types) are normally undetected by 2MASS except when viewed edge-on or nearly so. Not only does the disk surface brightness increase with inclination, bars would also be most easily detected edge-on. Since the near-infrared is much less affected by dust, bar features may dominate the light coming from a late-type galaxies at 2 μm (assuming the bar is composed of an older population of stars)—2MASS is ideally suited for studying bars in nearby spirals. We should point out that

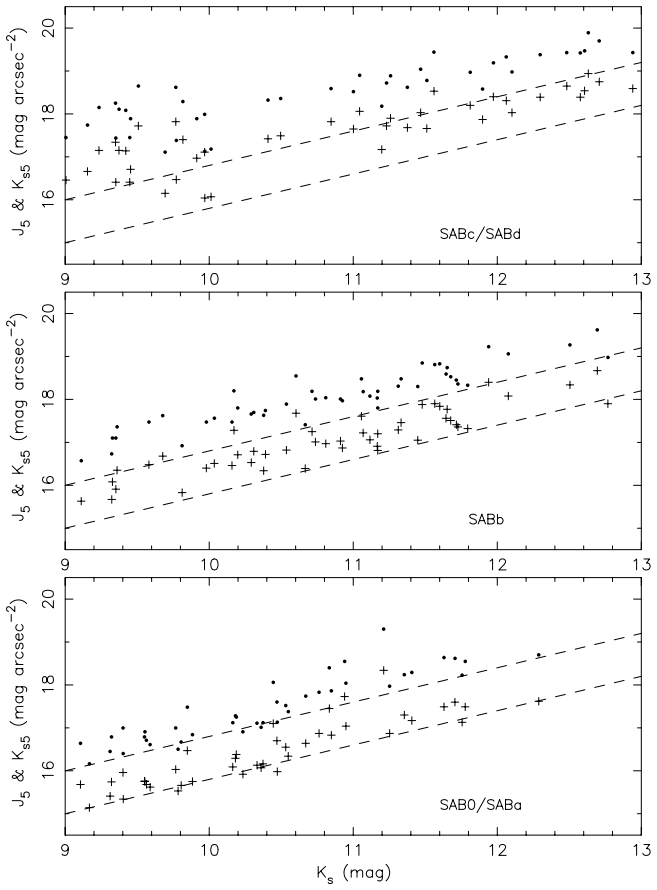

FIG. 11.—Near-infrared central surface brightness as a function of the K_s integrated flux for normal-barred transition spiral galaxies. See Fig. 9 legend for details.

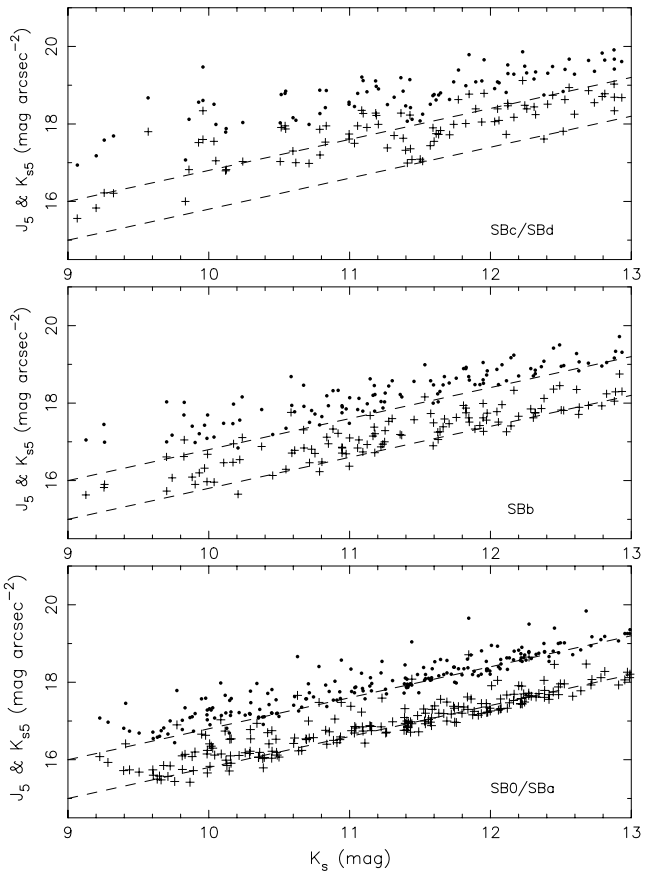

FIG. 12.—Near-infrared central surface brightness as a function of the K_s integrated flux for barred spiral galaxies. See Fig. 9 legend for details.

the respective axis ratios are determined at different surface brightness levels (18.8 vs. 25 mag arcsec^{-2}) and thus subject to different morphological features, moderating our overall interpretation of the results.

5.3. Surface Brightness and Integrated Flux

The K_s elliptical isophotal photometry includes the core, bulge, and disk components, representing a "total" integrated flux.[2] In contrast, the central surface brightness represents the flux coming from the core or bulge component. By comparing these two measures, we approximate the bulge-to-disk ratio that is traditionally used to construct the Hubble sequence.

The central surface brightness is measured both from the peak-pixel flux and from the mean value within 5″ of the nuclear peak. Due to the pixel undersampling and resolution (∼2″), the peak surface brightness is of only limited use. For the 2MASS catalog, the mean central surface brightness ($r \leq 5''$) is the most meaningful measure of the *central* surface brightness. In Figures 9–13 we show the resultant J and K_s-band surface brightness as a function of the K_s integrated flux for ellipticals (Fig. 9), normal spirals (Fig. 10), barred-transition spirals (Fig. 11), barred spirals (Fig. 12), and other types (Fig. 13). The 1.3 μm and 2.2 μm central surface brightness is labeled J_5 and K_{s5}, respectively. The J-band surface brightness is denoted with filled circle symbols and the K_s band with cross symbols (note that J is about 1 mag fainter than K_s). Here we have fit a line to the points corresponding to SA0/S0-type galaxies, denoted with dashed lines; also see solutions below. Here lenticulars represent the earliest *spiral* type. The same fit is shown for each morphological type for comparison. The panels are in sequence of early to late types (from bottom to top).

Elliptical and lenticular spirals have similar bulge surface brightness to total flux ratios (Fig. 9), with only a slightly higher surface brightness for E0 in comparison to S0. Although small, this result is consistent with elliptical–S0 evolution sequence. The ratios are more dramatic when

[2] A true total flux can only be estimated using a curve-of-growth and extrapolation technique; however, the isophotal photometry presented here does capture most of the flux from a galaxy, particularly for those with simple exponential radial profiles; see § 5.4 and Jarrett et al. (2000).

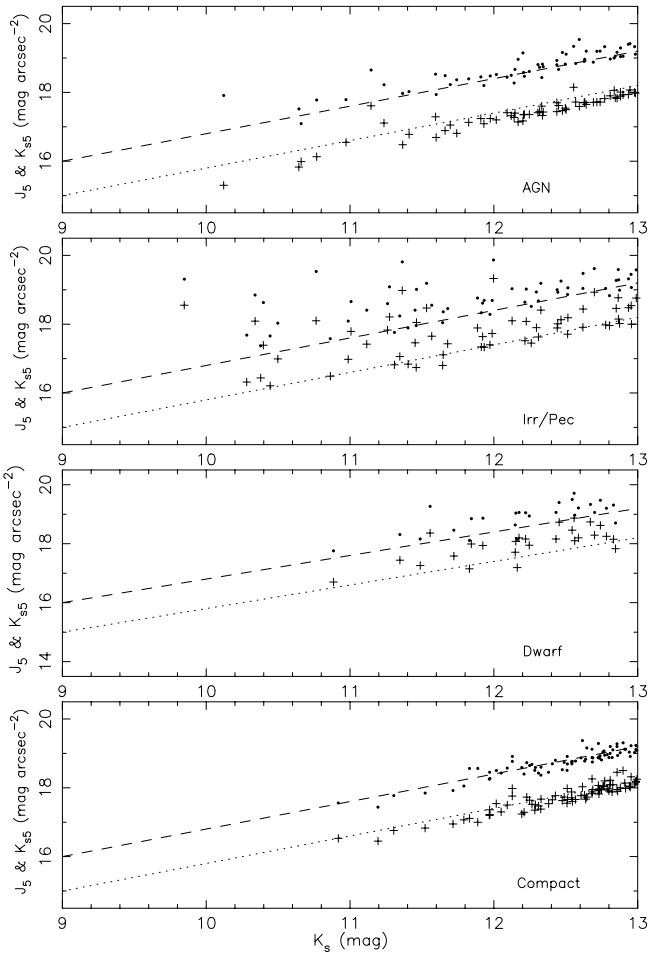

FIG. 13.—Near-infrared central surface brightness as a function of the K_s integrated flux for compact, dwarf, irregular, and AGN-type galaxies. See Fig. 9 legend for details.

comparing early-type spirals to late-type spirals (Figs. 10–12). In comparison to late-type spirals, early-type spirals exhibit both a higher surface brightness (i.e., more prominent bulges) and less dispersion in their distribution. The surface brightness difference between E0/S0 and Sc, for example, is large enough ($\sim$0.3 mag arcsec^{-2}) that it is possible to discriminate between individual lenticular or elliptical galaxies and disk-dominated spirals, at least for high S/N ($>$10) that are clearly resolved (apparent size $>20''$). This can be understood by plotting the *residuals* relative to the best-fit line to the SA0/S0 distribution:

$$J_5(\text{mag arcsec}^{-2}) = 0.700(K_s) + 7.500\ ,$$
$$K_{s0}(\text{mag arcsec}^{-2}) = 0.800(K_s) + 7.789\ . \qquad (1)$$

Figure 14 shows the S0/SA0 histogram distribution corresponding to the difference between the measured surface brightness (at K_s mag) and the best-fit solutions (eq. [1]). The J-band surface brightness residual is shown with a solid line and the K_s with a dotted line. Ignoring the low surface brightness tail, the residuals shows a dispersion of only $\sim$0.12 mag arcsec^{-2} (Fig. 14), a value smaller than the average surface brightness difference between early- and late-type spirals (Fig. 15). At the most extreme, late-type spirals are systematically $\sim$0.4–0.5 mag arcsec^2 fainter than elliptical/lenticular galaxies, although the dispersion is also greater due to the lower S/N for late-type disk galaxies (in addition to their more complex morphology; see Figs. 2–4). Intermediate-type spirals are systematically fainter than lenticulars by $\sim$0.2 mag arcsec^{-2}, while early-type spirals are $\sim$0.1 mag arcsec^{-2} fainter than lenticulars in their central cores. Even though these are statistical trends, it is clear that S0/E -type galaxies can be delineated from disk-dominated galaxies using only near-infrared measurements. This result is consistent with that of Grauer & Rieke (1998), who acquired deep 1–2 μm infrared imaging of many nearby UGC galaxies, finding that central surface brightness is strongly correlated with Hubble type. Interestingly, this surface brightness effect is much less prominent at optical wavelengths for some studies (see Odewahn & Aldering 1995).

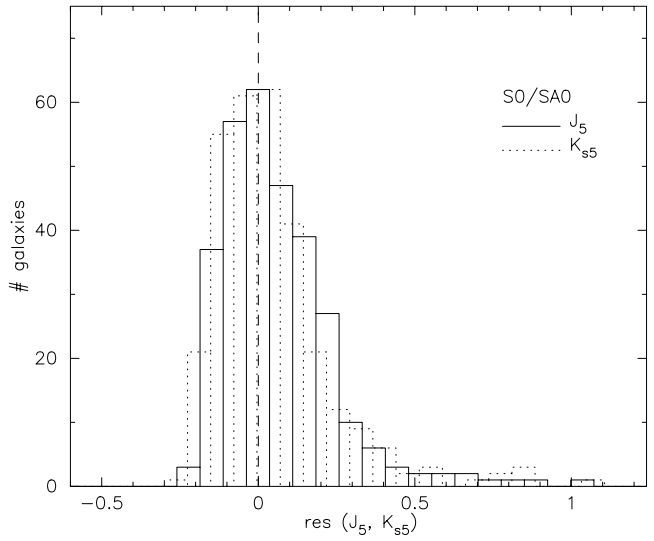

FIG. 14.—Residual central surface brightness for lenticular-type galaxies after subtracting the surface brightness to integrated flux relation (eq. [1]). The J-band residual is denoted with a solid line and the K_s with a dashed line. The distribution dispersion is $\sim$0.12 mag arcsec^{-2}.

Even with a crude measure of the mean central surface brightness, the Hubble galaxy types can be differentiated statistically. A cleaner separation between types should be possible using a better representation of the surface brightness, including those derived from the "effective" or half-light radius (see below). Similarly, by combining physical information such as disk scale length, isophotal size, and more precise (i.e., decoupled) bulge-to-disk surface brightness and color ratios as derived from infrared *and* optical

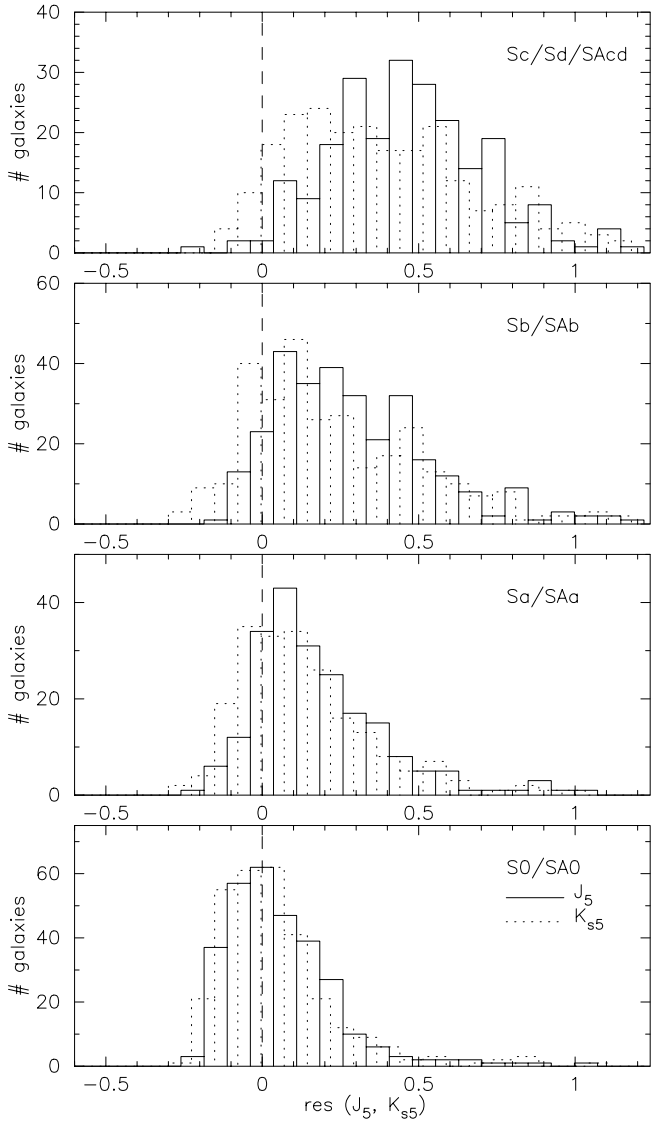

FIG. 15.—Residual central surface brightness for normal spiral galaxies after subtracting the lenticular surface brightness to integrated flux relation (eq. [1]).

imaging, more robust taxonomy of spiral and barred types should be possible.

5.4. Comparison with Optical Properties

Compared to visual-band imaging, ground-based infrared imaging (e.g., 2MASS) is not as sensitive to low surface brightness emission from galaxies due to the high backgrounds inherent to the 1–2 μm atmospheric windows. On the other hand, the NIR is less affected by dust extinction, both within our Galaxy and within the targeted galaxies. A detailed comparison between the bands provides the first step toward understanding the properties of the stellar light coming from the different large-scale components (see

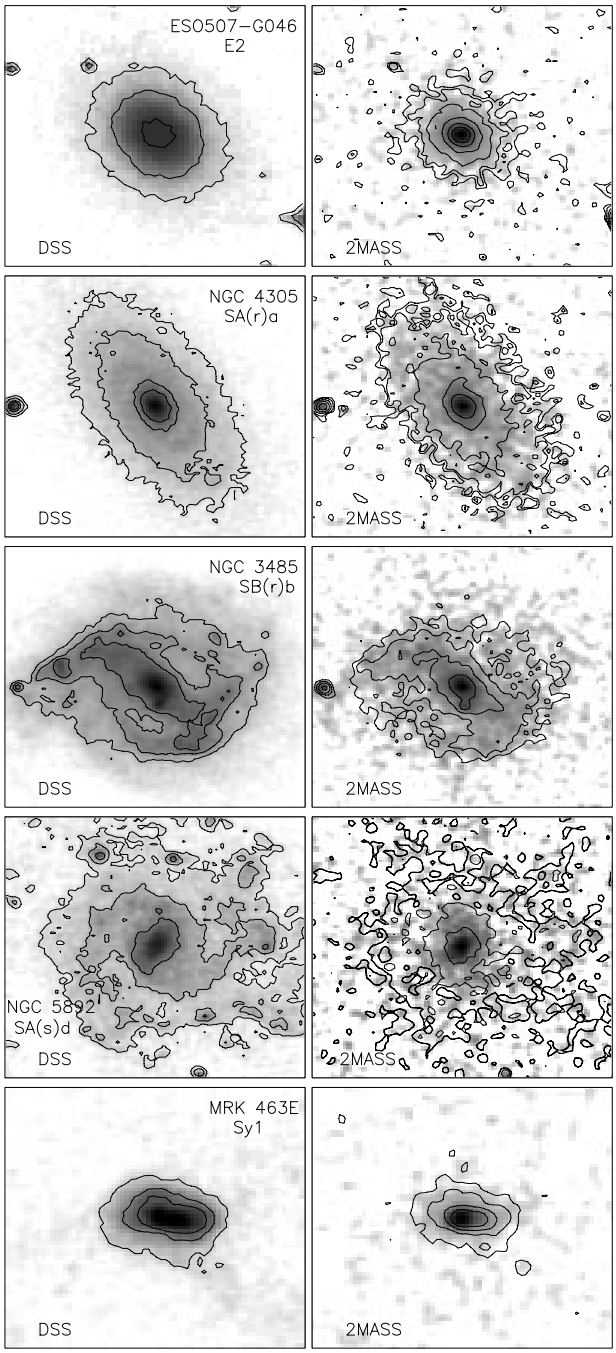

FIG. 16.—Comparison between optical and infrared imaging. Five galaxies are illustrated: spheroidal E2 galaxy (ESO 507-G046), early-type Sa spiral (NGC 4305), barred SBb spiral (NGC 3485), late-type Sd spiral (NGC 5892), and Seyfert-type active galaxy (Mrk 463E). The K_s-band integrated flux for each galaxy is $\sim$10.0 mag ($\sim$75 mJy). The left column show gray-scale Digitized Sky Survey images with contours overlaid. The right column shows 2MASS K_s-band images (*gray-scale halftone*), overlaid with J-band contours. The gray-scale stretch and contour levels were chosen to highlight similar features between the DSS and 2MASS data. The average surface brightness of the lowest contour for the optical images is $\sim$24.6, 24.0, 23.4, 23.0, and 24.0 mag arcsec^{-2}, reading from top to bottom (early to late types).

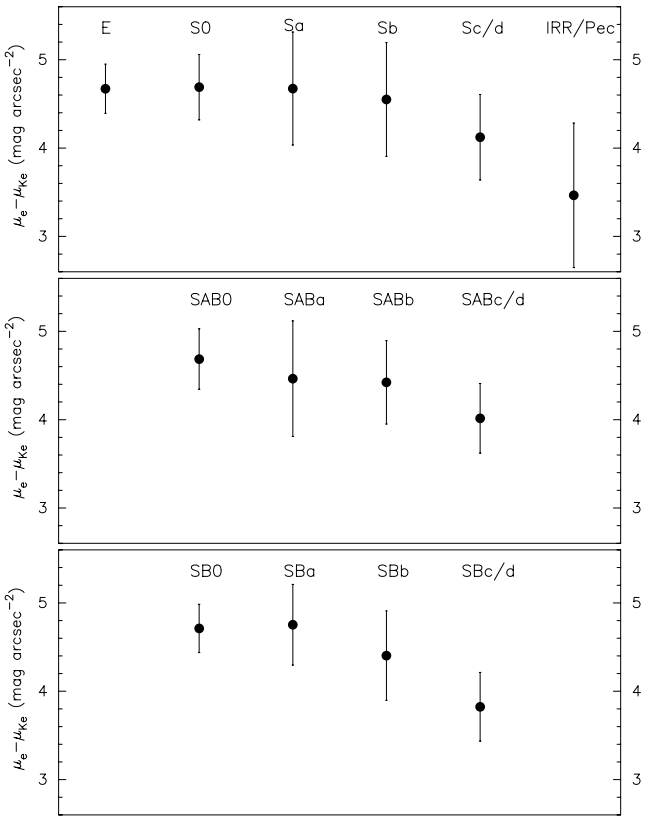

FIG. 17.— Comparison between the optical and near-infrared surface brightness for different Hubble types. The B-band surface brightness, μ_e, is computed from the RC3 "effective" aperture (half-light diameter, A_e). The K-band surface brightness, μ_{Ke}, is computed using a matched aperture. The error bars represent the rms scatter in the distribution.

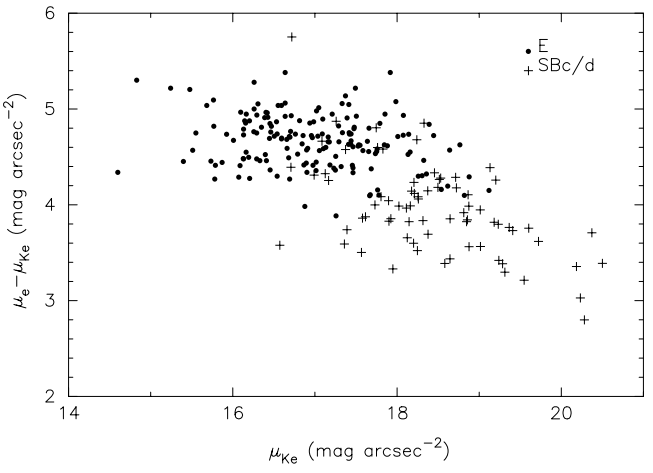

FIG. 18.—Comparison between the optical and near-infrared surface brightness for elliptical (*filled circles*) and late-type barred spirals (*crosses*). The B-band surface brightness, μ_e, is computed from the RC3 "effective" aperture (half-light diameter, A_e). The K-band surface brightness, μ_{Ke}, is computed using a matched aperture.

Grauer & Rieke 1998). Here we compare the NIR properties of 2MASS galaxies with the corresponding measures in the RC3 (de Vaucouleurs et al. 1991), including the size, total flux, central surface brightness, and elongation. To help define the context, we first begin with a qualitative comparison between optical and NIR images of bright galaxies.

In Figure 16 we show five different cases: spheroidal E2 galaxy (ESO 507-G046), early-type Sa spiral (NGC 4305), barred SBb spiral (NGC 3485), late-type Sd spiral (NGC 5892), and Seyfert-type active galaxy (Mrk 463E). The K_s-band flux for each galaxy is $\sim$10th mag ($\sim$75 mJy); they are relatively bright and large galaxies for 2MASS. The $J-K_s$ colors range from 0.8 to 1.0 mag, except for Mrk 463E, which has a very red color of 2.2 mag (see also Fig. 20*ay*). The galaxies were also chosen due to their mostly face-on orientation, which aids comparison of large-scale features. The left column represents visual imaging, where we display the Digitized Sky Survey (DSS) image using a gray-scale halftone with contours overlaid. The right column represents the 2MASS K_s band, shown with gray-scale halftone, overlaid with J-band contours. For both sets of data the gray-scale stretches and contours were chosen to highlight similar features, allowing for qualitative comparison. Moreover, the optical contours show the surface brightness difference between the optical and infrared for the Hubble sequence: the lowest level contour ranges between 24.5 and 23.0 B mag arcsec^{-2}, from early to late type.

The DSS images are more sensitive to low surface brightness emission, particularly for late-type ("blue") spirals, owing to their lower backgrounds and favorable colors. Nevertheless, the 2 μm images do show the same features as those seen in the 0.7 μm images, including spiral arms, bars, and asymmetries. For the active galaxy, Mrk 463E, the "double" nucleus feature is distinctly different between data sets, probably due to dust extinction. Although 2MASS imaging alone is not sufficiently sensitive to provide unambiguous classification between spiral subtypes, in combination with optical data it should be possible to clearly distinguish between the classic Hubble types of galaxies.

A detailed comparison is made with the RC3, including $\sim$900 galaxies with surface brightness measurements, delineated into 50–100 galaxies per Hubble type. Here we compute the ratio between the 2MASS isophotal size, D_{20}, corresponding to the 20 K mag arcsec^{-2} isophote, with the RC3 D_{25} isophotal size, corresponding to the 25 B mag arcsec^{-2} isophote. For the total flux comparison, we take the difference between the 2MASS integrated flux (from D_{20}) and the RC3 B_T mag (derived from D_{25}). For the axis ratio comparison, we multiply the K-band axis minor-to-major axis ratio ($K_{b/a}$; derived from the 3 σ contour, roughly equal to 18.8 K mag arcsec^{-2}) with the RC3 major-

to-minor axis ratio, R_{25}. Finally, for the central surface brightness, μ_e (B mag arcsec^{-2}), we use the RC3 "effective" aperture, A_e, roughly corresponding to the half-light radius. Since the current (first release) version of the 2MASS galaxy catalog does not include a half-light or "effective" aperture,[3] it was necessary to perform additional photometry on the 2MASS images using an aperture matched to the RC3 effective aperture, A_e. In order to minimize source contamination in the photometry, stars were carefully subtracted from the 2MASS images using the appropriate point-spread function (PSF) image.[4] To avoid the effects of undersampling, galaxies with an A_e diameter of less than 14″ were not included in the analysis. The absolute calibration uncertainty is estimated to be less than 5%. The resultant surface brightness, μ_{Ke} (K mag arcsec^{-2}), can be directly compared with corresponding optical version.

The results are shown in Table 2. For early types, the NIR isophotes extend down to about 75% of the corresponding optical size. Galaxies appear even smaller in the NIR for the later Sc/d types, ~56% of the optical size. For barred spirals the trend is similar from early to late-type, but the amplitude is smaller (76% vs. 67%), while the dispersion is significantly larger for late-types. The dispersion might be indicative of the lower S/N in the K-band images relative to the optical (see below). The results are also consistent with a more prominent bar in the NIR. The bar is increasing the apparent size and elongation, $K_{b/a} \times R_{25}$, of the galaxy (see also § 5.2). The effective (half-light) diameter of the optical images, A_e, is about 45%–60% in size of the K-band isophotal diameter (recall that 20 mag arcsec^{-2} is about 1 σ of the background noise), again showing the same trend from early to late types. For the total flux comparison, $B_T - K_s$, the average color is about 3.9–4.0 for early types, decreasing to 3.1 for late types (even bluer, 2.9 mag, for barred spirals). The NIR sensitivity is decreasing for the later type (i.e., "blue") galaxies.

This color effect is most clearly seen in the central surface brightness comparison, $\mu_e - \mu_{Ke}$, where we have matched the apertures. Now the early types are much redder, with colors between 4.6 and 4.7 mag arcsec^{-2}, while for the late types the color drops to ~3.8–4.1 mag arcsec^{-2} (Fig. 17). Compared to the *total* $B_T - K_s$, the *central* surface brightness color is redder from two effects: dust extinction (absorbing mostly blue light) and the presence of older (redder) stars in the core and halo of galaxies. The color gradient from early to late types (Fig. 17) maps the change in stellar populations. The gradient is strongest for the barred spirals, which suggests a younger massive population of stars associated with the bar feature (see also Fig. 18). It is interesting to note that irregular and peculiar galaxies, including mergers, tidal interactions, and starbursts, also have very blue colors similar to barred spirals. As the late-type galaxies evolve, their cores will gradually redden and brighten into early-type disks or spheroids.[5]

6. SUMMARY

We present an image atlas of a sample of galaxies observed with the Two Micron All-Sky Survey (Figs. 19 and 20). The images are separated according to the traditionally based Hubble type or morphological classification. In addition to the main elliptical/spheroidal and spiral-type classes, we also include examples of compact, dwarf, irregular/peculiar, and AGN/Seyfert types of extragalactic objects. A simple analysis of the atlas shows that the different classes are not as well separated with infrared colors (the exception being the extremely red class of AGN galaxies) but are clearly distinguished when comparing central surface brightness and total flux. A detailed comparison between optical and infrared properties, including sizes, elongation, colors, and surface brightness, reveals clear differences between spiral types and between barred and normal disk galaxies. With more sophisticated measurements (e.g., decoupled bulge-to-disk ratios) and methods (e.g., supervised neural networks), and in combination with optical imaging, it should be possible to derive morphological classifications for a data set that is numbered in the millions.

We thank Harold Corwin for his wise counsel and RC3 data sets. We thank Tom Chester, Joe Mazzerella, Barry Madore, Marion Schmitz, and George Helou for their insightful comments. We thank Steve Odewahn for a careful review of this paper. We thank Geraldine Jarrett for proofreading. This publication makes use of data products of the 2MASS, which is a joint project of the University of Massachusetts and the Infrared Processing and Analysis Center, funded by the NASA and NSF. This research has made use of the NASA/IPAC Extragalactic Database (NED), which is operated by the Jet Propulsion Laboratory, California Institute of Technology, under contract with NASA. The Digitized Sky Surveys were produced at the Space Telescope Science Institute. The images of these surveys are based on photographic data obtained using the Oschin Schmidt Telescope on Palomar Mountain and the UK Schmidt Telescope.

[3] The "effective" or half-light radius is difficult to derive robustly with automated processing. The 2MASS project decided to delay this procedure until the final processing, to be carried out in 2001.

[4] The PSF is well determined since 2MASS takes great pains to carefully track the PSF during a 6 minute "scan." See Jarrett et al. (2000) for details.

[5] Although it is by no means definitive how and where E-type spheroids form. Some ellipticals, for example, arise from merging galaxies, early in the history of the universe.

REFERENCES

Binggeli, B., Sandage, A., & Tammann, G. 1988, ARA&A, 26, 509
Buta, R. 1992, in Morphological and Physical Classification of Galaxies, ed. G. Longo, M. Capaccioli, & G. Busarello (Dordrecht: Kluwer), 1
———. 1995, ApJS, 96, 39
Buta, R., Mitra, S., de Vaucouleurs, G., & Corwin, H. G. 1994, AJ, 107, 118
de Vaucouleurs, G. 1959, Handbuch der Physik, 3, 275
———. 1977, in The Evolution of Galaxies and Stellar Populations, ed. B. Tinsley & R. Larson (New Haven: Yale Univ. Obs.), 43
de Vaucouleurs, G., de Vaucouleurs, A., Corwin, H. G., Jr., Buta, R., Paturel, G., & Fouqué, P. 1991, Third Reference Catalogue of Bright Galaxies (Berlin: Springer) (RC3)
de Vaucouleurs, G., & Freeman, K. C. 1972, Vistas Astron., 14, 163
Dressler, A. 1980, ApJ, 236, 351
Ferrini, F., & Galli, D. 1988, A&A, 195, 27
Giovanelli, R., & Haynes, M. P. 1983, AJ, 88, 881
Grauer, A. D., & Rieke, M. 1998, ApJS, 116, 29
Hoffman, G. L., Helou, G., Salpeter, E. E., & Lewis, B. M. 1989, ApJ, 339, 812
Holmberg, E. 1958, Medd. Lund. Astron. Obs. Ser., 2, 136
Hubble, E. 1926, ApJ, 64, 321
———. 1936, The Realm of the Nebulae (New Haven: Yale Univ. Obs.)
Hubble, E., & Humason, M. 1931, ApJ, 74, 43
Impey, C., & Bothun, G. 1997, ARA&A, 35, 267
Jarrett, T. H., Chester, T., Cutri, R., Schneider, S., & Huchra, J. 2000, AJ, 119, 2498
Jarrett, T. H., Chester, Schneider, S., & Huchra, J. 1997, in The Impact of Large-Scale Near-IR Sky Surveys, ed. F. Garzon et al. (Dordrecht: Kluwer), 213
Julian, W. H., Kooiman, B. L., & Sanders, W. L. 1997, PASP, 109, 297
Kormendy, J. A. 1977, ApJ, 218, 333
Mamon, G. 1992, ApJ, 401, L3
Odewahn, S. C., & Aldering, G. 1995, AJ, 110, 2009
Odewahn, S. C., Burstein, D., & Windhorst, R. 1997, AJ, 114, 2219
Odewahn, S. C., Windhorst, R., Driver, S. P., & Keel, W. C. 1996, ApJ, 472, L13
Osterbrock, D. E. 1993, ApJ, 404, 551
Postman, M., & Geller, M. J. 1984, ApJ, 281, 95
Roberts, M. S., & Haynes, M. P. 1994, ARA&A, 32, 115
Sandage, A. 1961, The Hubble Atlas (Washington, DC: Carnegie Inst. Washington)
———. 1975, in Stars and Stellar Systems, vol. 9, ed. A. Sandage, M. Sandage, & J. Kristian (Chicago: Univ. Chicago Press), 1
———. 1986, A&A, 161, 89
———. 1990, in Clusters of Galaxies, ed. W. Oegerle, M. Fitchett, & L. Danly (New York: Cambridge Univ. Press), 201
Sandage, A., & Binggeli, B. 1984, AJ, 89, 919
Skrutskie, M., et al. 1997, in The Impact of Large-Scale Near-IR Sky Surveys, ed. F. Garzon et al. (Dordrecht: Kluwer), 25
van den Bergh, S. 1994, AJ, 107, 153
———. 1998, Galaxy Morphology and Classification (New York: Cambridge Univ. Press)
Whitmore, B. C., Gilmore, D., & Jones, C. 1993, ApJ, 407, 489

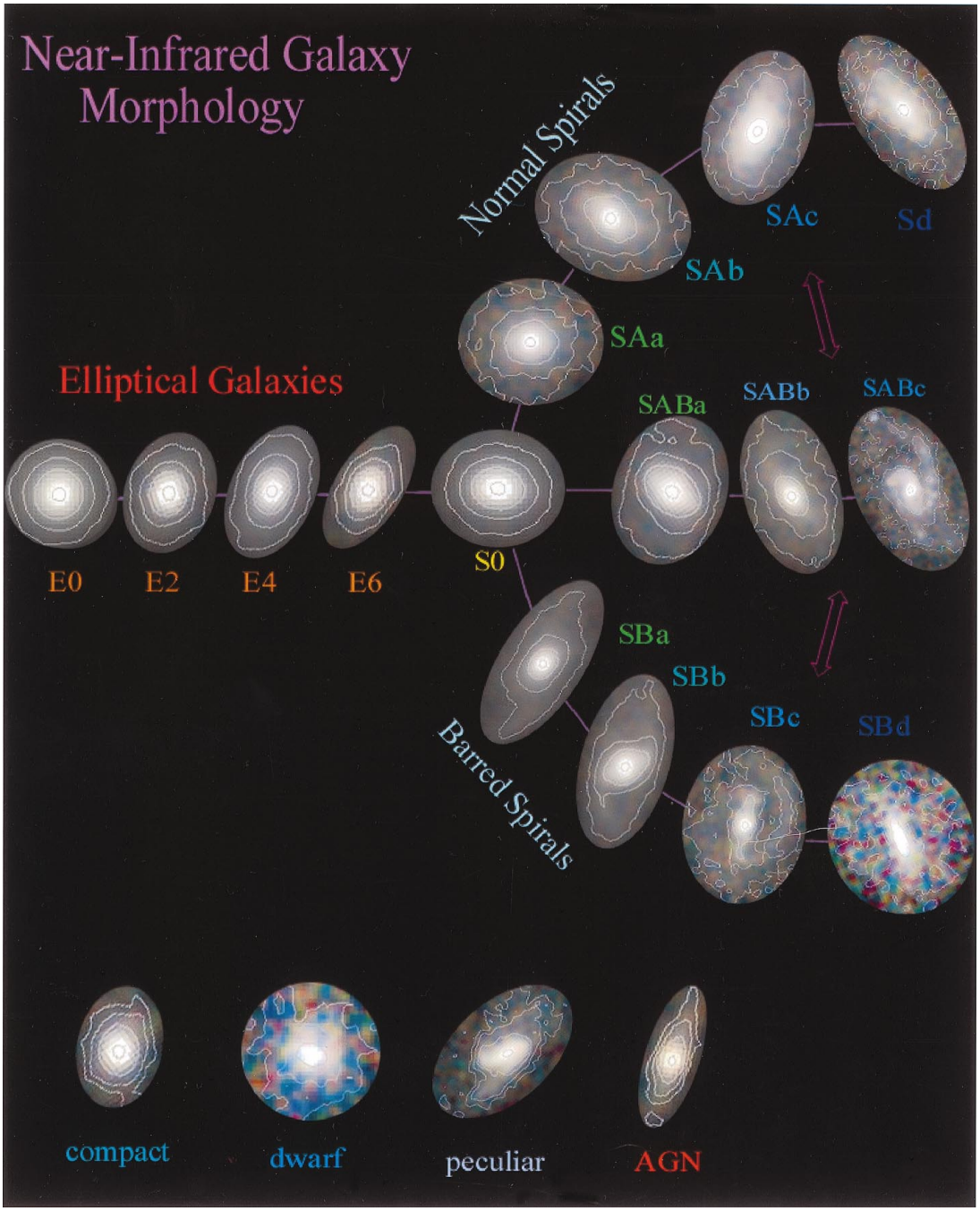

FIG. 19.—The 2MASS near-infrared galaxy morphology sequence "trident," analogous to the Hubble sequence "tuning fork." The images were created by combining the J, H, and K_s image data with an RGB color scale: J is assigned blue intensity levels, H green, and K_s red intensity levels. Also shown are J-band contours, corresponding to the 10%, 20%, 30%, . . ., etc., of the J-band peak flux. The integrated brightness ranges between 10.0 and 11.0 mag at 2.2 μm (30–70 mJy, respectively), and angular sizes range from 50″ to 100″. The 2MASS beam size, in comparison, is $\sim$2″.

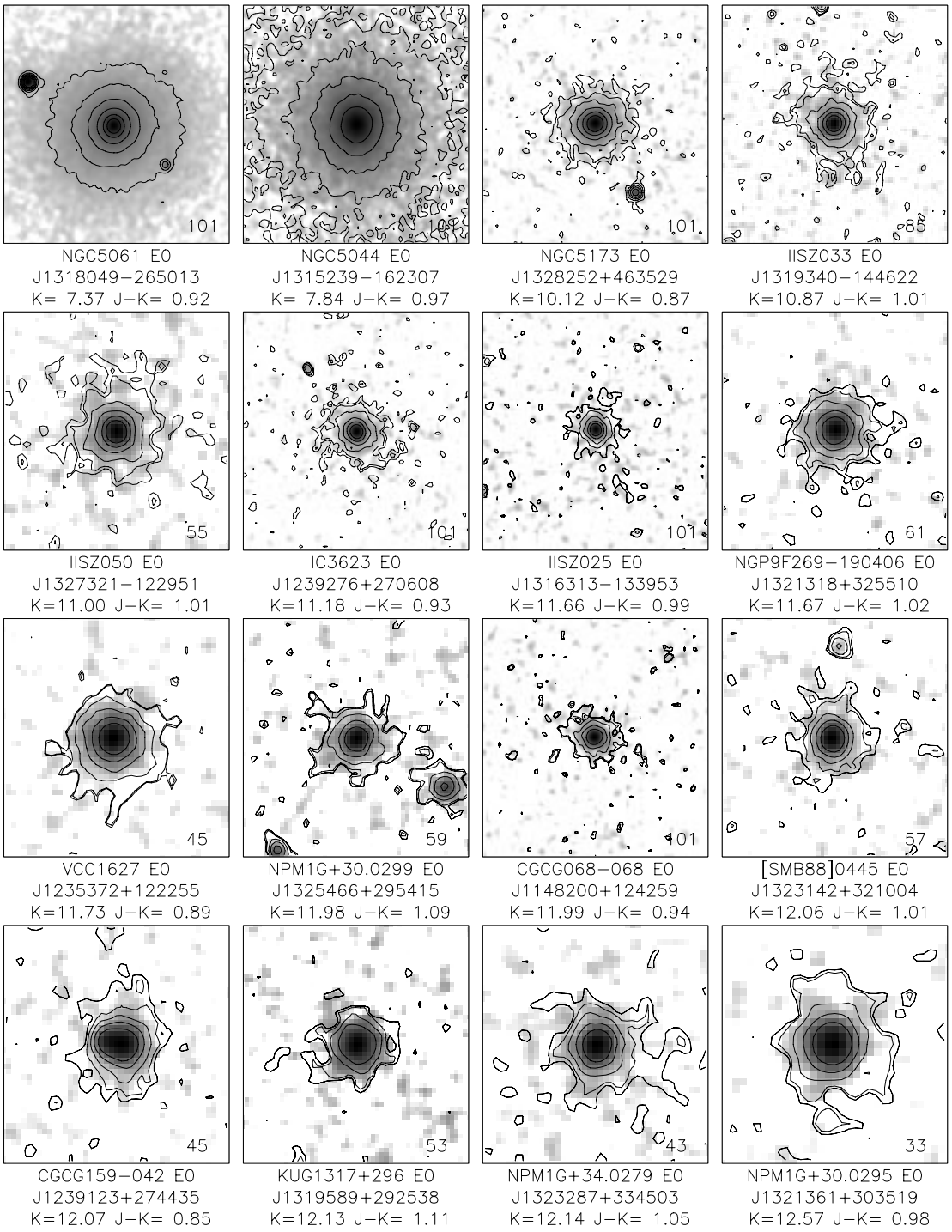

FIG. 20*a*

FIG. 20.—2MASS galaxy morphology atlas. Each "plate" consists of 16 different galaxy images, separated according to morphology and integrated flux (see Table 1). The images are presented as gray-scale halftones of the K_s (2.2. μm) image, overlaid with contours corresponding to the J-band (1.3 μm) image. The gray-scale ranges from 1 σ ($\sim$ 20 mag arcsec^{-2}) of the background noise to the peak pixel value for the galaxy (but with a lower threshold of 5 σ). The gray-scale stretch includes a base-10 logarithm transformation, which enhances the contrast in the underlying galaxy emission. The J-band contours correspond to the 1%, 2%, 4%, 8%, 16%, and 32% peak-intensity levels, with a minimum value corresponding to 2 σ ($\sim$ 20.8 mag arcsec^{-2}) of the J-band background. Also included are the catalog or NED name, morphological or Hubble type, 2MASS name, K_s mag, and $J - K_s$ color. The 2MASS name maps into the J2000 equatorial position of the source (Jhhmmss.s $\pm$ ddmmss). The angular size of the image is noted in the lower right-hand corner of the image, ranging from 21″ to 101″ (the beam size, in comparison, is $\sim$ 2″).

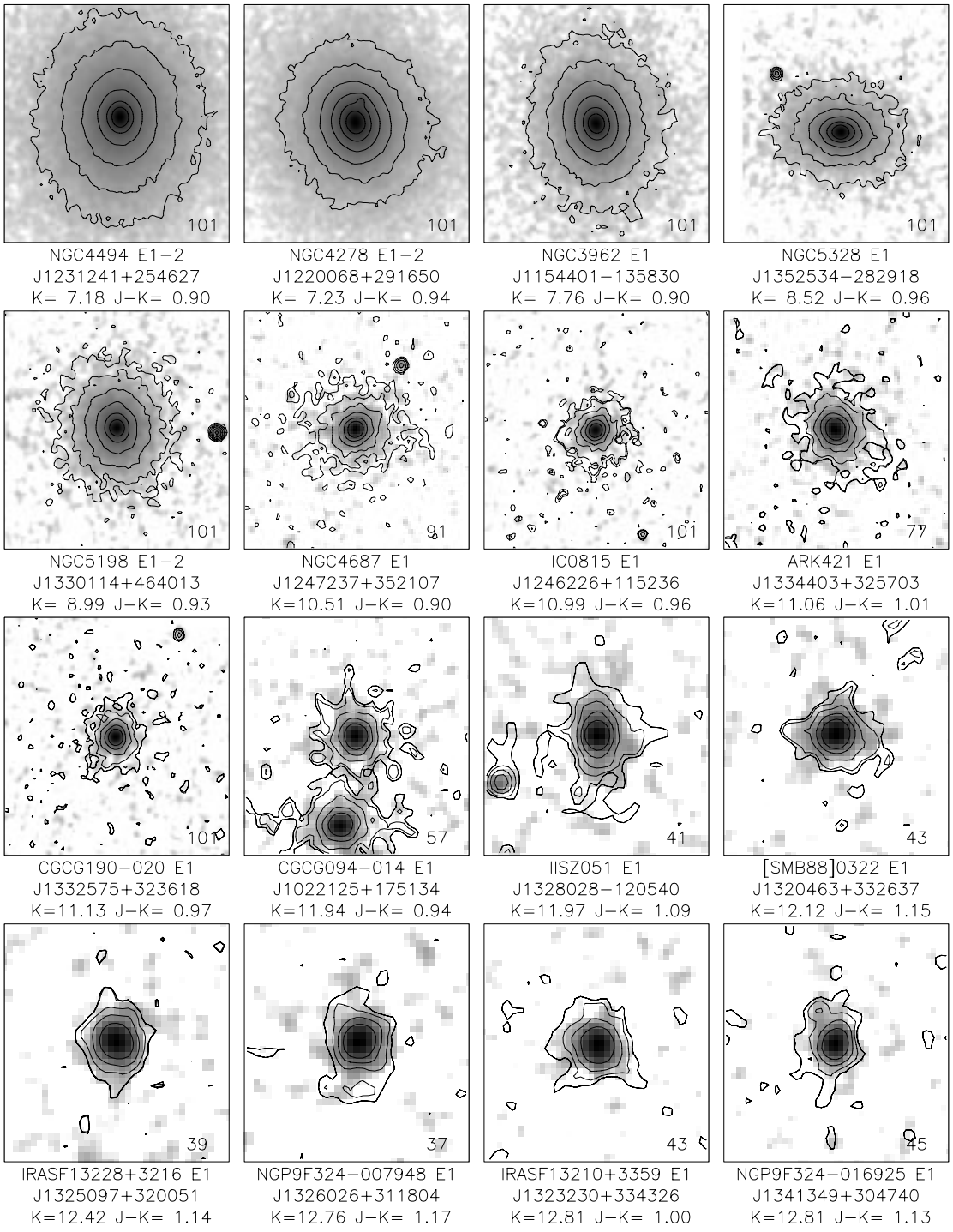
101
NGC4494 E1−2
J1231241+254627
K= 7.18 J−K= 0.90
101
NGC4278 E1−2
J1220068+291650
K= 7.23 J−K= 0.94
101
NGC3962 E1
J1154401−135830
K= 7.76 J−K= 0.90
101
NGC5328 E1
J1352534−282918
K= 8.52 J−K= 0.96
101
NGC5198 E1−2
J1330114+464013
K= 8.99 J−K= 0.93
91
NGC4687 E1
J1247237+352107
K=10.51 J−K= 0.90
101
IC0815 E1
J1246226+115236
K=10.99 J−K= 0.96
77
ARK421 E1
J1334403+325703
K=11.06 J−K= 1.01
101
CGCG190−020 E1
J1332575+323618
K=11.13 J−K= 0.97
57
CGCG094−014 E1
J1022125+175134
K=11.94 J−K= 0.94
41
IISZ051 E1
J1328028−120540
K=11.97 J−K= 1.09
43
[SMB88]0322 E1
J1320463+332637
K=12.12 J−K= 1.15
39
IRASF13228+3216 E1
J1325097+320051
K=12.42 J−K= 1.14
37
NGP9F324−007948 E1
J1326026+311804
K=12.76 J−K= 1.17
43
IRASF13210+3359 E1
J1323230+334326
K=12.81 J−K= 1.00
45
NGP9F324−016925 E1
J1341349+304740
K=12.81 J−K= 1.13

FIG. 20*b*

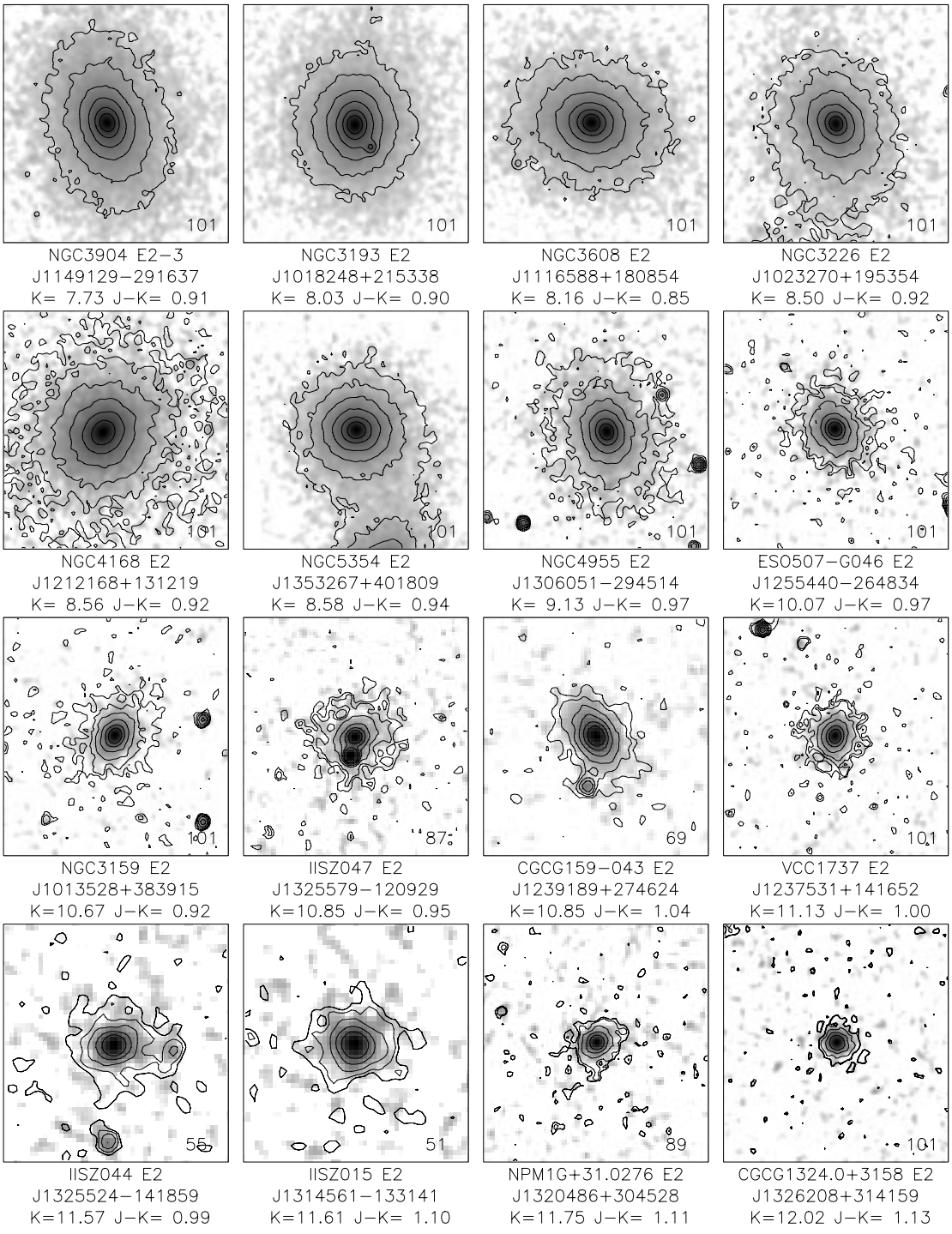
101
NGC3904 E2−3
J1149129−291637
K= 7.73 J−K= 0.91
101
NGC3193 E2
J1018248+215338
K= 8.03 J−K= 0.90
101
NGC3608 E2
J1116588+180854
K= 8.16 J−K= 0.85
101
NGC3226 E2
J1023270+195354
K= 8.50 J−K= 0.92
101
NGC4168 E2
J1212168+131219
K= 8.56 J−K= 0.92
101
NGC5354 E2
J1353267+401809
K= 8.58 J−K= 0.94
101
NGC4955 E2
J1306051−294514
K= 9.13 J−K= 0.97
101
ESO507−G046 E2
J1255440−264834
K=10.07 J−K= 0.97
101
NGC3159 E2
J1013528+383915
K=10.67 J−K= 0.92
87
IISZ047 E2
J1325579−120929
K=10.85 J−K= 0.95
69
CGCG159−043 E2
J1239189+274624
K=10.85 J−K= 1.04
101
VCC1737 E2
J1237531+141652
K=11.13 J−K= 1.00
55
IISZ044 E2
J1325524−141859
K=11.57 J−K= 0.99
51
IISZ015 E2
J1314561−133141
K=11.61 J−K= 1.10
89
NPM1G+31.0276 E2
J1320486+304528
K=11.75 J−K= 1.11
101
CGCG1324.0+3158 E2
J1326208+314159
K=12.02 J−K= 1.13

FIG. 20*c*

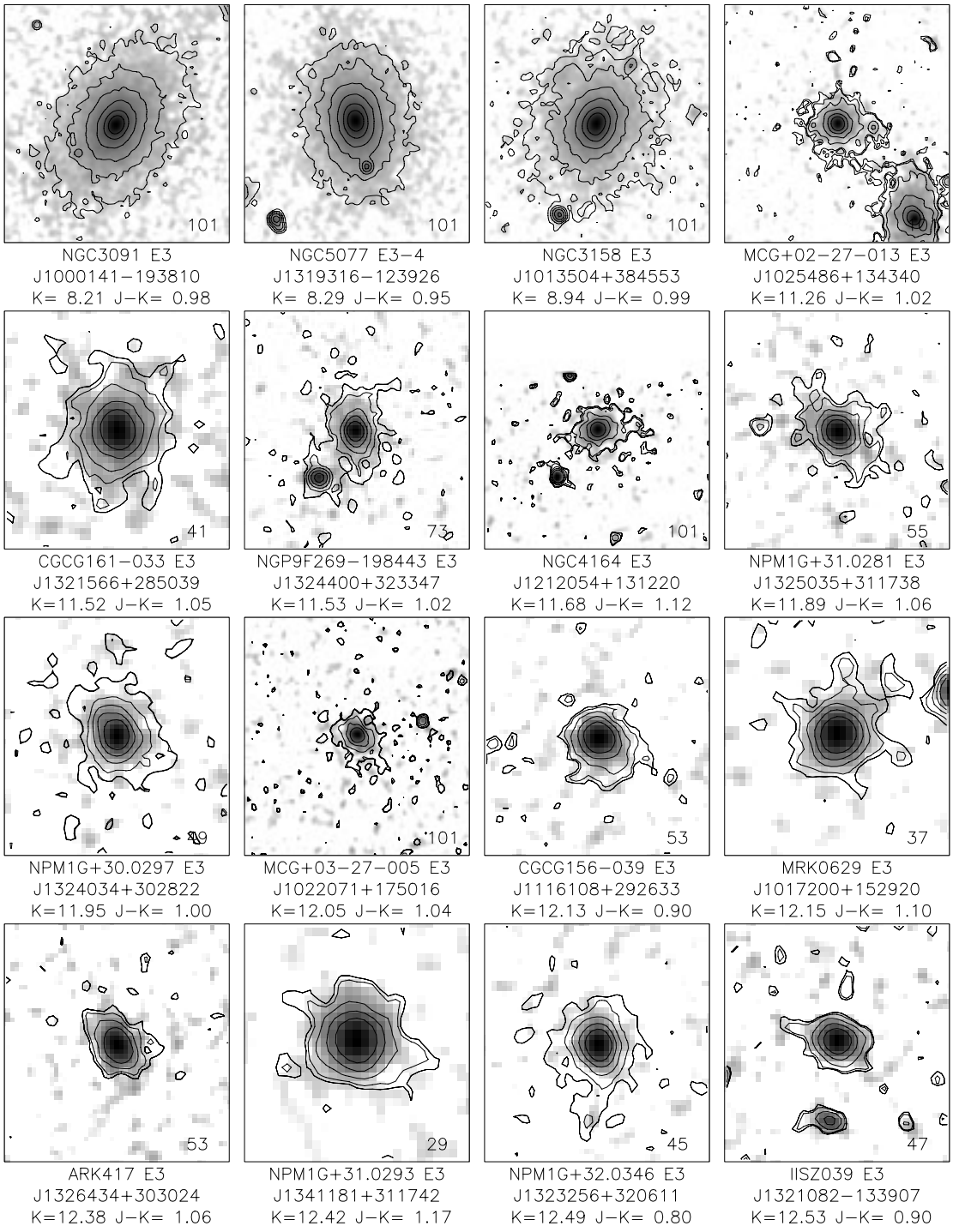
101
NGC3091 E3
J1000141−193810
K= 8.21 J−K= 0.98
101
NGC5077 E3−4
J1319316−123926
K= 8.29 J−K= 0.95
101
NGC3158 E3
J1013504+384553
K= 8.94 J−K= 0.99
MCG+02−27−013 E3
J1025486+134340
K=11.26 J−K= 1.02
41
CGCG161−033 E3
J1321566+285039
K=11.52 J−K= 1.05
73
NGP9F269−198443 E3
J1324400+323347
K=11.53 J−K= 1.02
101
NGC4164 E3
J1212054+131220
K=11.68 J−K= 1.12
55
NPM1G+31.0281 E3
J1325035+311738
K=11.89 J−K= 1.06
49
NPM1G+30.0297 E3
J1324034+302822
K=11.95 J−K= 1.00
101
MCG+03−27−005 E3
J1022071+175016
K=12.05 J−K= 1.04
53
CGCG156−039 E3
J1116108+292633
K=12.13 J−K= 0.90
37
MRK0629 E3
J1017200+152920
K=12.15 J−K= 1.10
53
ARK417 E3
J1326434+303024
K=12.38 J−K= 1.06
29
NPM1G+31.0293 E3
J1341181+311742
K=12.42 J−K= 1.17
45
NPM1G+32.0346 E3
J1323256+320611
K=12.49 J−K= 0.80
47
IISZ039 E3
J1321082−133907
K=12.53 J−K= 0.90

FIG. 20*d*

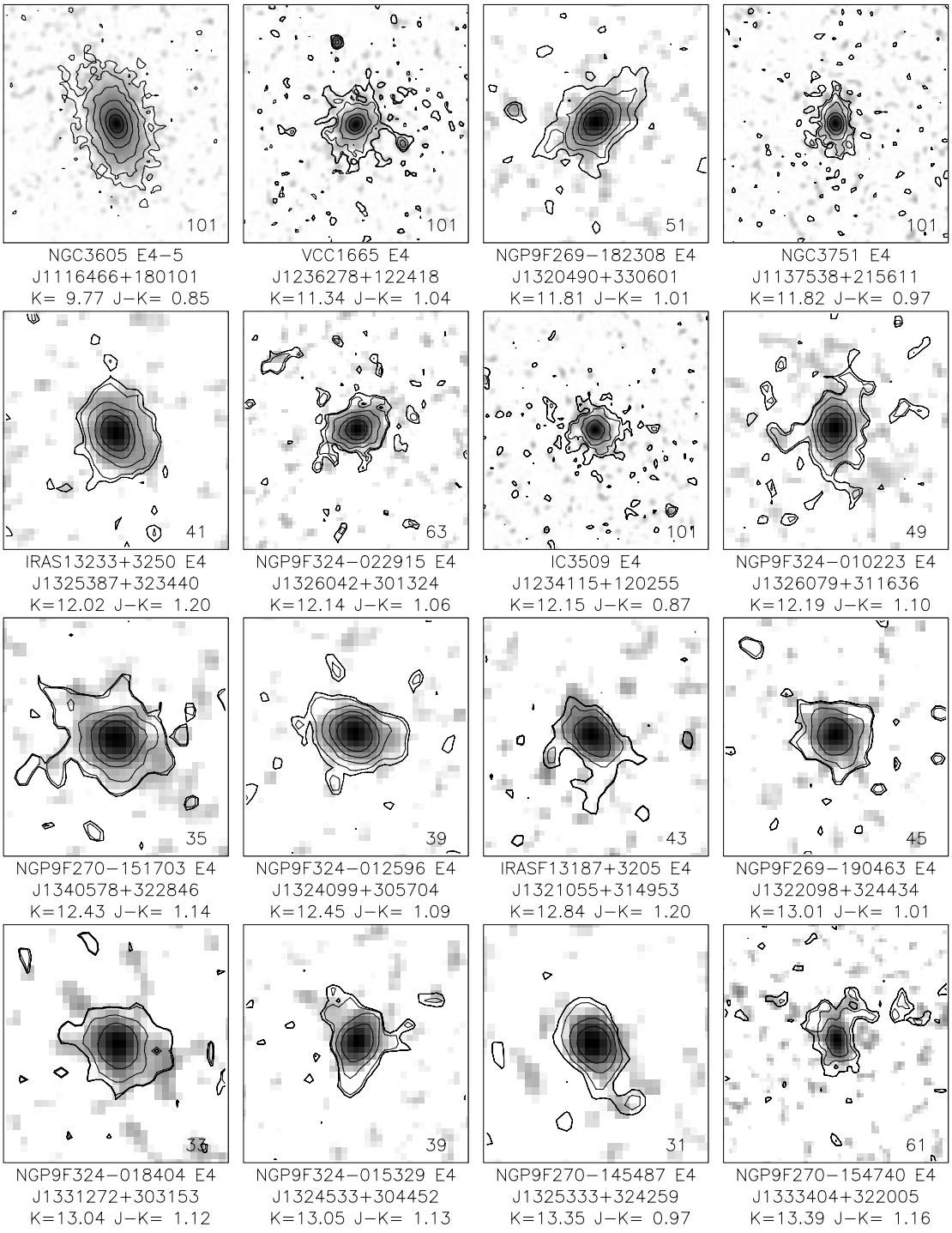
101
NGC3605 E4−5
J1116466+180101
K= 9.77 J−K= 0.85
101
VCC1665 E4
J1236278+122418
K=11.34 J−K= 1.04
51
NGP9F269−182308 E4
J1320490+330601
K=11.81 J−K= 1.01
101
NGC3751 E4
J1137538+215611
K=11.82 J−K= 0.97
41
IRAS13233+3250 E4
J1325387+323440
K=12.02 J−K= 1.20
63
NGP9F324−022915 E4
J1326042+301324
K=12.14 J−K= 1.06
101
IC3509 E4
J1234115+120255
K=12.15 J−K= 0.87
49
NGP9F324−010223 E4
J1326079+311636
K=12.19 J−K= 1.10
35
NGP9F270−151703 E4
J1340578+322846
K=12.43 J−K= 1.14
39
NGP9F324−012596 E4
J1324099+305704
K=12.45 J−K= 1.09
43
IRASF13187+3205 E4
J1321055+314953
K=12.84 J−K= 1.20
45
NGP9F269−190463 E4
J1322098+324434
K=13.01 J−K= 1.01
33
NGP9F324−018404 E4
J1331272+303153
K=13.04 J−K= 1.12
39
NGP9F324−015329 E4
J1324533+304452
K=13.05 J−K= 1.13
31
NGP9F270−145487 E4
J1325333+324259
K=13.35 J−K= 0.97
61
NGP9F270−154740 E4
J1333404+322005
K=13.39 J−K= 1.16

FIG. 20*e*

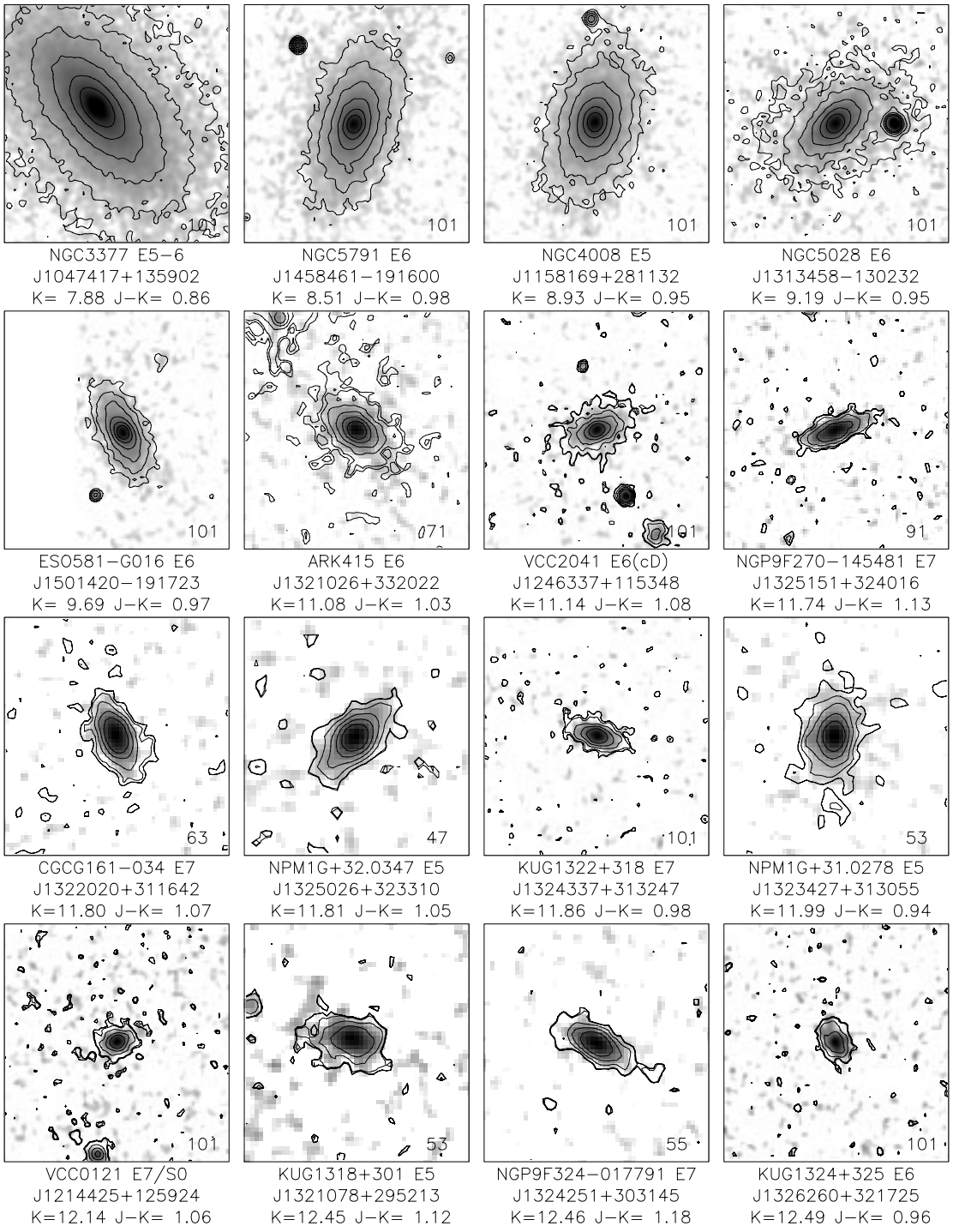
101
NGC3377 E5−6
J1047417+135902
K= 7.88 J−K= 0.86
101
NGC5791 E6
J1458461−191600
K= 8.51 J−K= 0.98
101
NGC4008 E5
J1158169+281132
K= 8.93 J−K= 0.95
101
NGC5028 E6
J1313458−130232
K= 9.19 J−K= 0.95
101
ESO581−G016 E6
J1501420−191723
K= 9.69 J−K= 0.97
071
ARK415 E6
J1321026+332022
K=11.08 J−K= 1.03
101
VCC2041 E6(cD)
J1246337+115348
K=11.14 J−K= 1.08
91
NGP9F270−145481 E7
J1325151+324016
K=11.74 J−K= 1.13
63
CGCG161−034 E7
J1322020+311642
K=11.80 J−K= 1.07
47
NPM1G+32.0347 E5
J1325026+323310
K=11.81 J−K= 1.05
101
KUG1322+318 E7
J1324337+313247
K=11.86 J−K= 0.98
53
NPM1G+31.0278 E5
J1323427+313055
K=11.99 J−K= 0.94
101
VCC0121 E7/S0
J1214425+125924
K=12.14 J−K= 1.06
53
KUG1318+301 E5
J1321078+295213
K=12.45 J−K= 1.12
55
NGP9F324−017791 E7
J1324251+303145
K=12.46 J−K= 1.18
101
KUG1324+325 E6
J1326260+321725
K=12.49 J−K= 0.96

FIG. 20*f*

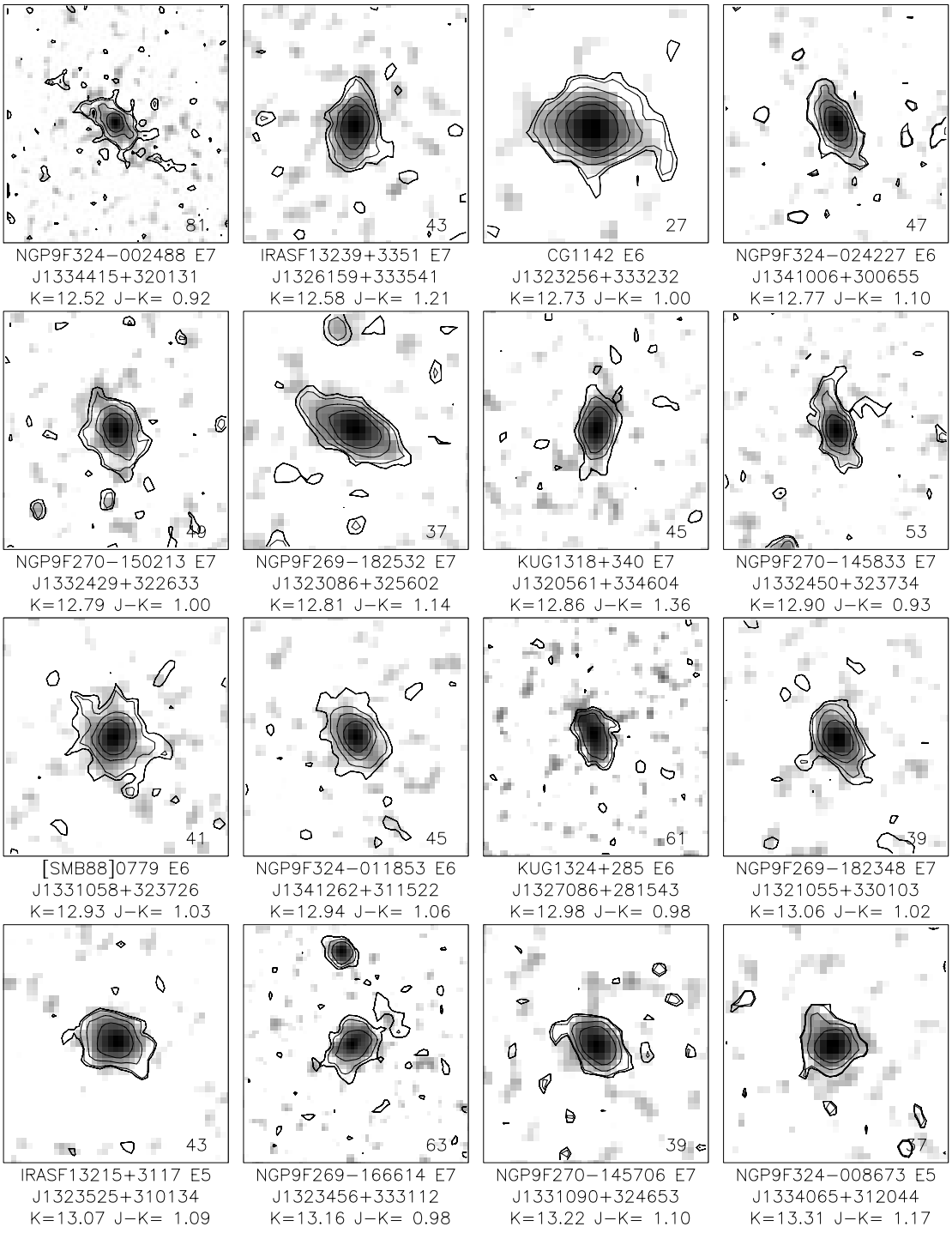
81
NGP9F324−002488 E7
J1334415+320131
K=12.52 J−K= 0.92
43
IRASF13239+3351 E7
J1326159+333541
K=12.58 J−K= 1.21
27
CG1142 E6
J1323256+333232
K=12.73 J−K= 1.00
47
NGP9F324−024227 E6
J1341006+300655
K=12.77 J−K= 1.10
49
NGP9F270−150213 E7
J1332429+322633
K=12.79 J−K= 1.00
37
NGP9F269−182532 E7
J1323086+325602
K=12.81 J−K= 1.14
45
KUG1318+340 E7
J1320561+334604
K=12.86 J−K= 1.36
53
NGP9F270−145833 E7
J1332450+323734
K=12.90 J−K= 0.93
41
[SMB88]0779 E6
J1331058+323726
K=12.93 J−K= 1.03
45
NGP9F324−011853 E6
J1341262+311522
K=12.94 J−K= 1.06
61
KUG1324+285 E6
J1327086+281543
K=12.98 J−K= 0.98
39
NGP9F269−182348 E7
J1321055+330103
K=13.06 J−K= 1.02
43
IRASF13215+3117 E5
J1323525+310134
K=13.07 J−K= 1.09
63
NGP9F269−166614 E7
J1323456+333112
K=13.16 J−K= 0.98
39
NGP9F270−145706 E7
J1331090+324653
K=13.22 J−K= 1.10
37
NGP9F324−008673 E5
J1334065+312044
K=13.31 J−K= 1.17

FIG. 20*g*

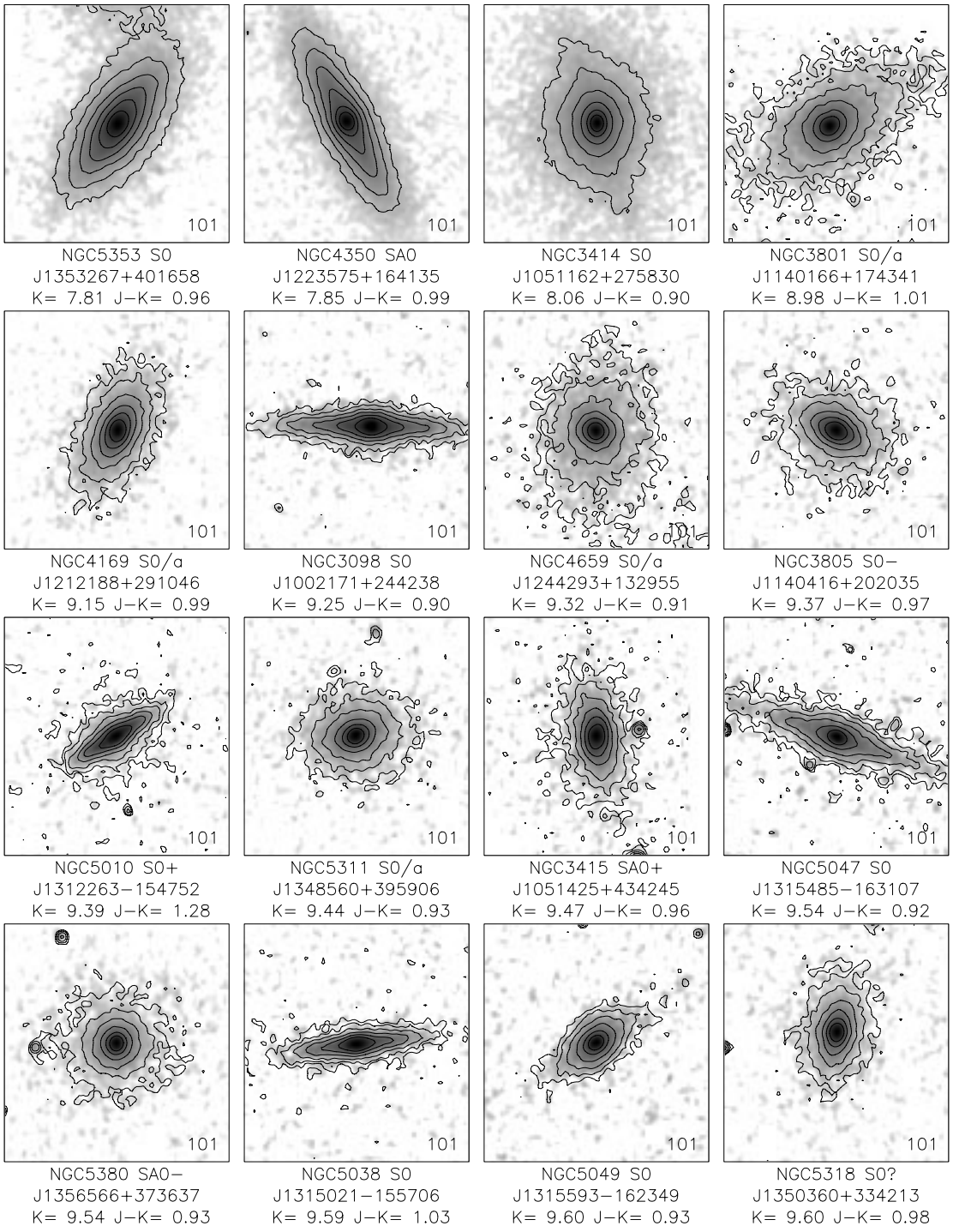
101
NGC5353 S0
J1353267+401658
K= 7.81 J−K= 0.96
NGC4350 SA0
J1223575+164135
K= 7.85 J−K= 0.99
NGC3414 S0
J1051162+275830
K= 8.06 J−K= 0.90
NGC3801 S0/a
J1140166+174341
K= 8.98 J−K= 1.01
NGC4169 S0/a
J1212188+291046
K= 9.15 J−K= 0.99
NGC3098 S0
J1002171+244238
K= 9.25 J−K= 0.90
NGC4659 S0/a
J1244293+132955
K= 9.32 J−K= 0.91
NGC3805 S0−
J1140416+202035
K= 9.37 J−K= 0.97
NGC5010 S0+
J1312263−154752
K= 9.39 J−K= 1.28
NGC5311 S0/a
J1348560+395906
K= 9.44 J−K= 0.93
NGC3415 SA0+
J1051425+434245
K= 9.47 J−K= 0.96
NGC5047 S0
J1315485−163107
K= 9.54 J−K= 0.92
NGC5380 SA0−
J1356566+373637
K= 9.54 J−K= 0.93
NGC5038 S0
J1315021−155706
K= 9.59 J−K= 1.03
NGC5049 S0
J1315593−162349
K= 9.60 J−K= 0.93
NGC5318 S0?
J1350360+334213
K= 9.60 J−K= 0.98

FIG. 20*h*

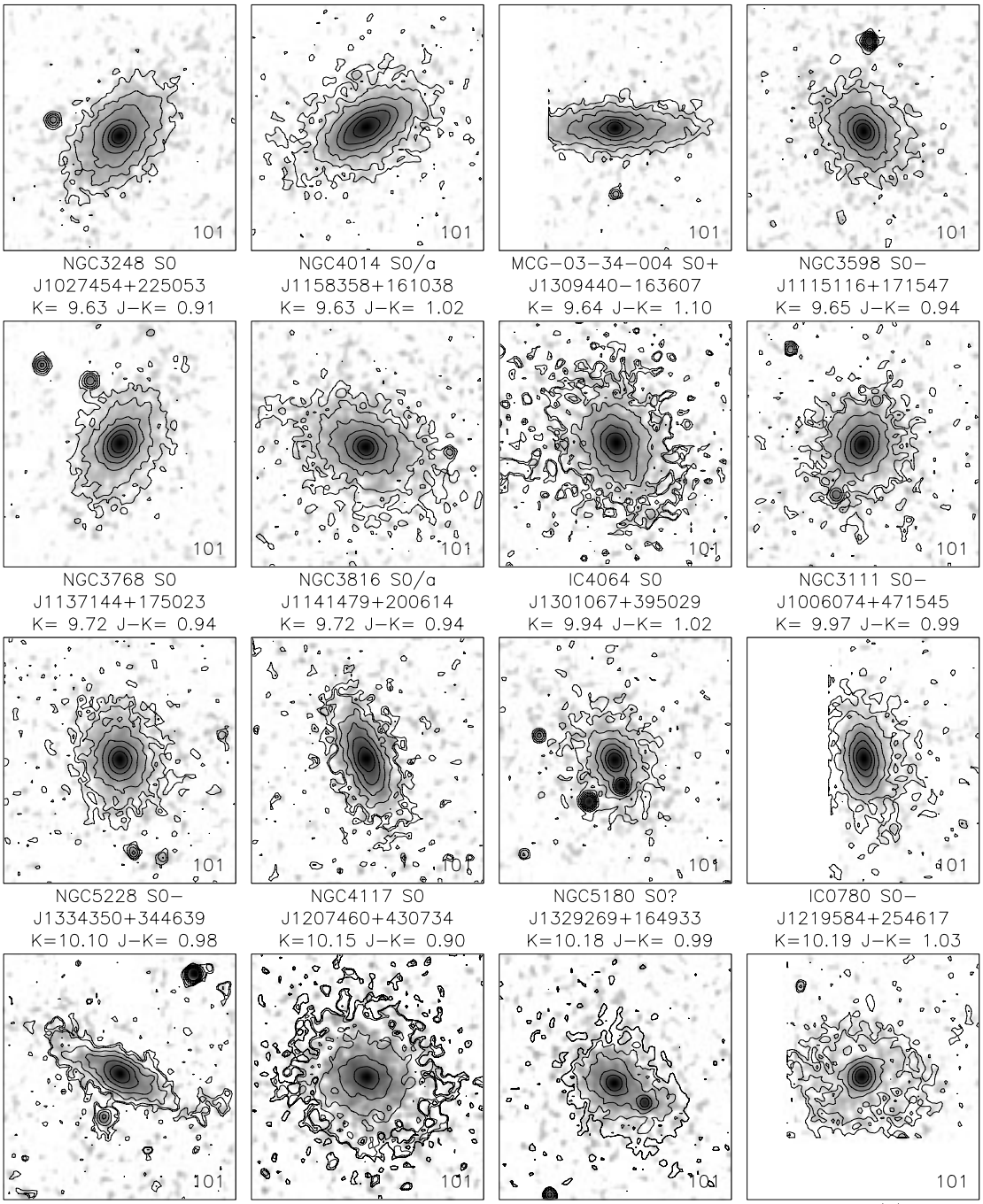
NGC3248 S0
J1027454+225053
K= 9.63 J−K= 0.91
NGC4014 S0/a
J1158358+161038
K= 9.63 J−K= 1.02
MCG−03−34−004 S0+
J1309440−163607
K= 9.64 J−K= 1.10
NGC3598 S0−
J1115116+171547
K= 9.65 J−K= 0.94
NGC3768 S0
J1137144+175023
K= 9.72 J−K= 0.94
NGC3816 S0/a
J1141479+200614
K= 9.72 J−K= 0.94
IC4064 S0
J1301067+395029
K= 9.94 J−K= 1.02
NGC3111 S0−
J1006074+471545
K= 9.97 J−K= 0.99
NGC5228 S0−
J1334350+344639
K=10.10 J−K= 0.98
NGC4117 S0
J1207460+430734
K=10.15 J−K= 0.90
NGC5180 S0?
J1329269+164933
K=10.18 J−K= 0.99
IC0780 S0−
J1219584+254617
K=10.19 J−K= 1.03
MCG−03−27−026 S0
J1042188−173855
K=10.31 J−K= 1.01
NGC4620 S0
J1241593+125634
K=10.32 J−K= 0.89
MCG−02−33−028 S0
J1251151−151159
K=10.35 J−K= 1.03
UGC05936 (R)SA0+
J1050072+362030
K=10.43 J−K= 0.98

FIG. 20*i*

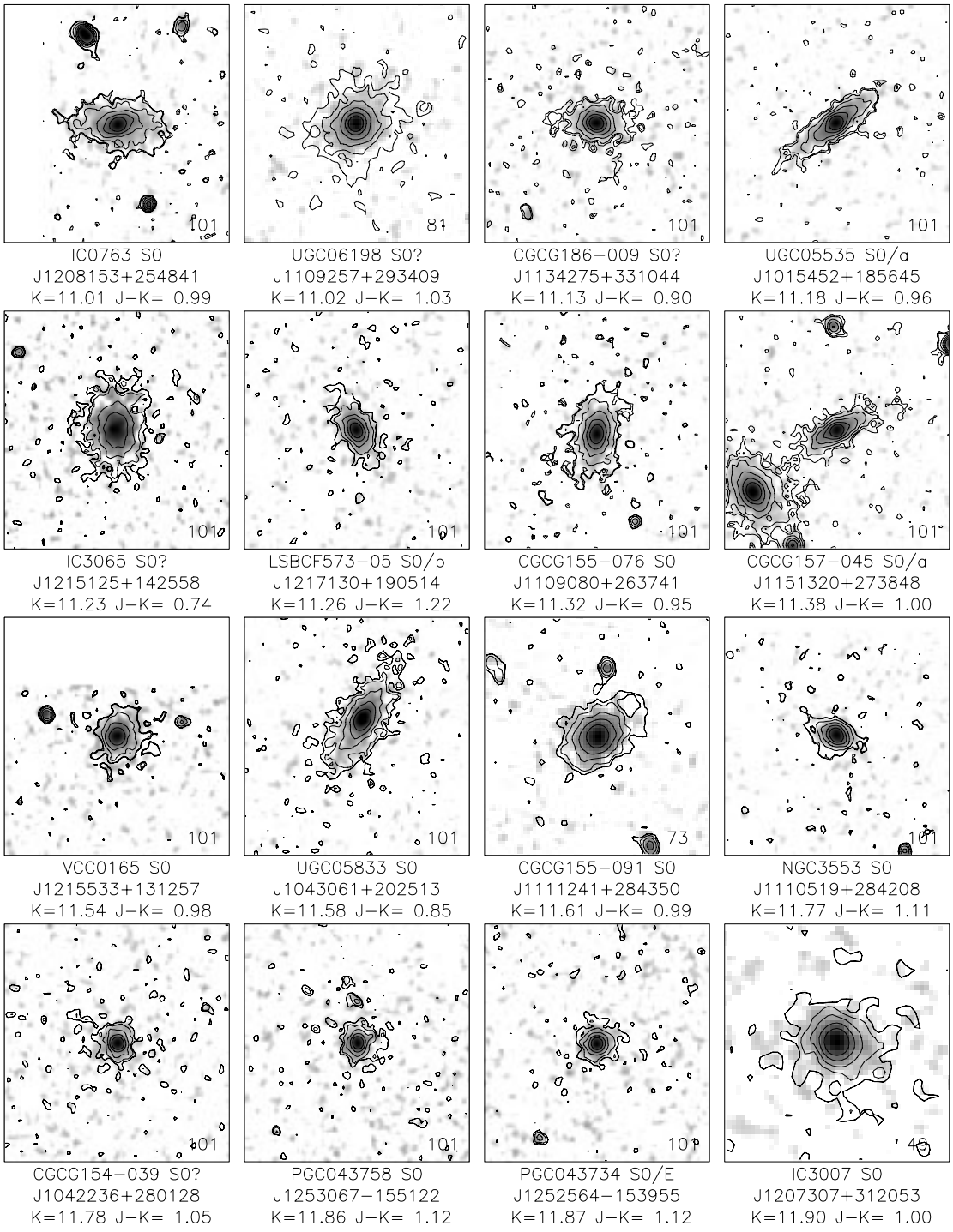
IC0763 S0
J1208153+254841
K=11.01 J−K= 0.99
UGC06198 S0?
J1109257+293409
K=11.02 J−K= 1.03
CGCG186−009 S0?
J1134275+331044
K=11.13 J−K= 0.90
UGC05535 S0/a
J1015452+185645
K=11.18 J−K= 0.96
IC3065 S0?
J1215125+142558
K=11.23 J−K= 0.74
LSBCF573−05 S0/p
J1217130+190514
K=11.26 J−K= 1.22
CGCG155−076 S0
J1109080+263741
K=11.32 J−K= 0.95
CGCG157−045 S0/a
J1151320+273848
K=11.38 J−K= 1.00
VCC0165 S0
J1215533+131257
K=11.54 J−K= 0.98
UGC05833 S0
J1043061+202513
K=11.58 J−K= 0.85
CGCG155−091 S0
J1111241+284350
K=11.61 J−K= 0.99
NGC3553 S0
J1110519+284208
K=11.77 J−K= 1.11
CGCG154−039 S0?
J1042236+280128
K=11.78 J−K= 1.05
PGC043758 S0
J1253067−155122
K=11.86 J−K= 1.12
PGC043734 S0/E
J1252564−153955
K=11.87 J−K= 1.12
IC3007 S0
J1207307+312053
K=11.90 J−K= 1.00

FIG. 20*j*

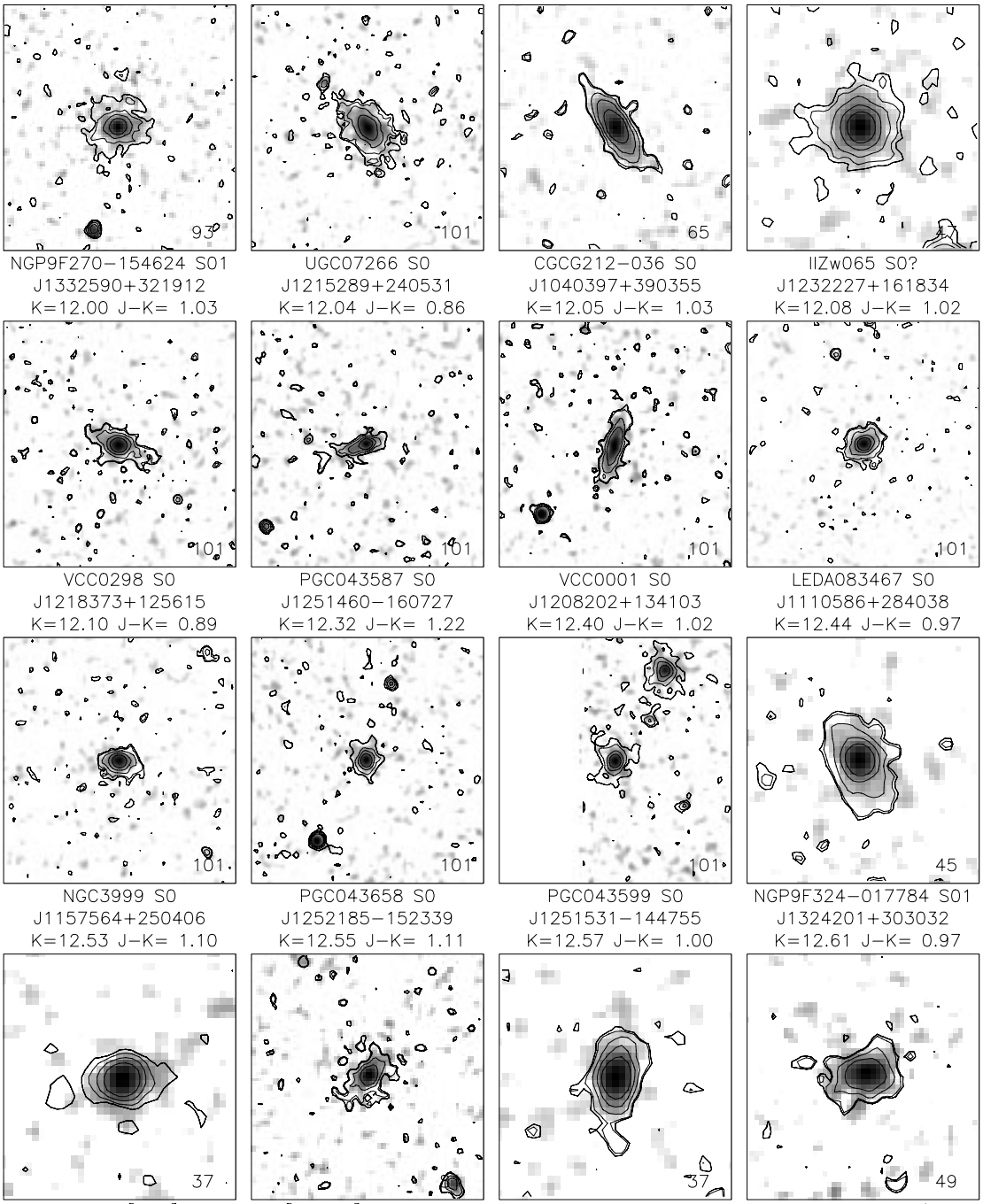
93
NGP9F270−154624 S01
J1332590+321912
K=12.00 J−K= 1.03
101
UGC07266 S0
J1215289+240531
K=12.04 J−K= 0.86
65
CGCG212−036 S0
J1040397+390355
K=12.05 J−K= 1.03
IIZw065 S0?
J1232227+161834
K=12.08 J−K= 1.02
101
VCC0298 S0
J1218373+125615
K=12.10 J−K= 0.89
101
PGC043587 S0
J1251460−160727
K=12.32 J−K= 1.22
101
VCC0001 S0
J1208202+134103
K=12.40 J−K= 1.02
101
LEDA083467 S0
J1110586+284038
K=12.44 J−K= 0.97
101
NGC3999 S0
J1157564+250406
K=12.53 J−K= 1.10
101
PGC043658 S0
J1252185−152339
K=12.55 J−K= 1.11
101
PGC043599 S0
J1251531−144755
K=12.57 J−K= 1.00
45
NGP9F324−017784 S01
J1324201+303032
K=12.61 J−K= 0.97
37
ABELL1631[D80] S0
J1252301−151028
K=12.62 J−K= 1.24
[SMB88]0507 S01
J1324409+310134
K=12.77 J−K= 1.07
37
LEDA083469 S0
J1111341+284517
K=12.98 J−K= 0.99
49
UGC06684 S0/a
J1143326+312728
K=12.98 J−K= 0.88

FIG. 20*k*

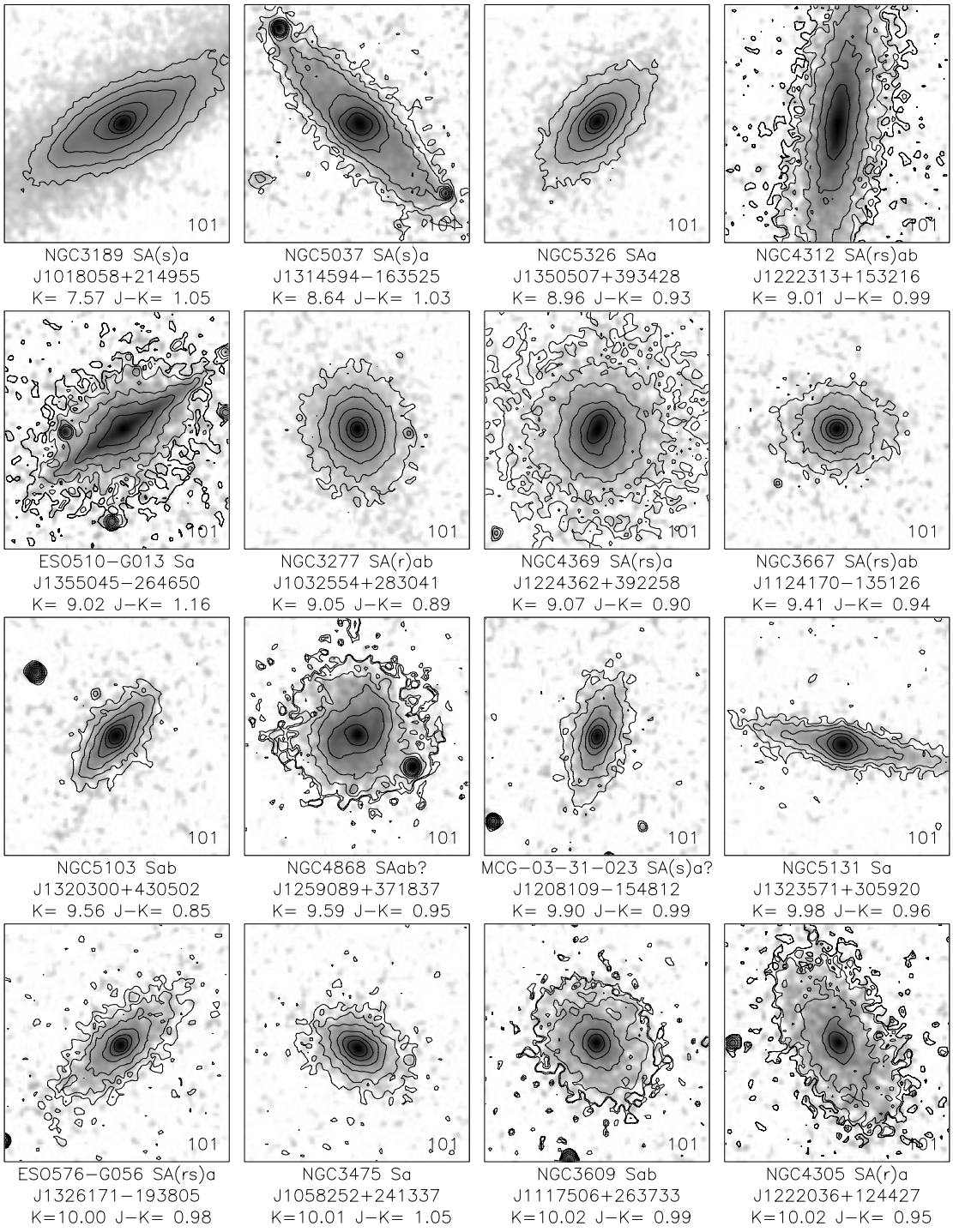
NGC3189 SA(s)a
J1018058+214955
K= 7.57 J−K= 1.05
NGC5037 SA(s)a
J1314594−163525
K= 8.64 J−K= 1.03
NGC5326 SAa
J1350507+393428
K= 8.96 J−K= 0.93
NGC4312 SA(rs)ab
J1222313+153216
K= 9.01 J−K= 0.99
ESO510−G013 Sa
J1355045−264650
K= 9.02 J−K= 1.16
NGC3277 SA(r)ab
J1032554+283041
K= 9.05 J−K= 0.89
NGC4369 SA(rs)a
J1224362+392258
K= 9.07 J−K= 0.90
NGC3667 SA(rs)ab
J1124170−135126
K= 9.41 J−K= 0.94
NGC5103 Sab
J1320300+430502
K= 9.56 J−K= 0.85
NGC4868 SAab?
J1259089+371837
K= 9.59 J−K= 0.95
MCG−03−31−023 SA(s)a?
J1208109−154812
K= 9.90 J−K= 0.99
NGC5131 Sa
J1323571+305920
K= 9.98 J−K= 0.96
ESO576−G056 SA(rs)a
J1326171−193805
K=10.00 J−K= 0.98
NGC3475 Sa
J1058252+241337
K=10.01 J−K= 1.05
NGC3609 Sab
J1117506+263733
K=10.02 J−K= 0.99
NGC4305 SA(r)a
J1222036+124427
K=10.02 J−K= 0.95

FIG. 20*l*

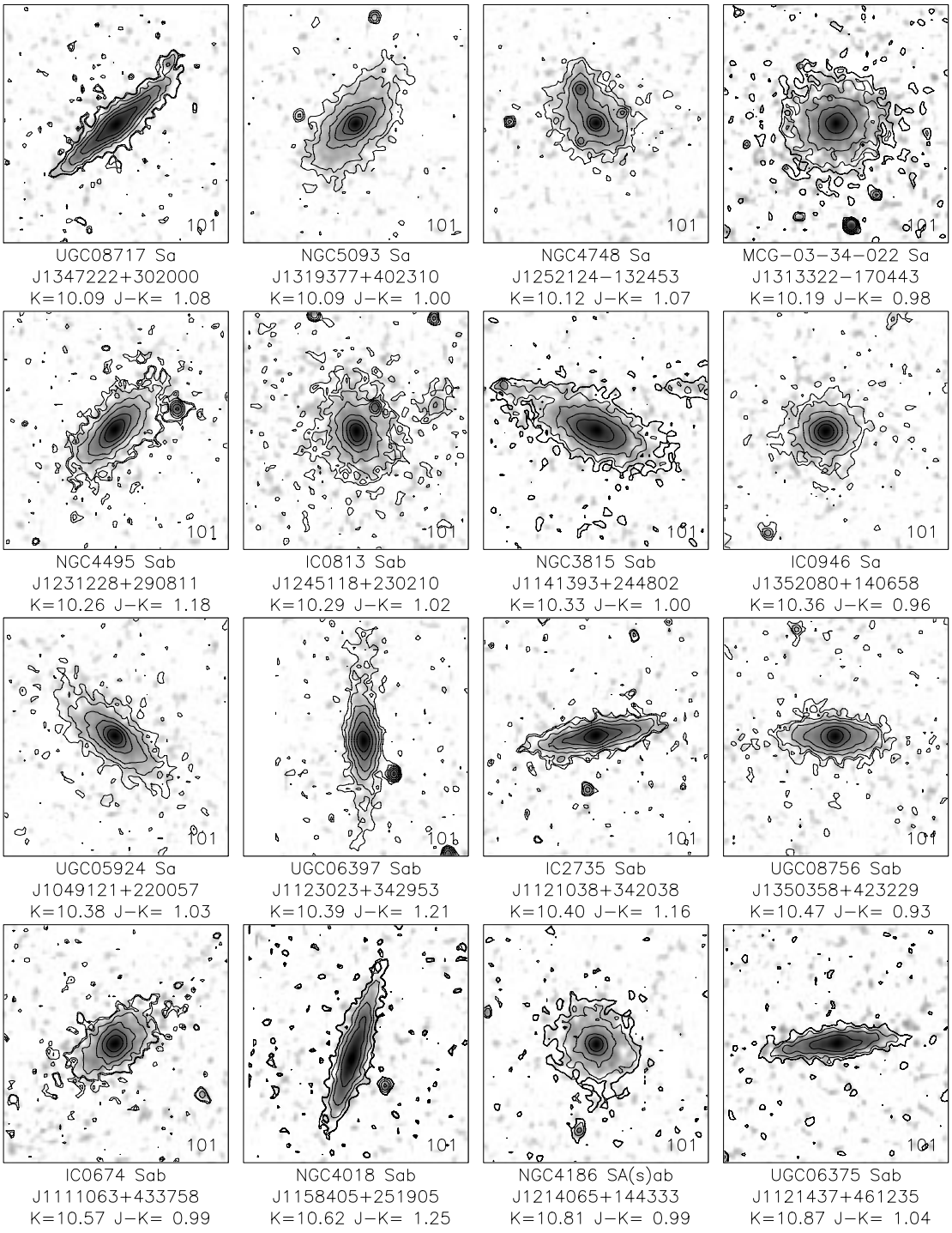
UGC08717 Sa
J1347222+302000
K=10.09 J−K= 1.08
NGC5093 Sa
J1319377+402310
K=10.09 J−K= 1.00
NGC4748 Sa
J1252124−132453
K=10.12 J−K= 1.07
MCG−03−34−022 Sa
J1313322−170443
K=10.19 J−K= 0.98
NGC4495 Sab
J1231228+290811
K=10.26 J−K= 1.18
IC0813 Sab
J1245118+230210
K=10.29 J−K= 1.02
NGC3815 Sab
J1141393+244802
K=10.33 J−K= 1.00
IC0946 Sa
J1352080+140658
K=10.36 J−K= 0.96
UGC05924 Sa
J1049121+220057
K=10.38 J−K= 1.03
UGC06397 Sab
J1123023+342953
K=10.39 J−K= 1.21
IC2735 Sab
J1121038+342038
K=10.40 J−K= 1.16
UGC08756 Sab
J1350358+423229
K=10.47 J−K= 0.93
IC0674 Sab
J1111063+433758
K=10.57 J−K= 0.99
NGC4018 Sab
J1158405+251905
K=10.62 J−K= 1.25
NGC4186 SA(s)ab
J1214065+144333
K=10.81 J−K= 0.99
UGC06375 Sab
J1121437+461235
K=10.87 J−K= 1.04

FIG. 20*m*

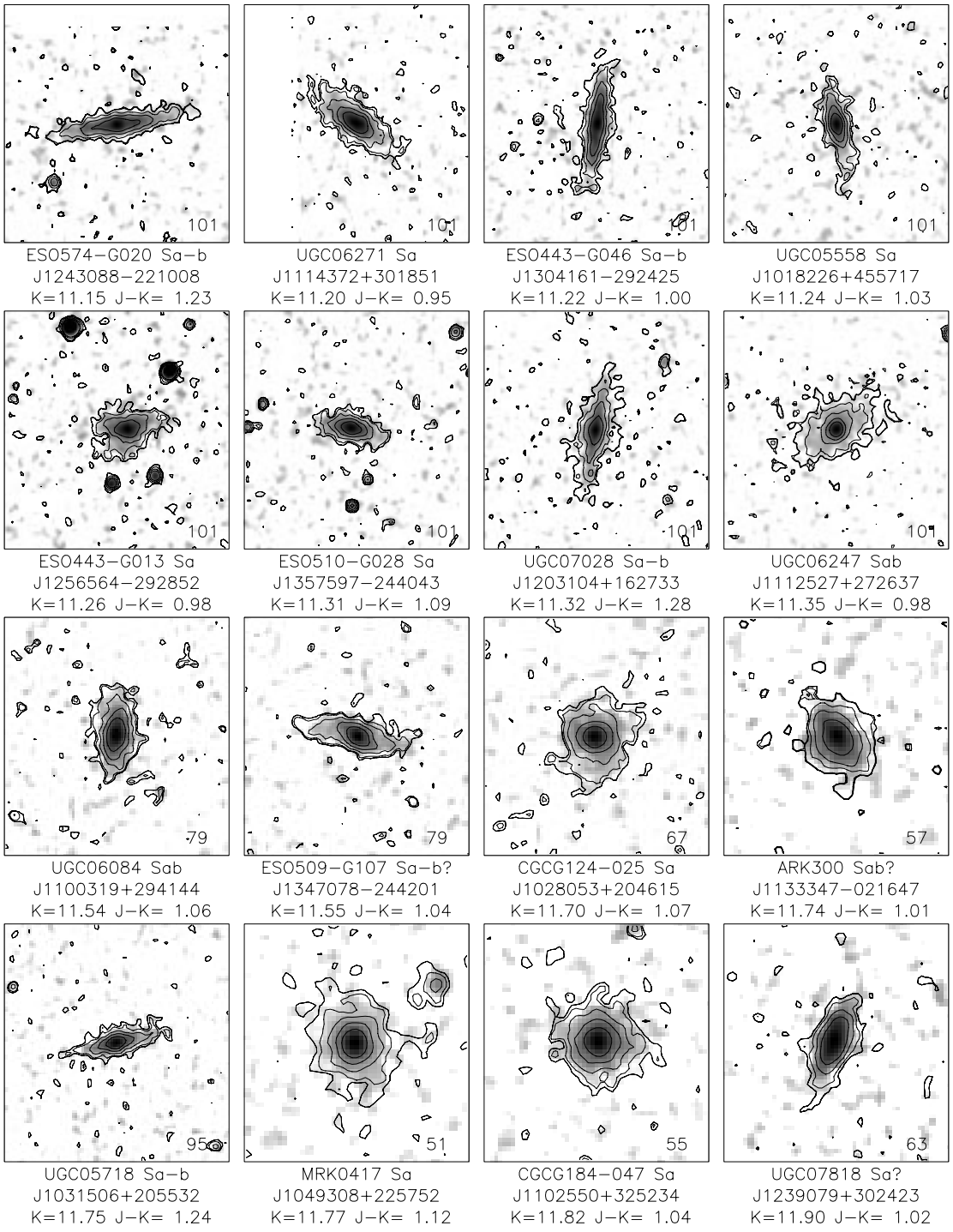
101
ESO574−G020 Sa−b
J1243088−221008
K=11.15 J−K= 1.23
101
UGC06271 Sa
J1114372+301851
K=11.20 J−K= 0.95
101
ESO443−G046 Sa−b
J1304161−292425
K=11.22 J−K= 1.00
101
UGC05558 Sa
J1018226+455717
K=11.24 J−K= 1.03
101
ESO443−G013 Sa
J1256564−292852
K=11.26 J−K= 0.98
101
ESO510−G028 Sa
J1357597−244043
K=11.31 J−K= 1.09
101
UGC07028 Sa−b
J1203104+162733
K=11.32 J−K= 1.28
101
UGC06247 Sab
J1112527+272637
K=11.35 J−K= 0.98
79
UGC06084 Sab
J1100319+294144
K=11.54 J−K= 1.06
79
ESO509−G107 Sa−b?
J1347078−244201
K=11.55 J−K= 1.04
67
CGCG124−025 Sa
J1028053+204615
K=11.70 J−K= 1.07
57
ARK300 Sab?
J1133347−021647
K=11.74 J−K= 1.01
95
UGC05718 Sa−b
J1031506+205532
K=11.75 J−K= 1.24
51
MRK0417 Sa
J1049308+225752
K=11.77 J−K= 1.12
55
CGCG184−047 Sa
J1102550+325234
K=11.82 J−K= 1.04
63
UGC07818 Sa?
J1239079+302423
K=11.90 J−K= 1.02

FIG. 20*n*

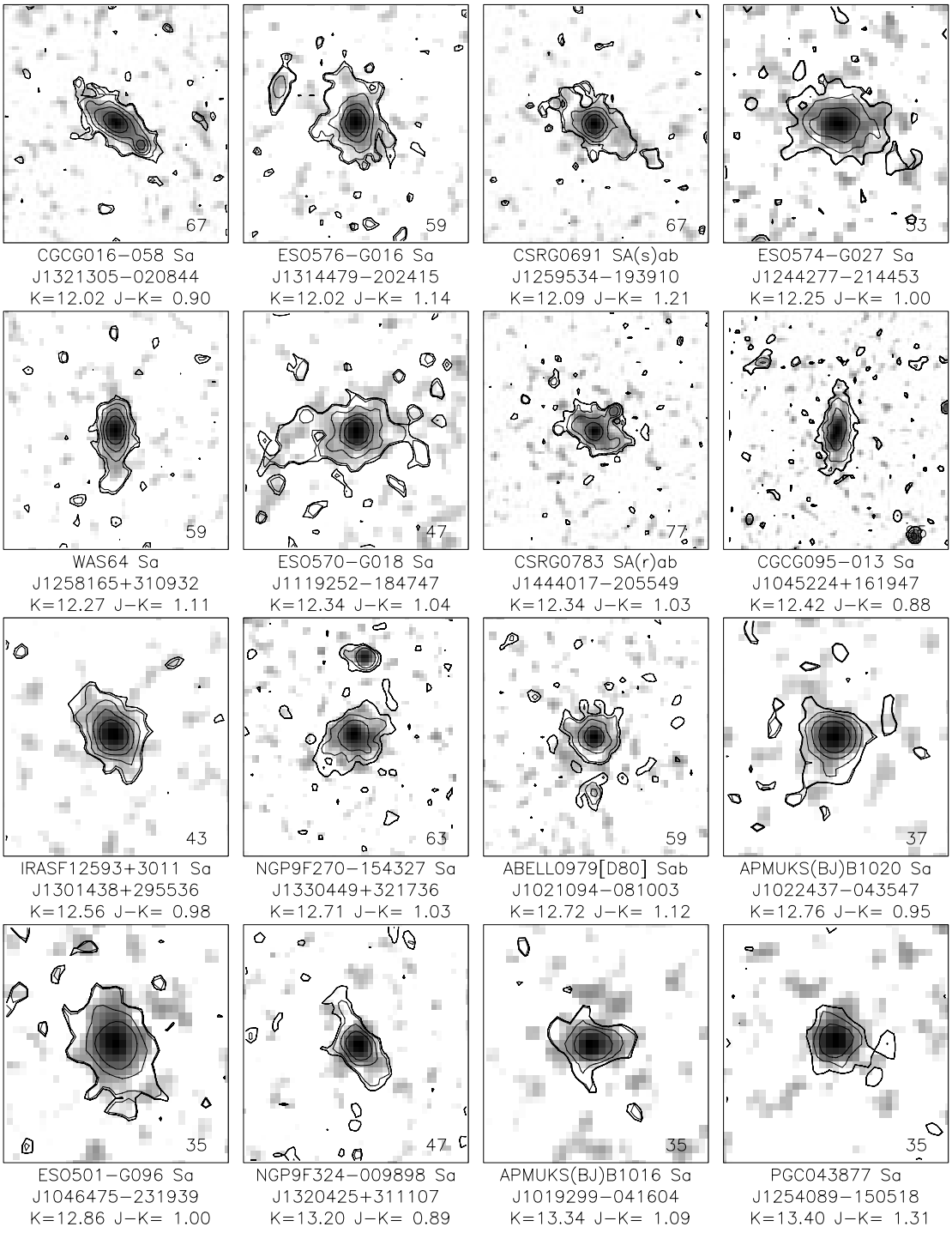
67
CGCG016−058 Sa
J1321305−020844
K=12.02 J−K= 0.90
59
ESO576−G016 Sa
J1314479−202415
K=12.02 J−K= 1.14
67
CSRG0691 SA(s)ab
J1259534−193910
K=12.09 J−K= 1.21
93
ESO574−G027 Sa
J1244277−214453
K=12.25 J−K= 1.00
59
WAS64 Sa
J1258165+310932
K=12.27 J−K= 1.11
47
ESO570−G018 Sa
J1119252−184747
K=12.34 J−K= 1.04
77
CSRG0783 SA(r)ab
J1444017−205549
K=12.34 J−K= 1.03
CGCG095−013 Sa
J1045224+161947
K=12.42 J−K= 0.88
43
IRASF12593+3011 Sa
J1301438+295536
K=12.56 J−K= 0.98
63
NGP9F270−154327 Sa
J1330449+321736
K=12.71 J−K= 1.03
59
ABELL0979[D80] Sab
J1021094−081003
K=12.72 J−K= 1.12
37
APMUKS(BJ)B1020 Sa
J1022437−043547
K=12.76 J−K= 0.95
35
ESO501−G096 Sa
J1046475−231939
K=12.86 J−K= 1.00
47
NGP9F324−009898 Sa
J1320425+311107
K=13.20 J−K= 0.89
35
APMUKS(BJ)B1016 Sa
J1019299−041604
K=13.34 J−K= 1.09
35
PGC043877 Sa
J1254089−150518
K=13.40 J−K= 1.31

FIG. 20*o*

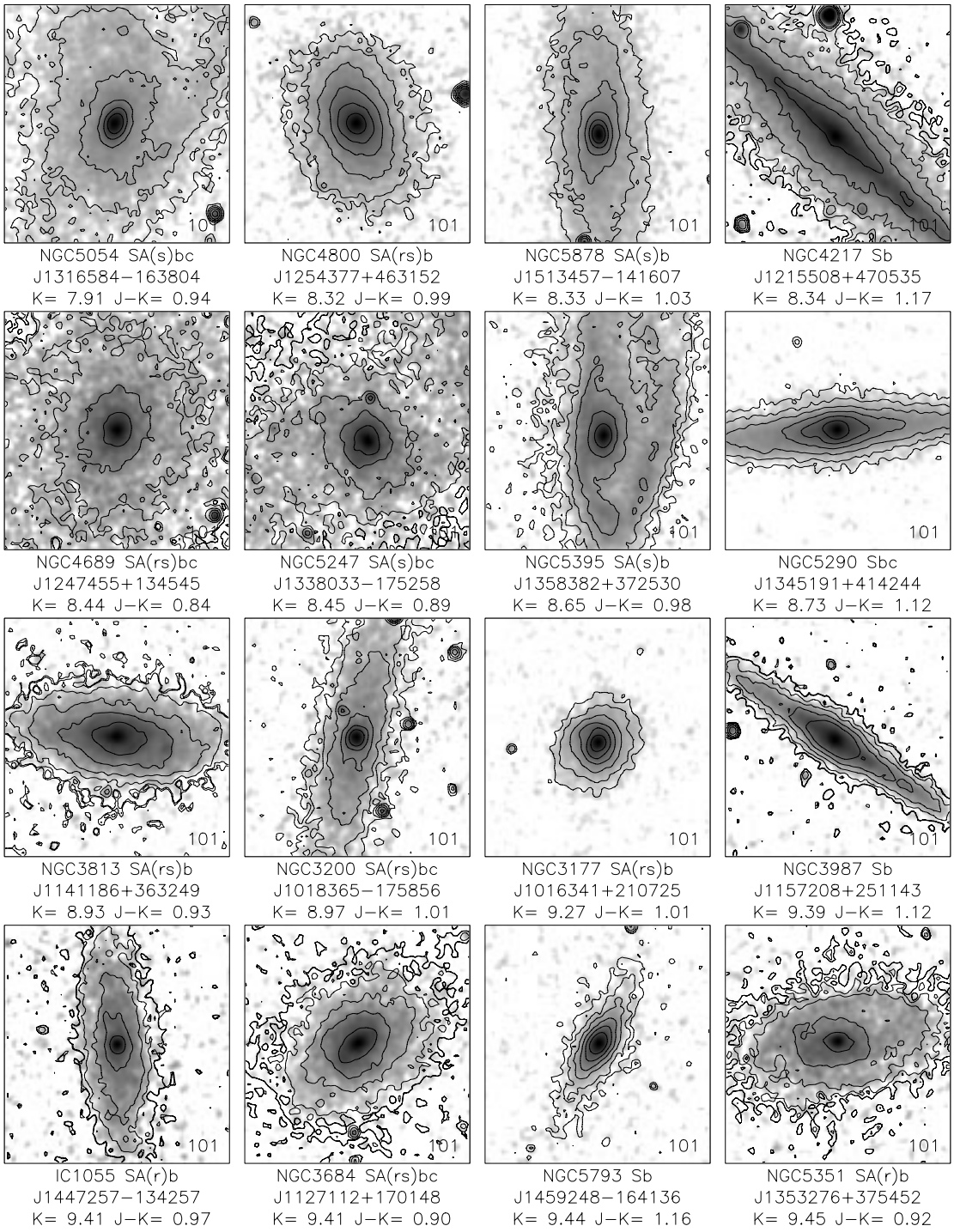
NGC5054 SA(s)bc
J1316584−163804
K= 7.91 J−K= 0.94
NGC4800 SA(rs)b
J1254377+463152
K= 8.32 J−K= 0.99
NGC5878 SA(s)b
J1513457−141607
K= 8.33 J−K= 1.03
NGC4217 Sb
J1215508+470535
K= 8.34 J−K= 1.17
NGC4689 SA(rs)bc
J1247455+134545
K= 8.44 J−K= 0.84
NGC5247 SA(s)bc
J1338033−175258
K= 8.45 J−K= 0.89
NGC5395 SA(s)b
J1358382+372530
K= 8.65 J−K= 0.98
NGC5290 Sbc
J1345191+414244
K= 8.73 J−K= 1.12
NGC3813 SA(rs)b
J1141186+363249
K= 8.93 J−K= 0.93
NGC3200 SA(rs)bc
J1018365−175856
K= 8.97 J−K= 1.01
NGC3177 SA(rs)b
J1016341+210725
K= 9.27 J−K= 1.01
NGC3987 Sb
J1157208+251143
K= 9.39 J−K= 1.12
IC1055 SA(r)b
J1447257−134257
K= 9.41 J−K= 0.97
NGC3684 SA(rs)bc
J1127112+170148
K= 9.41 J−K= 0.90
NGC5793 Sb
J1459248−164136
K= 9.44 J−K= 1.16
NGC5351 SA(r)b
J1353276+375452
K= 9.45 J−K= 0.92

FIG. 20*p*

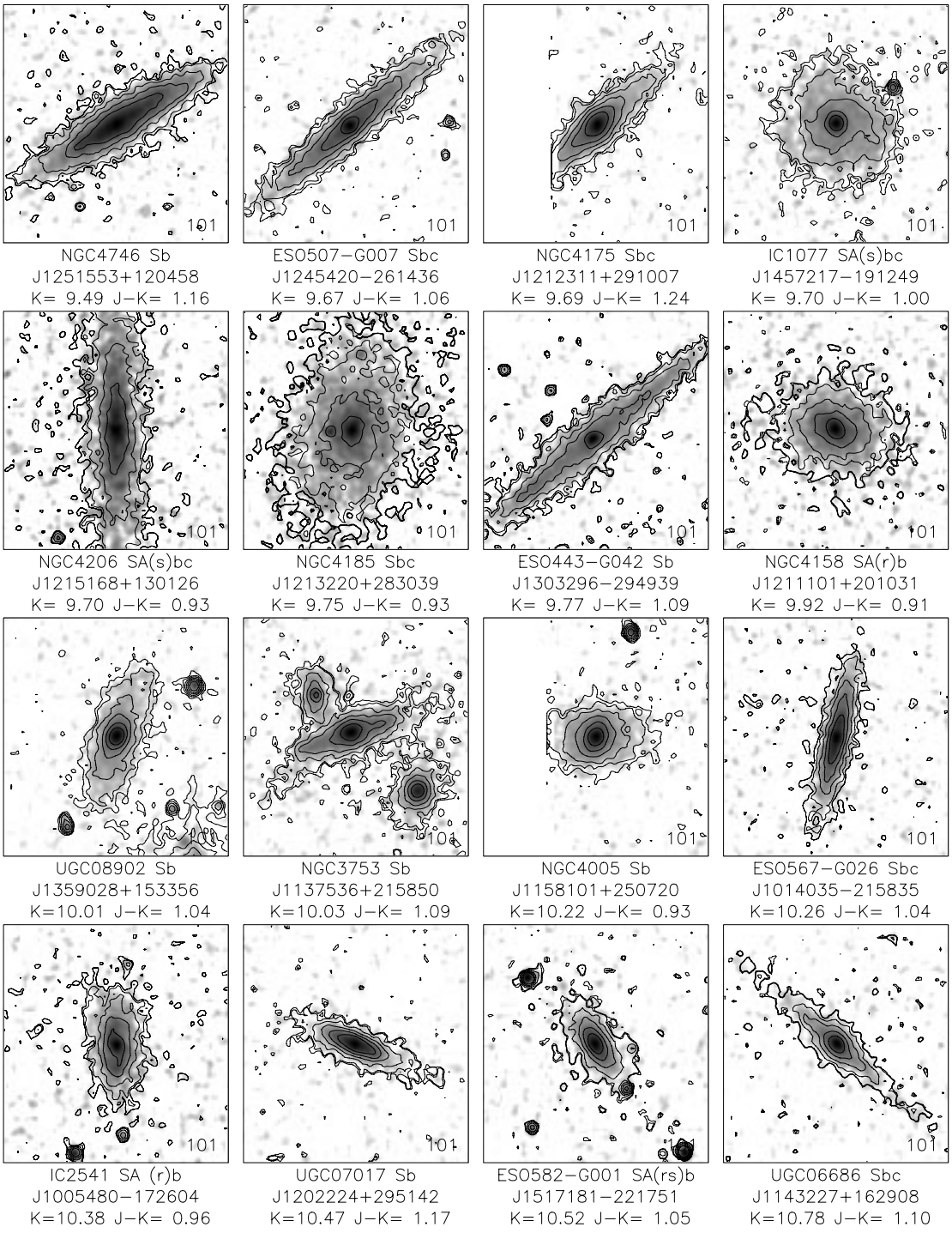
NGC4746 Sb
J1251553+120458
K= 9.49 J−K= 1.16
ESO507−G007 Sbc
J1245420−261436
K= 9.67 J−K= 1.06
NGC4175 Sbc
J1212311+291007
K= 9.69 J−K= 1.24
IC1077 SA(s)bc
J1457217−191249
K= 9.70 J−K= 1.00
NGC4206 SA(s)bc
J1215168+130126
K= 9.70 J−K= 0.93
NGC4185 Sbc
J1213220+283039
K= 9.75 J−K= 0.93
ESO443−G042 Sb
J1303296−294939
K= 9.77 J−K= 1.09
NGC4158 SA(r)b
J1211101+201031
K= 9.92 J−K= 0.91
UGC08902 Sb
J1359028+153356
K=10.01 J−K= 1.04
NGC3753 Sb
J1137536+215850
K=10.03 J−K= 1.09
NGC4005 Sb
J1158101+250720
K=10.22 J−K= 0.93
ESO567−G026 Sbc
J1014035−215835
K=10.26 J−K= 1.04
IC2541 SA (r)b
J1005480−172604
K=10.38 J−K= 0.96
UGC07017 Sb
J1202224+295142
K=10.47 J−K= 1.17
ESO582−G001 SA(rs)b
J1517181−221751
K=10.52 J−K= 1.05
UGC06686 Sbc
J1143227+162908
K=10.78 J−K= 1.10

FIG. 20*q*

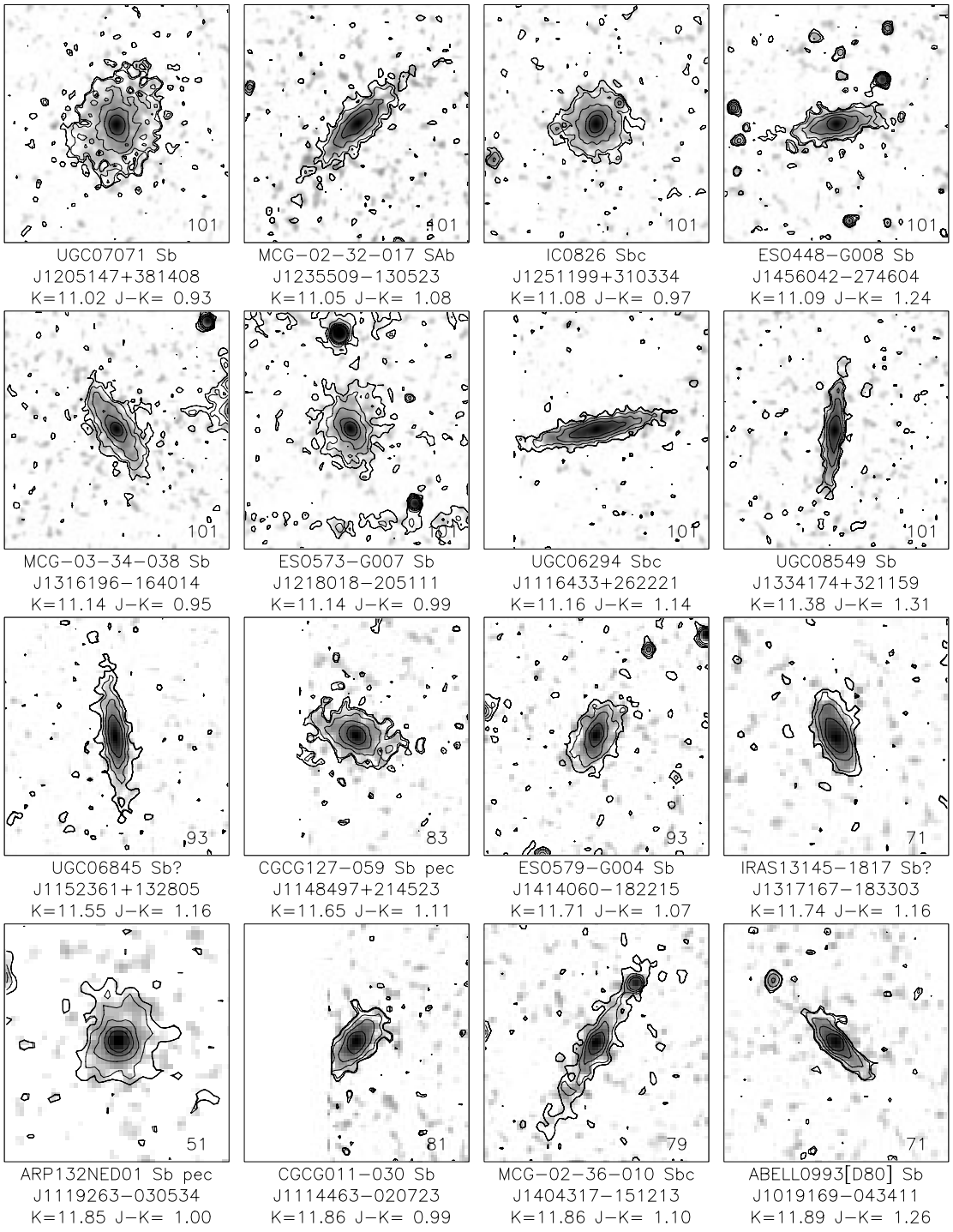
101
UGC07071 Sb
J1205147+381408
K=11.02 J−K= 0.93
101
MCG−02−32−017 SAb
J1235509−130523
K=11.05 J−K= 1.08
101
IC0826 Sbc
J1251199+310334
K=11.08 J−K= 0.97
101
ESO448−G008 Sb
J1456042−274604
K=11.09 J−K= 1.24
101
MCG−03−34−038 Sb
J1316196−164014
K=11.14 J−K= 0.95
101
ESO573−G007 Sb
J1218018−205111
K=11.14 J−K= 0.99
101
UGC06294 Sbc
J1116433+262221
K=11.16 J−K= 1.14
101
UGC08549 Sb
J1334174+321159
K=11.38 J−K= 1.31
93
UGC06845 Sb?
J1152361+132805
K=11.55 J−K= 1.16
83
CGCG127−059 Sb pec
J1148497+214523
K=11.65 J−K= 1.11
93
ESO579−G004 Sb
J1414060−182215
K=11.71 J−K= 1.07
71
IRAS13145−1817 Sb?
J1317167−183303
K=11.74 J−K= 1.16
51
ARP132NED01 Sb pec
J1119263−030534
K=11.85 J−K= 1.00
81
CGCG011−030 Sb
J1114463−020723
K=11.86 J−K= 0.99
79
MCG−02−36−010 Sbc
J1404317−151213
K=11.86 J−K= 1.10
71
ABELL0993[D80] Sb
J1019169−043411
K=11.89 J−K= 1.26

FIG. 20*r*

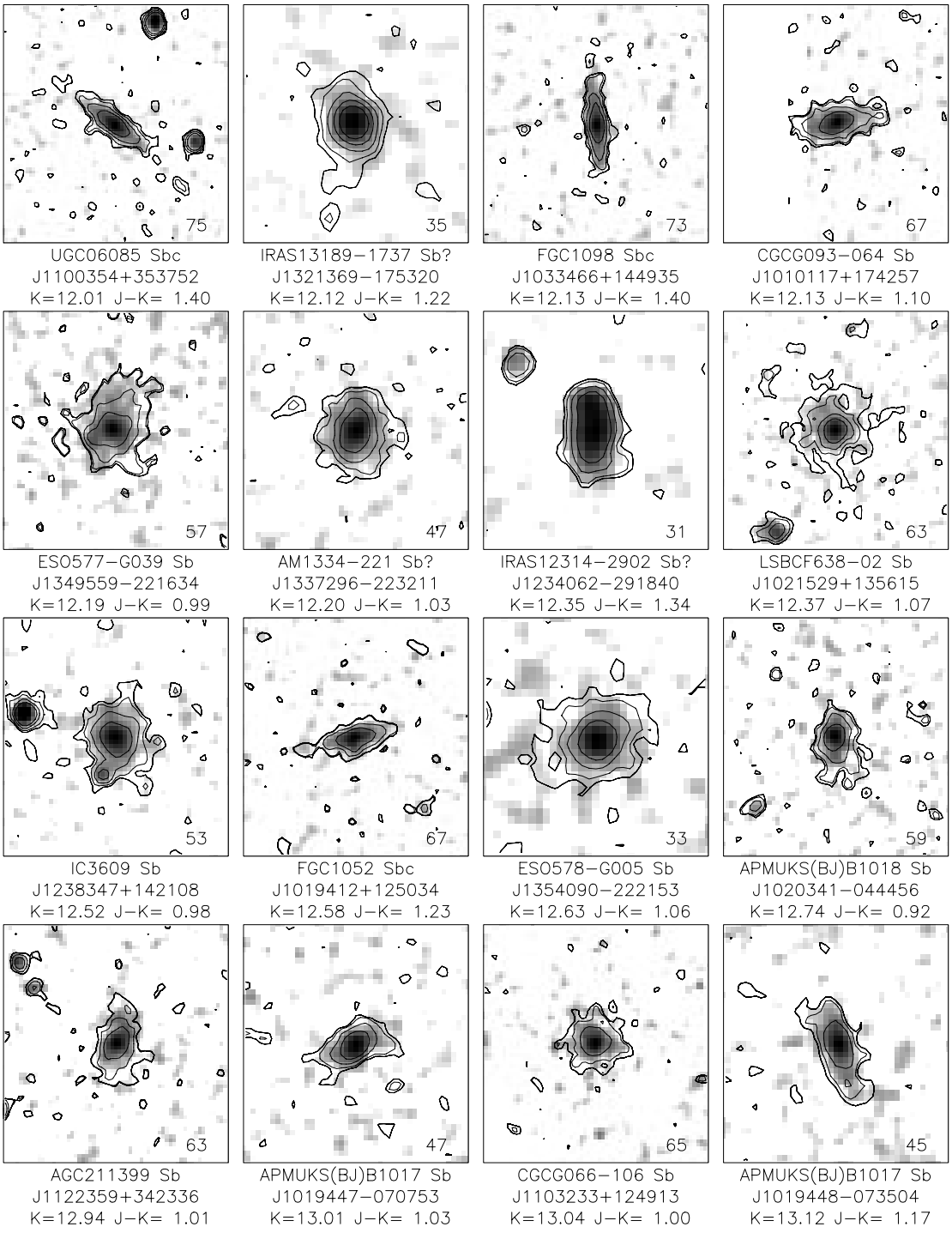
75
UGC06085 Sbc
J1100354+353752
K=12.01 J−K= 1.40
35
IRAS13189−1737 Sb?
J1321369−175320
K=12.12 J−K= 1.22
73
FGC1098 Sbc
J1033466+144935
K=12.13 J−K= 1.40
67
CGCG093−064 Sb
J1010117+174257
K=12.13 J−K= 1.10
57
ESO577−G039 Sb
J1349559−221634
K=12.19 J−K= 0.99
47
AM1334−221 Sb?
J1337296−223211
K=12.20 J−K= 1.03
31
IRAS12314−2902 Sb?
J1234062−291840
K=12.35 J−K= 1.34
63
LSBCF638−02 Sb
J1021529+135615
K=12.37 J−K= 1.07
53
IC3609 Sb
J1238347+142108
K=12.52 J−K= 0.98
67
FGC1052 Sbc
J1019412+125034
K=12.58 J−K= 1.23
33
ESO578−G005 Sb
J1354090−222153
K=12.63 J−K= 1.06
59
APMUKS(BJ)B1018 Sb
J1020341−044456
K=12.74 J−K= 0.92
63
AGC211399 Sb
J1122359+342336
K=12.94 J−K= 1.01
47
APMUKS(BJ)B1017 Sb
J1019447−070753
K=13.01 J−K= 1.03
65
CGCG066−106 Sb
J1103233+124913
K=13.04 J−K= 1.00
45
APMUKS(BJ)B1017 Sb
J1019448−073504
K=13.12 J−K= 1.17

FIG. 20*s*

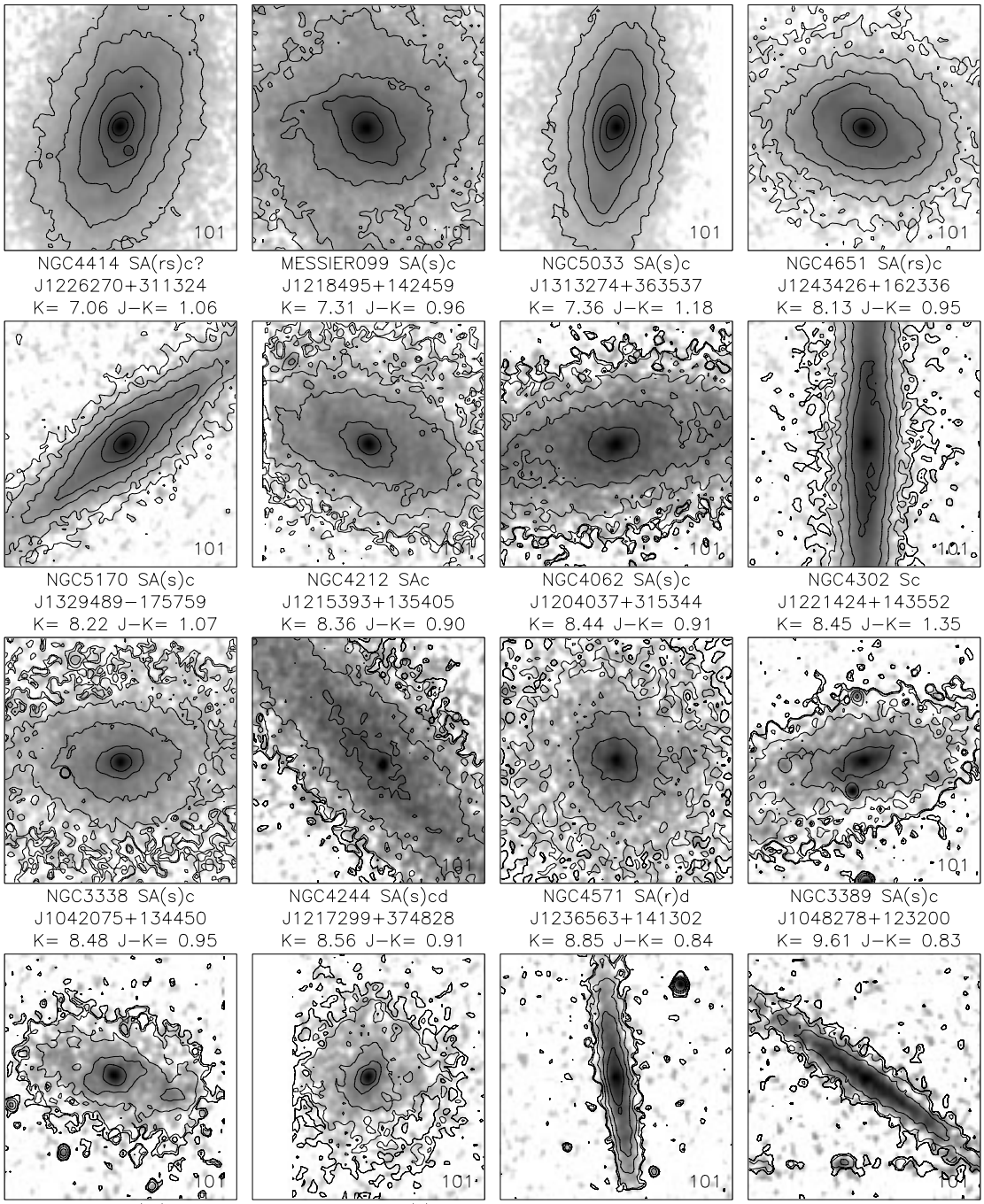
NGC4414 SA(rs)c?
J1226270+311324
K= 7.06 J−K= 1.06
MESSIER099 SA(s)c
J1218495+142459
K= 7.31 J−K= 0.96
NGC5033 SA(s)c
J1313274+363537
K= 7.36 J−K= 1.18
NGC4651 SA(rs)c
J1243426+162336
K= 8.13 J−K= 0.95
NGC5170 SA(s)c
J1329489−175759
K= 8.22 J−K= 1.07
NGC4212 SAc
J1215393+135405
K= 8.36 J−K= 0.90
NGC4062 SA(s)c
J1204037+315344
K= 8.44 J−K= 0.91
NGC4302 Sc
J1221424+143552
K= 8.45 J−K= 1.35
NGC3338 SA(s)c
J1042075+134450
K= 8.48 J−K= 0.95
NGC4244 SA(s)cd
J1217299+374828
K= 8.56 J−K= 0.91
NGC4571 SA(r)d
J1236563+141302
K= 8.85 J−K= 0.84
NGC3389 SA(s)c
J1048278+123200
K= 9.61 J−K= 0.83
NGC4177 SA(rs)c pec
J1212410−140053
K= 9.80 J−K= 0.90
NGC5230 SA(s)c
J1335318+134034
K= 9.91 J−K= 0.91
MCG−03−30−003 Scd
J1137594−171400
K= 9.96 J−K= 1.13
NGC4222 Sc
J1216226+131826
K=10.15 J−K= 1.07

FIG. 20*t*

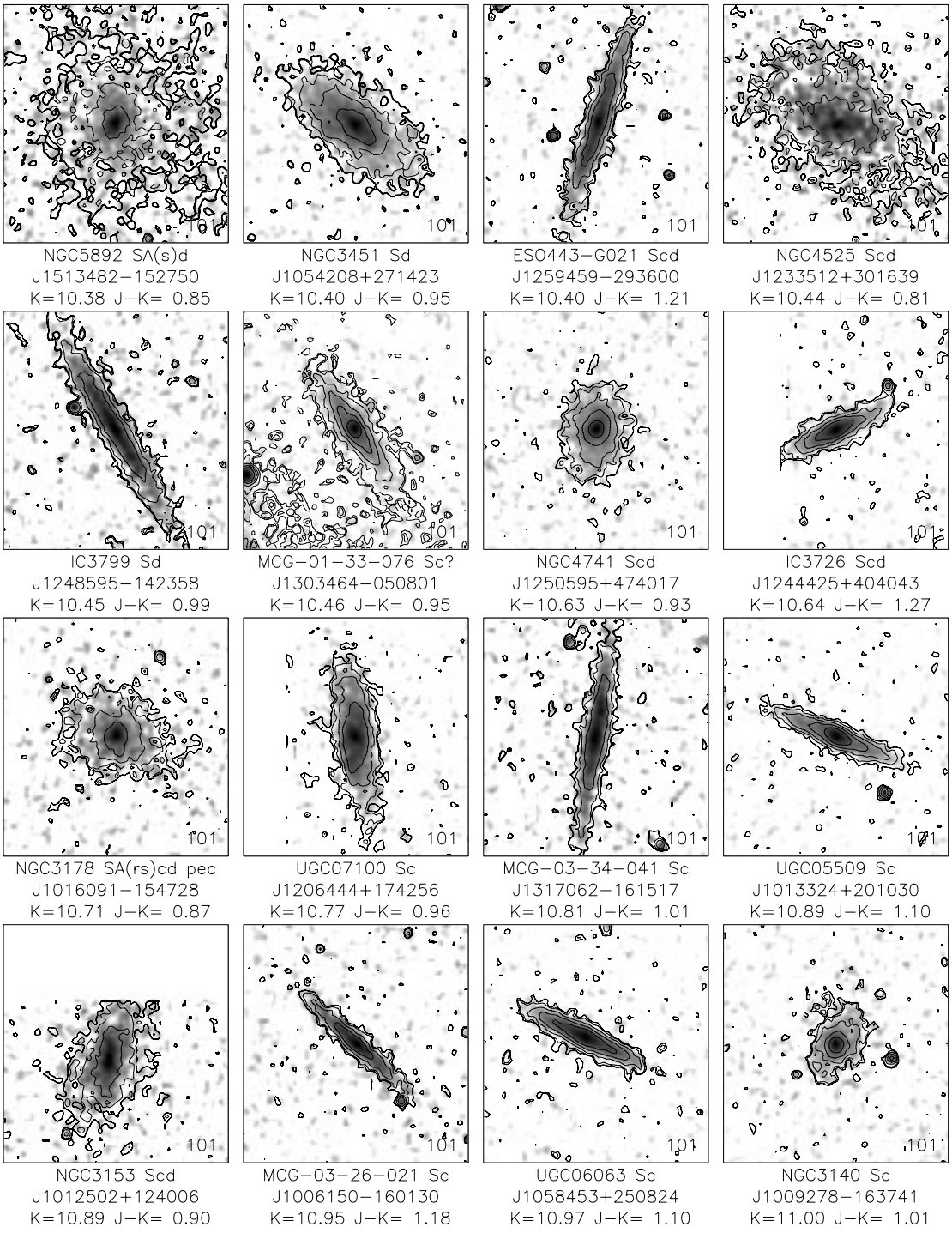
NGC5892 SA(s)d
J1513482−152750
K=10.38 J−K= 0.85
NGC3451 Sd
J1054208+271423
K=10.40 J−K= 0.95
ESO443−G021 Scd
J1259459−293600
K=10.40 J−K= 1.21
NGC4525 Scd
J1233512+301639
K=10.44 J−K= 0.81
IC3799 Sd
J1248595−142358
K=10.45 J−K= 0.99
MCG−01−33−076 Sc?
J1303464−050801
K=10.46 J−K= 0.95
NGC4741 Scd
J1250595+474017
K=10.63 J−K= 0.93
IC3726 Scd
J1244425+404043
K=10.64 J−K= 1.27
NGC3178 SA(rs)cd pec
J1016091−154728
K=10.71 J−K= 0.87
UGC07100 Sc
J1206444+174256
K=10.77 J−K= 0.96
MCG−03−34−041 Sc
J1317062−161517
K=10.81 J−K= 1.01
UGC05509 Sc
J1013324+201030
K=10.89 J−K= 1.10
NGC3153 Scd
J1012502+124006
K=10.89 J−K= 0.90
MCG−03−26−021 Sc
J1006150−160130
K=10.95 J−K= 1.18
UGC06063 Sc
J1058453+250824
K=10.97 J−K= 1.10
NGC3140 Sc
J1009278−163741
K=11.00 J−K= 1.01

FIG. 20*u*

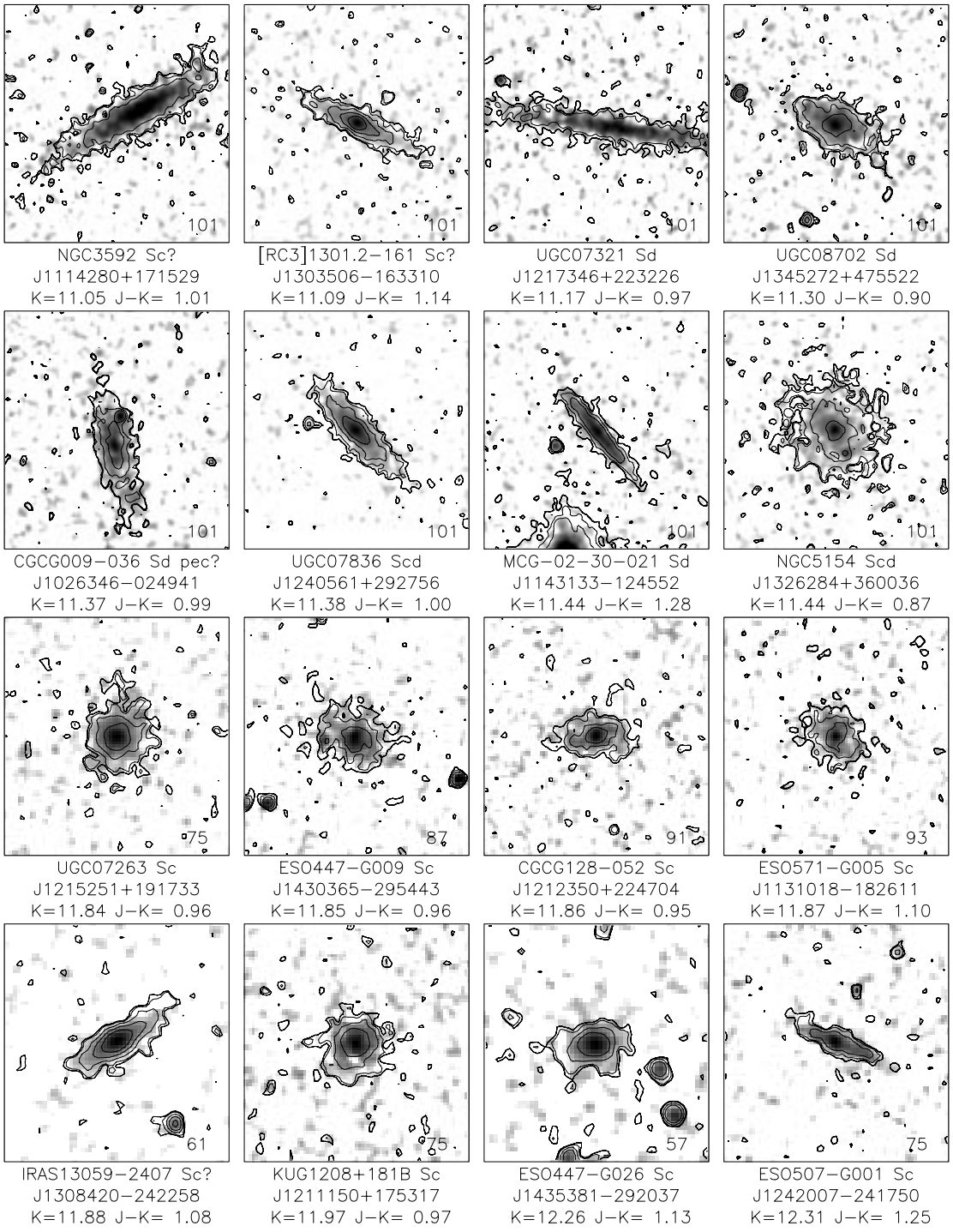
101
NGC3592 Sc?
J1114280+171529
K=11.05 J−K= 1.01
101
[RC3]1301.2−161 Sc?
J1303506−163310
K=11.09 J−K= 1.14
101
UGC07321 Sd
J1217346+223226
K=11.17 J−K= 0.97
101
UGC08702 Sd
J1345272+475522
K=11.30 J−K= 0.90
101
CGCG009−036 Sd pec?
J1026346−024941
K=11.37 J−K= 0.99
101
UGC07836 Scd
J1240561+292756
K=11.38 J−K= 1.00
101
MCG−02−30−021 Sd
J1143133−124552
K=11.44 J−K= 1.28
101
NGC5154 Scd
J1326284+360036
K=11.44 J−K= 0.87
75
UGC07263 Sc
J1215251+191733
K=11.84 J−K= 0.96
87
ESO447−G009 Sc
J1430365−295443
K=11.85 J−K= 0.96
91
CGCG128−052 Sc
J1212350+224704
K=11.86 J−K= 0.95
93
ESO571−G005 Sc
J1131018−182611
K=11.87 J−K= 1.10
61
IRAS13059−2407 Sc?
J1308420−242258
K=11.88 J−K= 1.08
75
KUG1208+181B Sc
J1211150+175317
K=11.97 J−K= 0.97
57
ESO447−G026 Sc
J1435381−292037
K=12.26 J−K= 1.13
75
ESO507−G001 Sc
J1242007−241750
K=12.31 J−K= 1.25

FIG. 20*v*

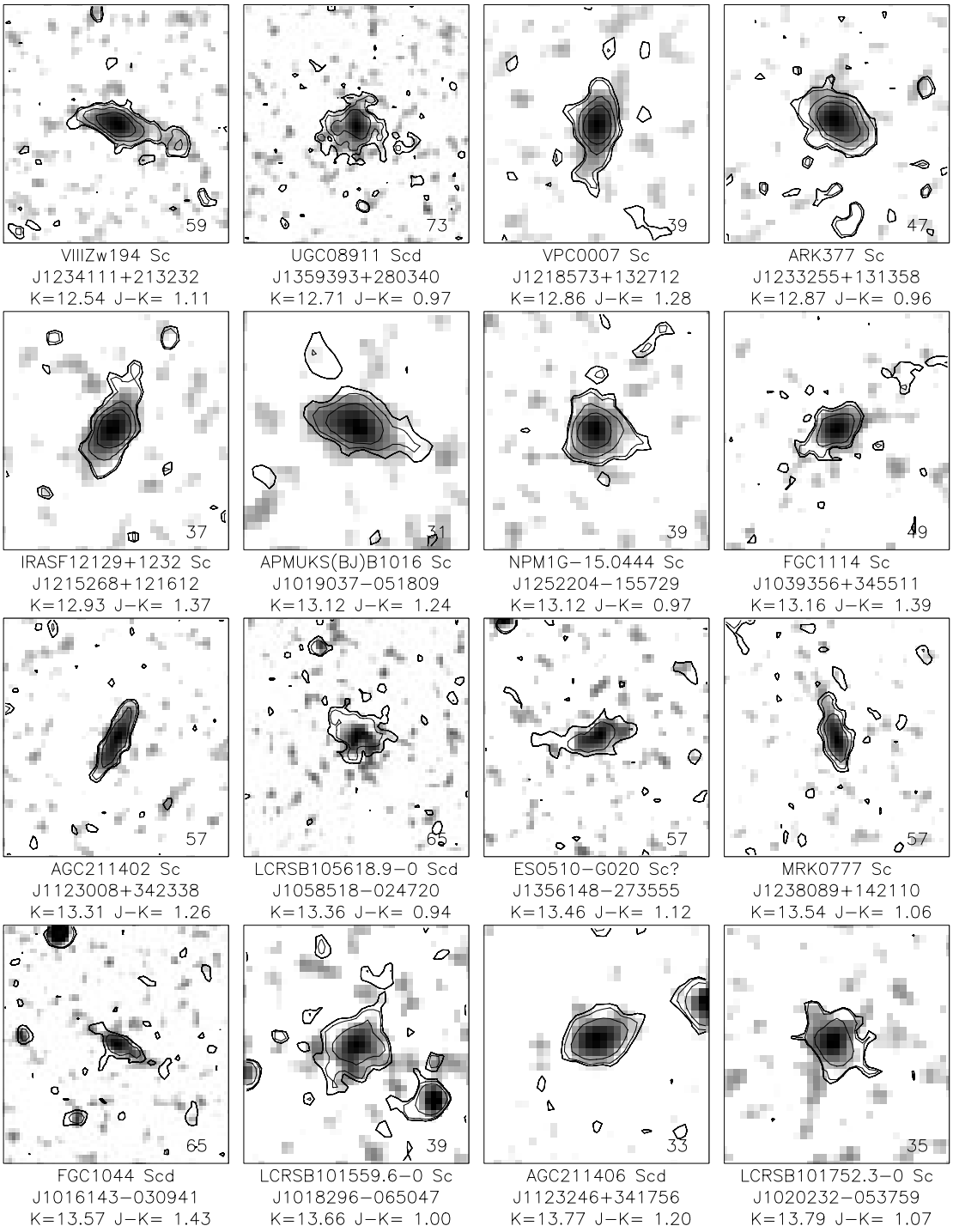
59
VIIIZw194 Sc
J1234111+213232
K=12.54 J−K= 1.11
73
UGC08911 Scd
J1359393+280340
K=12.71 J−K= 0.97
39
VPC0007 Sc
J1218573+132712
K=12.86 J−K= 1.28
47
ARK377 Sc
J1233255+131358
K=12.87 J−K= 0.96
37
IRASF12129+1232 Sc
J1215268+121612
K=12.93 J−K= 1.37
31
APMUKS(BJ)B1016 Sc
J1019037−051809
K=13.12 J−K= 1.24
39
NPM1G−15.0444 Sc
J1252204−155729
K=13.12 J−K= 0.97
49
FGC1114 Sc
J1039356+345511
K=13.16 J−K= 1.39
57
AGC211402 Sc
J1123008+342338
K=13.31 J−K= 1.26
65
LCRSB105618.9−0 Scd
J1058518−024720
K=13.36 J−K= 0.94
57
ESO510−G020 Sc?
J1356148−273555
K=13.46 J−K= 1.12
57
MRK0777 Sc
J1238089+142110
K=13.54 J−K= 1.06
65
FGC1044 Scd
J1016143−030941
K=13.57 J−K= 1.43
39
LCRSB101559.6−0 Sc
J1018296−065047
K=13.66 J−K= 1.00
33
AGC211406 Scd
J1123246+341756
K=13.77 J−K= 1.20
35
LCRSB101752.3−0 Sc
J1020232−053759
K=13.79 J−K= 1.07

FIG. 20*w*

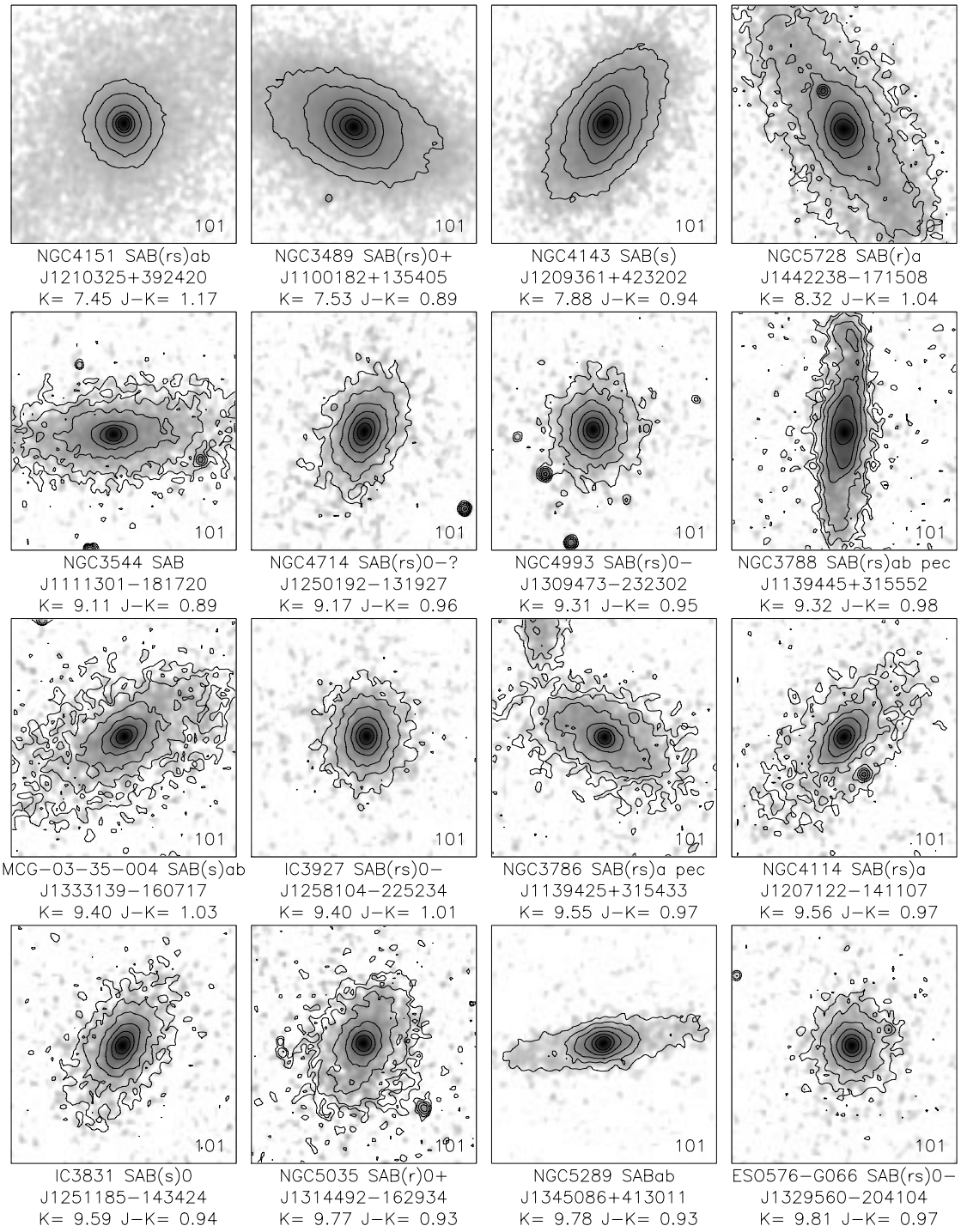
101
NGC4151 SAB(rs)ab
J1210325+392420
K= 7.45 J−K= 1.17
NGC3489 SAB(rs)0+
J1100182+135405
K= 7.53 J−K= 0.89
NGC4143 SAB(s)
J1209361+423202
K= 7.88 J−K= 0.94
NGC5728 SAB(r)a
J1442238−171508
K= 8.32 J−K= 1.04
NGC3544 SAB
J1111301−181720
K= 9.11 J−K= 0.89
NGC4714 SAB(rs)0−?
J1250192−131927
K= 9.17 J−K= 0.96
NGC4993 SAB(rs)0−
J1309473−232302
K= 9.31 J−K= 0.95
NGC3788 SAB(rs)ab pec
J1139445+315552
K= 9.32 J−K= 0.98
MCG−03−35−004 SAB(s)ab
J1333139−160717
K= 9.40 J−K= 1.03
IC3927 SAB(rs)0−
J1258104−225234
K= 9.40 J−K= 1.01
NGC3786 SAB(rs)a pec
J1139425+315433
K= 9.55 J−K= 0.97
NGC4114 SAB(rs)a
J1207122−141107
K= 9.56 J−K= 0.97
IC3831 SAB(s)0
J1251185−143424
K= 9.59 J−K= 0.94
NGC5035 SAB(r)0+
J1314492−162934
K= 9.77 J−K= 0.93
NGC5289 SABab
J1345086+413011
K= 9.78 J−K= 0.93
ESO576−G066 SAB(rs)0−
J1329560−204104
K= 9.81 J−K= 0.97

FIG. 20*x*

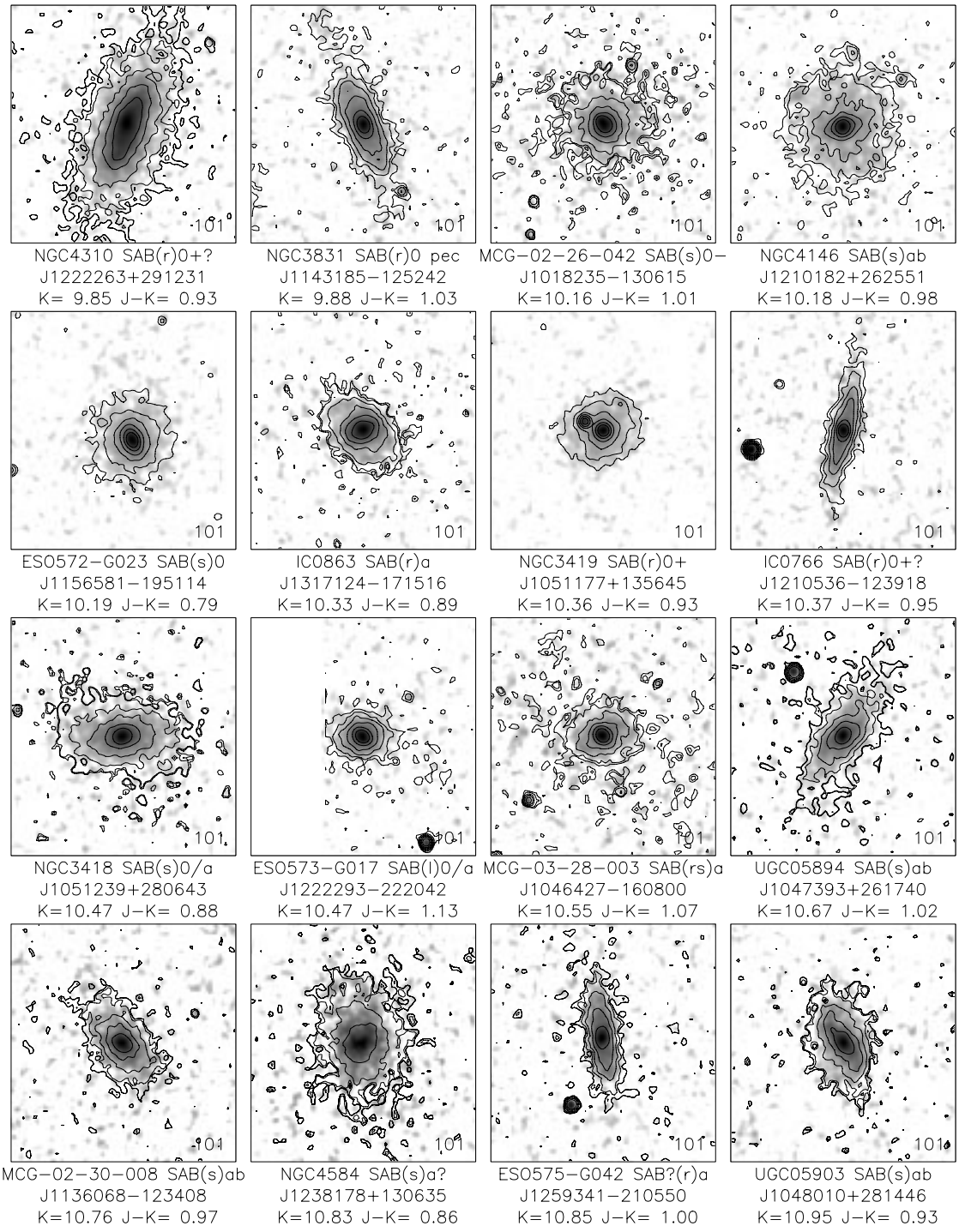
NGC4310 SAB(r)0+?
J1222263+291231
K= 9.85 J−K= 0.93
NGC3831 SAB(r)0 pec
J1143185−125242
K= 9.88 J−K= 1.03
MCG−02−26−042 SAB(s)0−
J1018235−130615
K=10.16 J−K= 1.01
NGC4146 SAB(s)ab
J1210182+262551
K=10.18 J−K= 0.98
ESO572−G023 SAB(s)0
J1156581−195114
K=10.19 J−K= 0.79
IC0863 SAB(r)a
J1317124−171516
K=10.33 J−K= 0.89
NGC3419 SAB(r)0+
J1051177+135645
K=10.36 J−K= 0.93
IC0766 SAB(r)0+?
J1210536−123918
K=10.37 J−K= 0.95
NGC3418 SAB(s)0/a
J1051239+280643
K=10.47 J−K= 0.88
ESO573−G017 SAB(l)0/a
J1222293−222042
K=10.47 J−K= 1.13
MCG−03−28−003 SAB(rs)a
J1046427−160800
K=10.55 J−K= 1.07
UGC05894 SAB(s)ab
J1047393+261740
K=10.67 J−K= 1.02
MCG−02−30−008 SAB(s)ab
J1136068−123408
K=10.76 J−K= 0.97
NGC4584 SAB(s)a?
J1238178+130635
K=10.83 J−K= 0.86
ESO575−G042 SAB?(r)a
J1259341−210550
K=10.85 J−K= 1.00
UGC05903 SAB(s)ab
J1048010+281446
K=10.95 J−K= 0.93

FIG. 20*y*

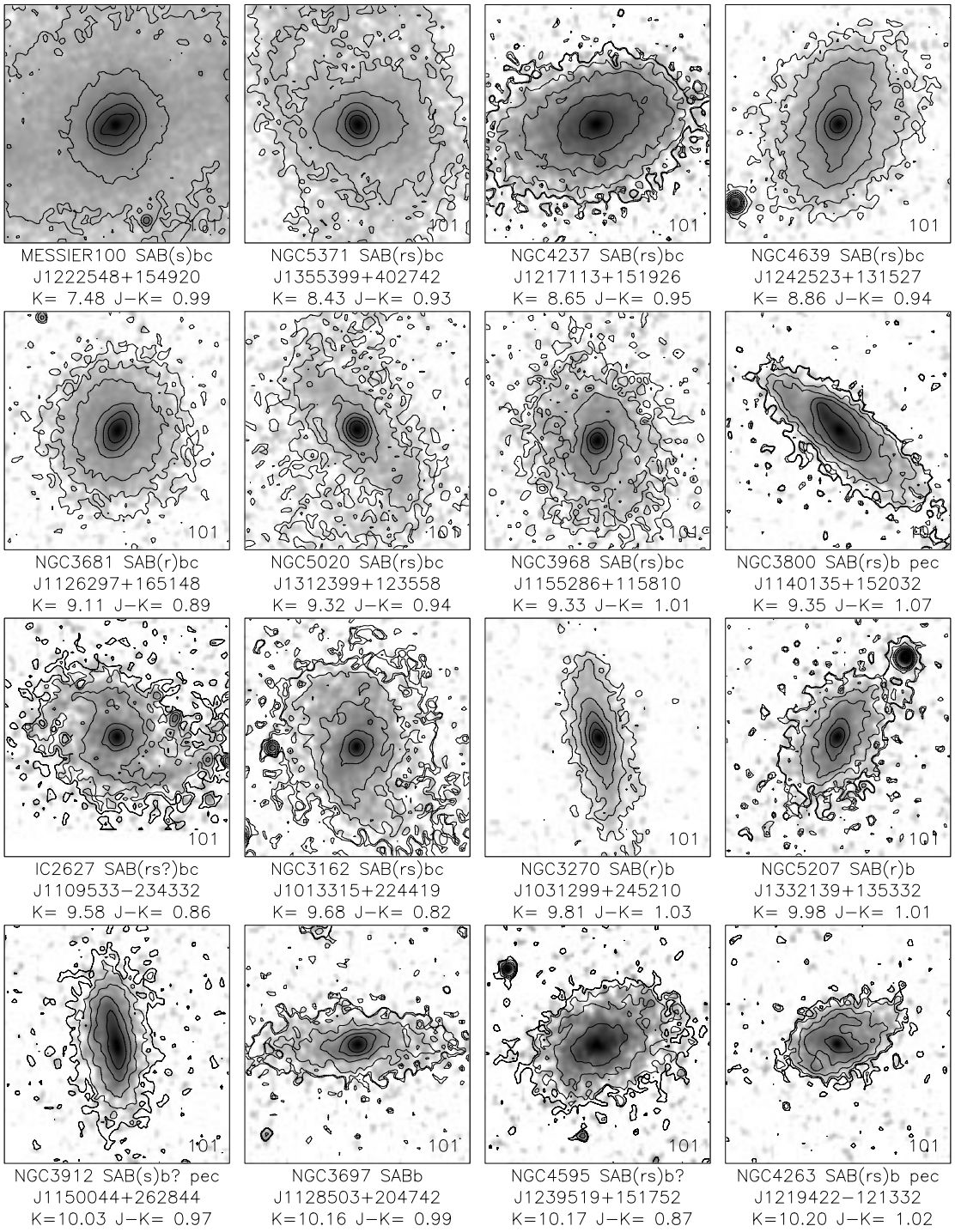
MESSIER100 SAB(s)bc
J1222548+154920
K= 7.48 J−K= 0.99
NGC5371 SAB(rs)bc
J1355399+402742
K= 8.43 J−K= 0.93
NGC4237 SAB(rs)bc
J1217113+151926
K= 8.65 J−K= 0.95
NGC4639 SAB(rs)bc
J1242523+131527
K= 8.86 J−K= 0.94
NGC3681 SAB(r)bc
J1126297+165148
K= 9.11 J−K= 0.89
NGC5020 SAB(rs)bc
J1312399+123558
K= 9.32 J−K= 0.94
NGC3968 SAB(rs)bc
J1155286+115810
K= 9.33 J−K= 1.01
NGC3800 SAB(rs)b pec
J1140135+152032
K= 9.35 J−K= 1.07
IC2627 SAB(rs?)bc
J1109533−234332
K= 9.58 J−K= 0.86
NGC3162 SAB(rs)bc
J1013315+224419
K= 9.68 J−K= 0.82
NGC3270 SAB(r)b
J1031299+245210
K= 9.81 J−K= 1.03
NGC5207 SAB(r)b
J1332139+135332
K= 9.98 J−K= 1.01
NGC3912 SAB(s)b? pec
J1150044+262844
K=10.03 J−K= 0.97
NGC3697 SABb
J1128503+204742
K=10.16 J−K= 0.99
NGC4595 SAB(rs)b?
J1239519+151752
K=10.17 J−K= 0.87
NGC4263 SAB(rs)b pec
J1219422−121332
K=10.20 J−K= 1.02

FIG. 20*z*

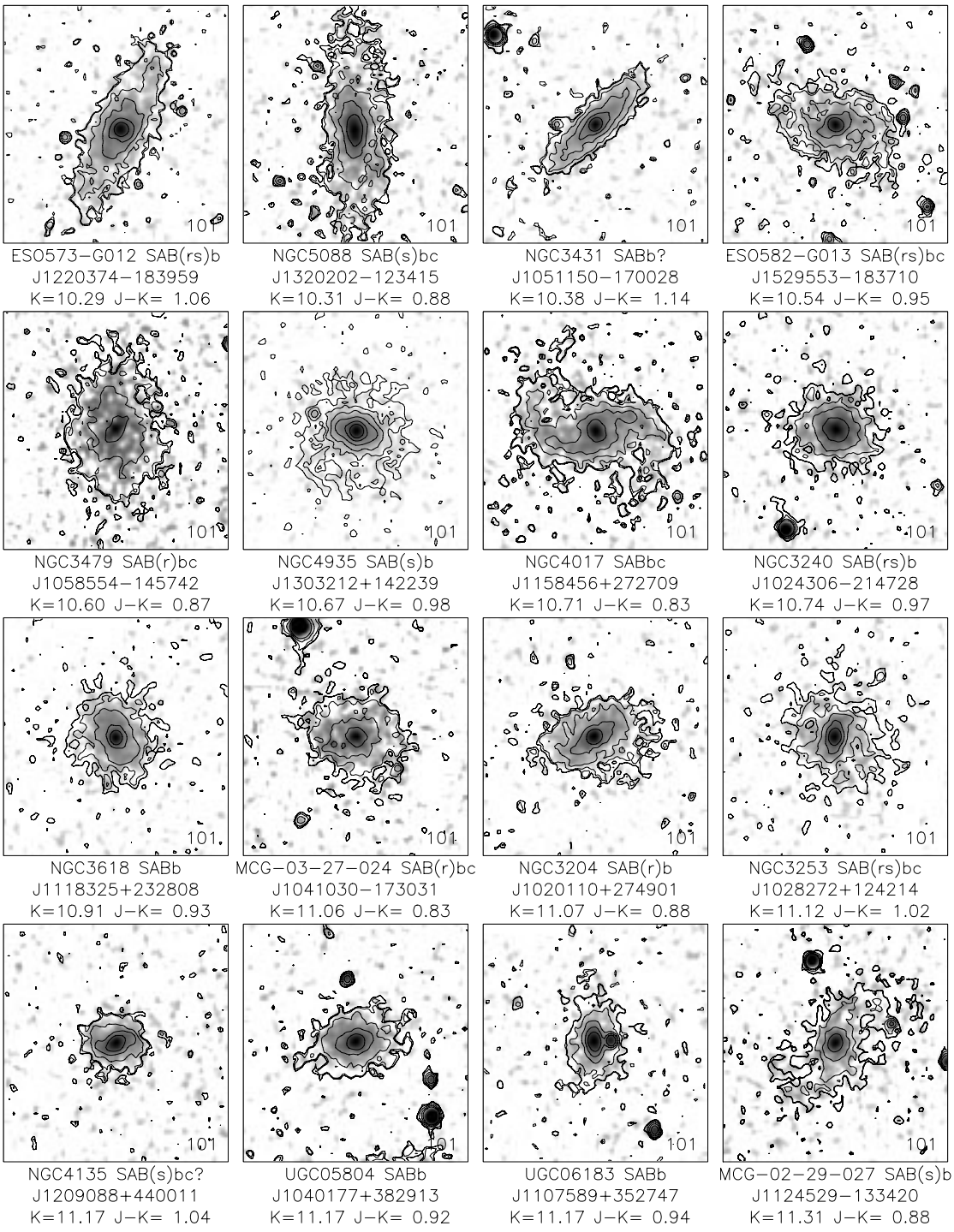
ESO573−G012 SAB(rs)b
J1220374−183959
K=10.29 J−K= 1.06
NGC5088 SAB(s)bc
J1320202−123415
K=10.31 J−K= 0.88
NGC3431 SABb?
J1051150−170028
K=10.38 J−K= 1.14
ESO582−G013 SAB(rs)bc
J1529553−183710
K=10.54 J−K= 0.95
NGC3479 SAB(r)bc
J1058554−145742
K=10.60 J−K= 0.87
NGC4935 SAB(s)b
J1303212+142239
K=10.67 J−K= 0.98
NGC4017 SABbc
J1158456+272709
K=10.71 J−K= 0.83
NGC3240 SAB(rs)b
J1024306−214728
K=10.74 J−K= 0.97
NGC3618 SABb
J1118325+232808
K=10.91 J−K= 0.93
MCG−03−27−024 SAB(r)bc
J1041030−173031
K=11.06 J−K= 0.83
NGC3204 SAB(r)b
J1020110+274901
K=11.07 J−K= 0.88
NGC3253 SAB(rs)bc
J1028272+124214
K=11.12 J−K= 1.02
NGC4135 SAB(s)bc?
J1209088+440011
K=11.17 J−K= 1.04
UGC05804 SABb
J1040177+382913
K=11.17 J−K= 0.92
UGC06183 SABb
J1107589+352747
K=11.17 J−K= 0.94
MCG−02−29−027 SAB(s)b
J1124529−133420
K=11.31 J−K= 0.88

FIG. 20*aa*

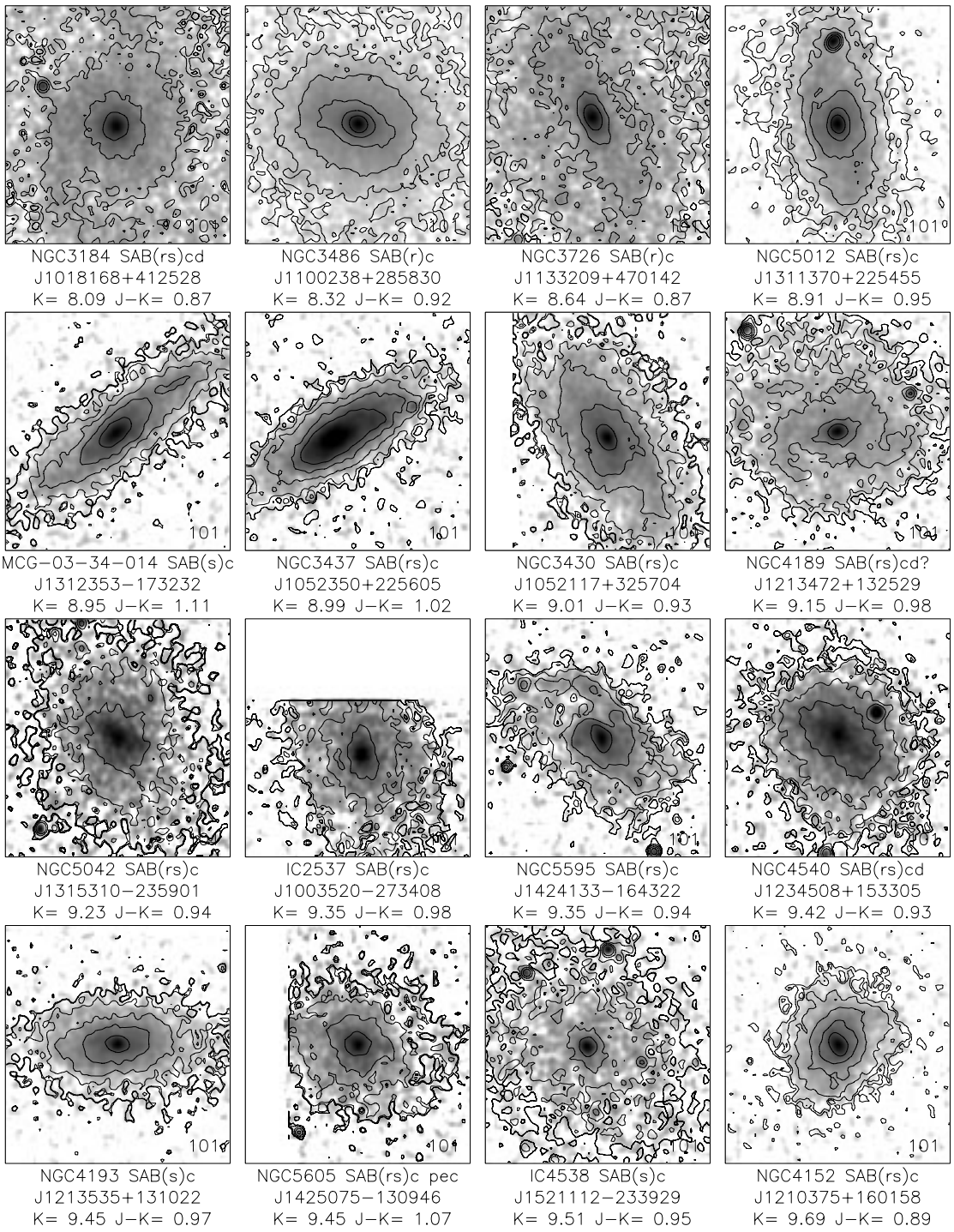
NGC3184 SAB(rs)cd
J1018168+412528
K= 8.09 J−K= 0.87
NGC3486 SAB(r)c
J1100238+285830
K= 8.32 J−K= 0.92
NGC3726 SAB(r)c
J1133209+470142
K= 8.64 J−K= 0.87
NGC5012 SAB(rs)c
J1311370+225455
K= 8.91 J−K= 0.95
MCG−03−34−014 SAB(s)c
J1312353−173232
K= 8.95 J−K= 1.11
NGC3437 SAB(rs)c
J1052350+225605
K= 8.99 J−K= 1.02
NGC3430 SAB(rs)c
J1052117+325704
K= 9.01 J−K= 0.93
NGC4189 SAB(rs)cd?
J1213472+132529
K= 9.15 J−K= 0.98
NGC5042 SAB(rs)c
J1315310−235901
K= 9.23 J−K= 0.94
IC2537 SAB(rs)c
J1003520−273408
K= 9.35 J−K= 0.98
NGC5595 SAB(rs)c
J1424133−164322
K= 9.35 J−K= 0.94
NGC4540 SAB(rs)cd
J1234508+153305
K= 9.42 J−K= 0.93
NGC4193 SAB(s)c
J1213535+131022
K= 9.45 J−K= 0.97
NGC5605 SAB(rs)c pec
J1425075−130946
K= 9.45 J−K= 1.07
IC4538 SAB(s)c
J1521112−233929
K= 9.51 J−K= 0.95
NGC4152 SAB(rs)c
J1210375+160158
K= 9.69 J−K= 0.89

FIG. 20*ab*

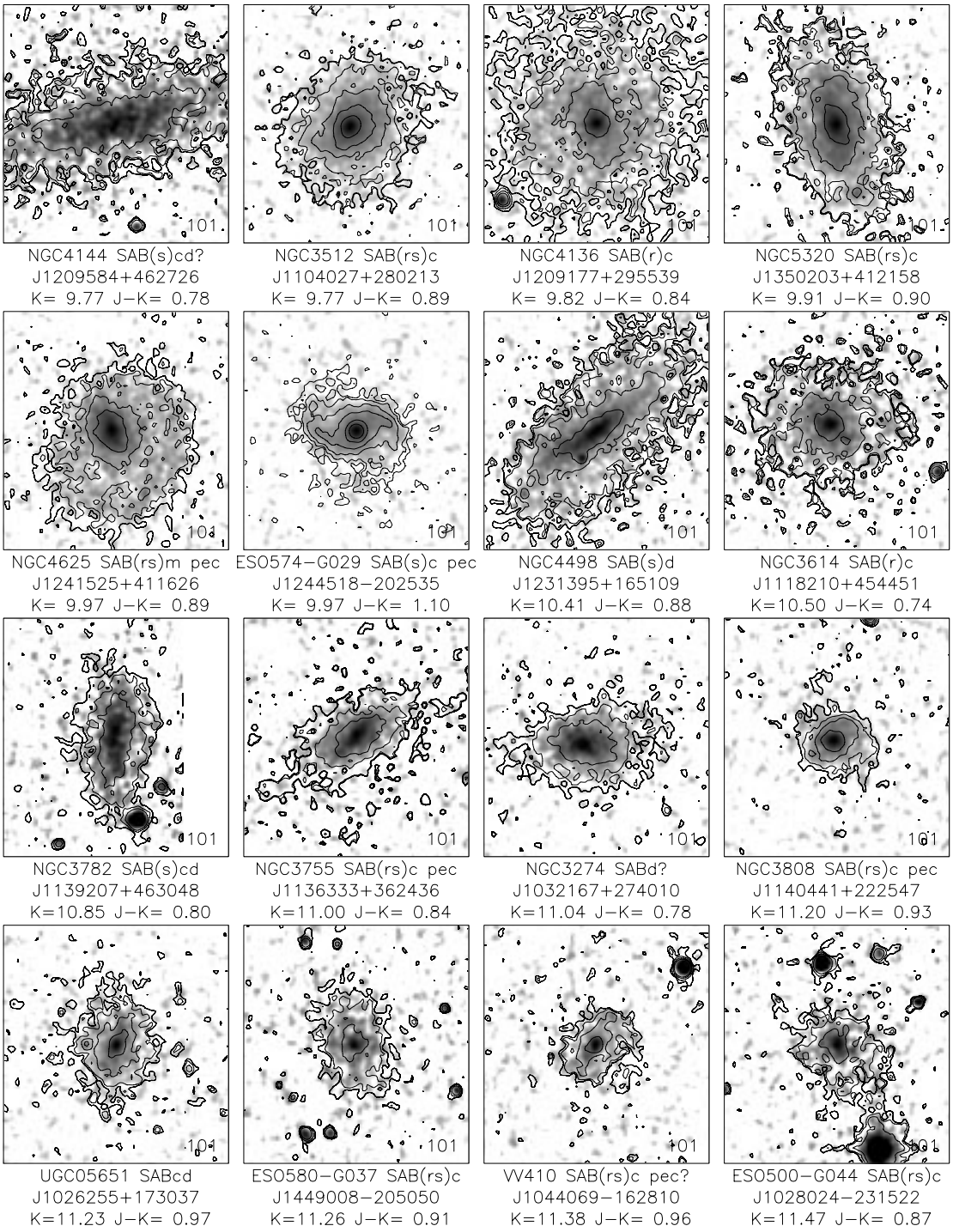
NGC4144 SAB(s)cd?
J1209584+462726
K= 9.77 J−K= 0.78
NGC3512 SAB(rs)c
J1104027+280213
K= 9.77 J−K= 0.89
NGC4136 SAB(r)c
J1209177+295539
K= 9.82 J−K= 0.84
NGC5320 SAB(rs)c
J1350203+412158
K= 9.91 J−K= 0.90
NGC4625 SAB(rs)m pec
J1241525+411626
K= 9.97 J−K= 0.89
ESO574−G029 SAB(s)c pec
J1244518−202535
K= 9.97 J−K= 1.10
NGC4498 SAB(s)d
J1231395+165109
K=10.41 J−K= 0.88
NGC3614 SAB(r)c
J1118210+454451
K=10.50 J−K= 0.74
NGC3782 SAB(s)cd
J1139207+463048
K=10.85 J−K= 0.80
NGC3755 SAB(rs)c pec
J1136333+362436
K=11.00 J−K= 0.84
NGC3274 SABd?
J1032167+274010
K=11.04 J−K= 0.78
NGC3808 SAB(rs)c pec
J1140441+222547
K=11.20 J−K= 0.93
UGC05651 SABcd
J1026255+173037
K=11.23 J−K= 0.97
ESO580−G037 SAB(rs)c
J1449008−205050
K=11.26 J−K= 0.91
VV410 SAB(rs)c pec?
J1044069−162810
K=11.38 J−K= 0.96
ESO500−G044 SAB(rs)c
J1028024−231522
K=11.47 J−K= 0.87

FIG. 20*ac*

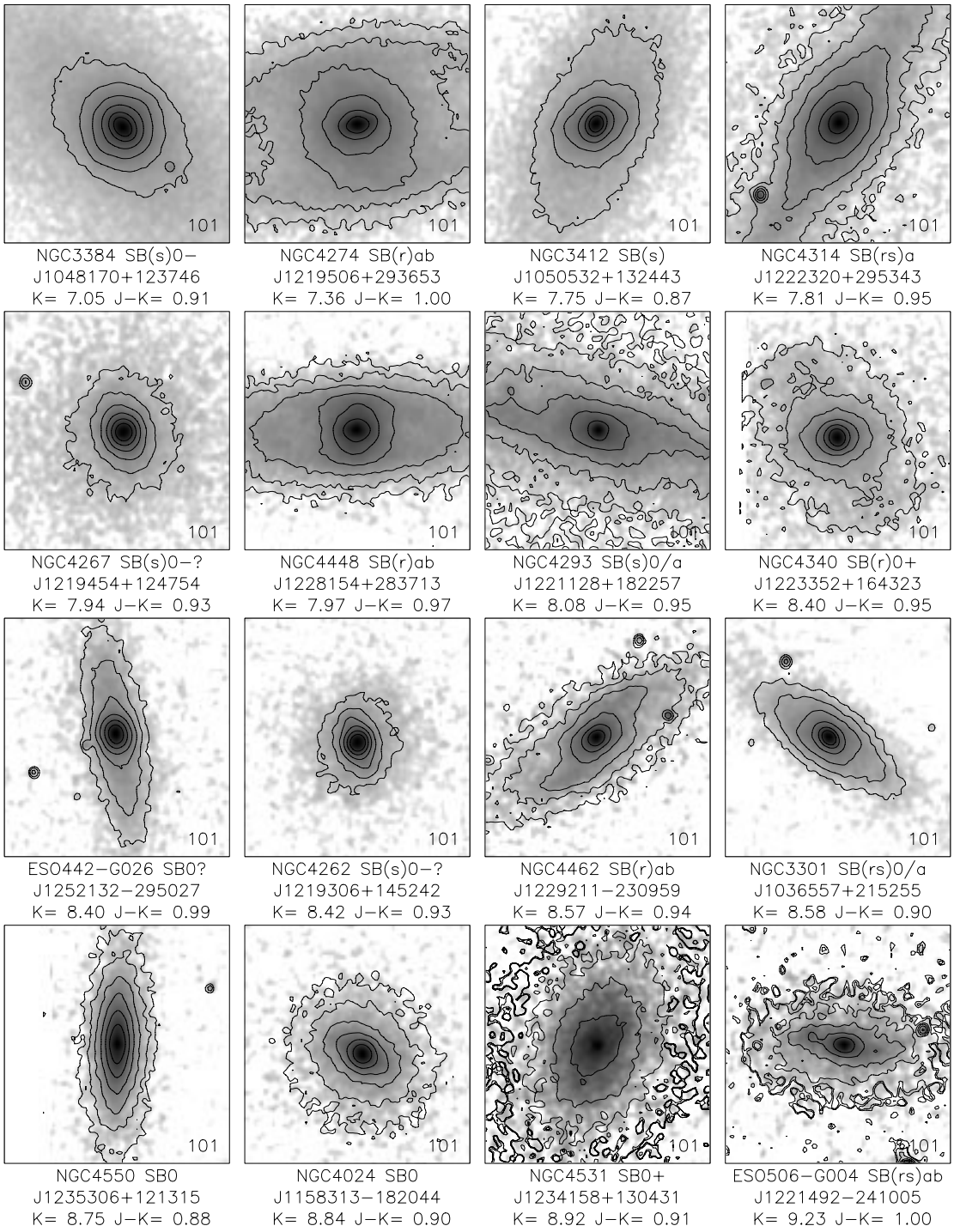
NGC3384 SB(s)0−
J1048170+123746
K= 7.05 J−K= 0.91
NGC4274 SB(r)ab
J1219506+293653
K= 7.36 J−K= 1.00
NGC3412 SB(s)
J1050532+132443
K= 7.75 J−K= 0.87
NGC4314 SB(rs)a
J1222320+295343
K= 7.81 J−K= 0.95
NGC4267 SB(s)0−?
J1219454+124754
K= 7.94 J−K= 0.93
NGC4448 SB(r)ab
J1228154+283713
K= 7.97 J−K= 0.97
NGC4293 SB(s)0/a
J1221128+182257
K= 8.08 J−K= 0.95
NGC4340 SB(r)0+
J1223352+164323
K= 8.40 J−K= 0.95
ESO442−G026 SB0?
J1252132−295027
K= 8.40 J−K= 0.99
NGC4262 SB(s)0−?
J1219306+145242
K= 8.42 J−K= 0.93
NGC4462 SB(r)ab
J1229211−230959
K= 8.57 J−K= 0.94
NGC3301 SB(rs)0/a
J1036557+215255
K= 8.58 J−K= 0.90
NGC4550 SB0
J1235306+121315
K= 8.75 J−K= 0.88
NGC4024 SB0
J1158313−182044
K= 8.84 J−K= 0.90
NGC4531 SB0+
J1234158+130431
K= 8.92 J−K= 0.91
ESO506−G004 SB(rs)ab
J1221492−241005
K= 9.23 J−K= 1.00

FIG. 20*ad*

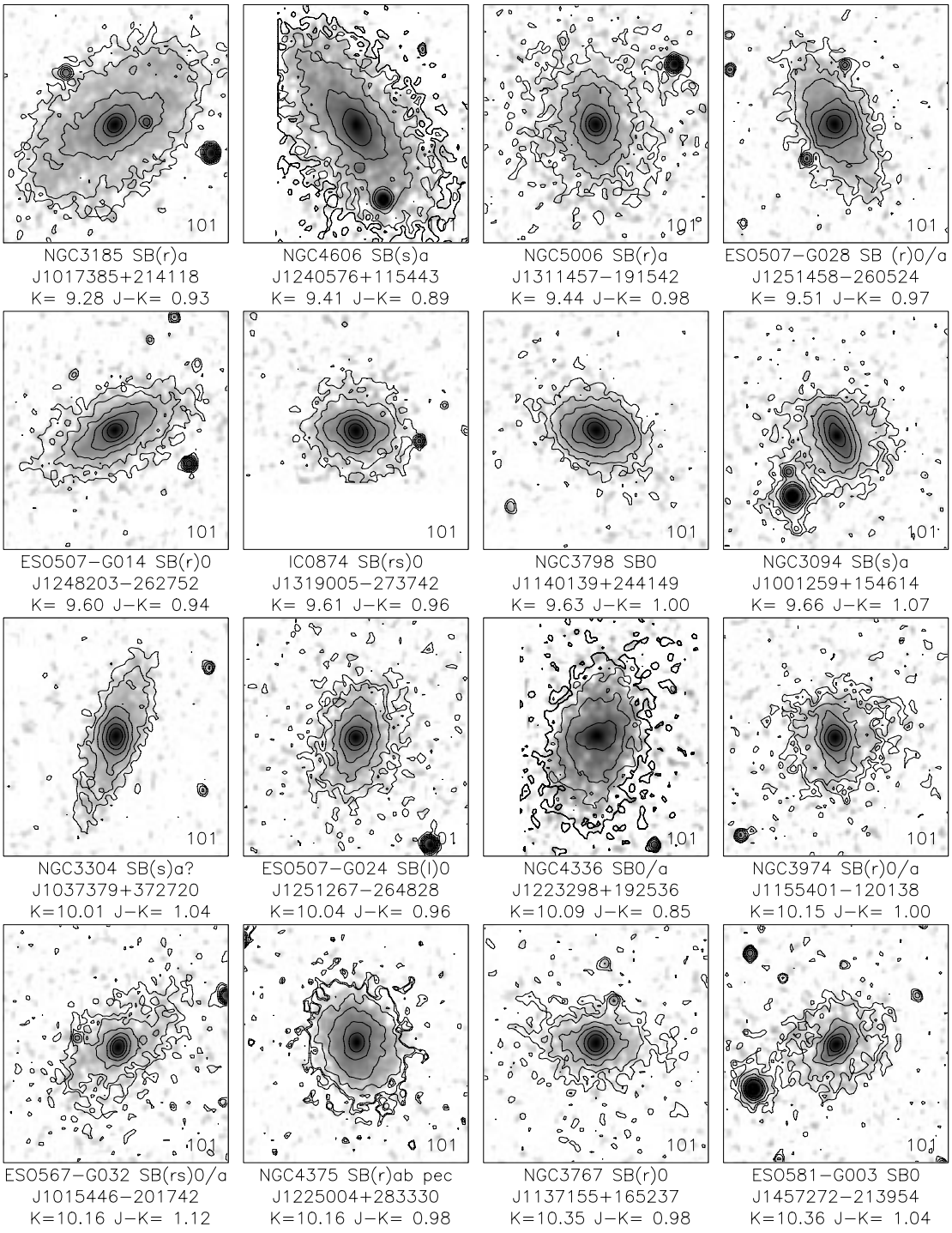
NGC3185 SB(r)a
J1017385+214118
K= 9.28 J−K= 0.93
NGC4606 SB(s)a
J1240576+115443
K= 9.41 J−K= 0.89
NGC5006 SB(r)a
J1311457−191542
K= 9.44 J−K= 0.98
ESO507−G028 SB (r)0/a
J1251458−260524
K= 9.51 J−K= 0.97
ESO507−G014 SB(r)0
J1248203−262752
K= 9.60 J−K= 0.94
IC0874 SB(rs)0
J1319005−273742
K= 9.61 J−K= 0.96
NGC3798 SB0
J1140139+244149
K= 9.63 J−K= 1.00
NGC3094 SB(s)a
J1001259+154614
K= 9.66 J−K= 1.07
NGC3304 SB(s)a?
J1037379+372720
K=10.01 J−K= 1.04
ESO507−G024 SB(l)0
J1251267−264828
K=10.04 J−K= 0.96
NGC4336 SB0/a
J1223298+192536
K=10.09 J−K= 0.85
NGC3974 SB(r)0/a
J1155401−120138
K=10.15 J−K= 1.00
ESO567−G032 SB(rs)0/a
J1015446−201742
K=10.16 J−K= 1.12
NGC4375 SB(r)ab pec
J1225004+283330
K=10.16 J−K= 0.98
NGC3767 SB(r)0
J1137155+165237
K=10.35 J−K= 0.98
ESO581−G003 SB0
J1457272−213954
K=10.36 J−K= 1.04

FIG. 20*ae*

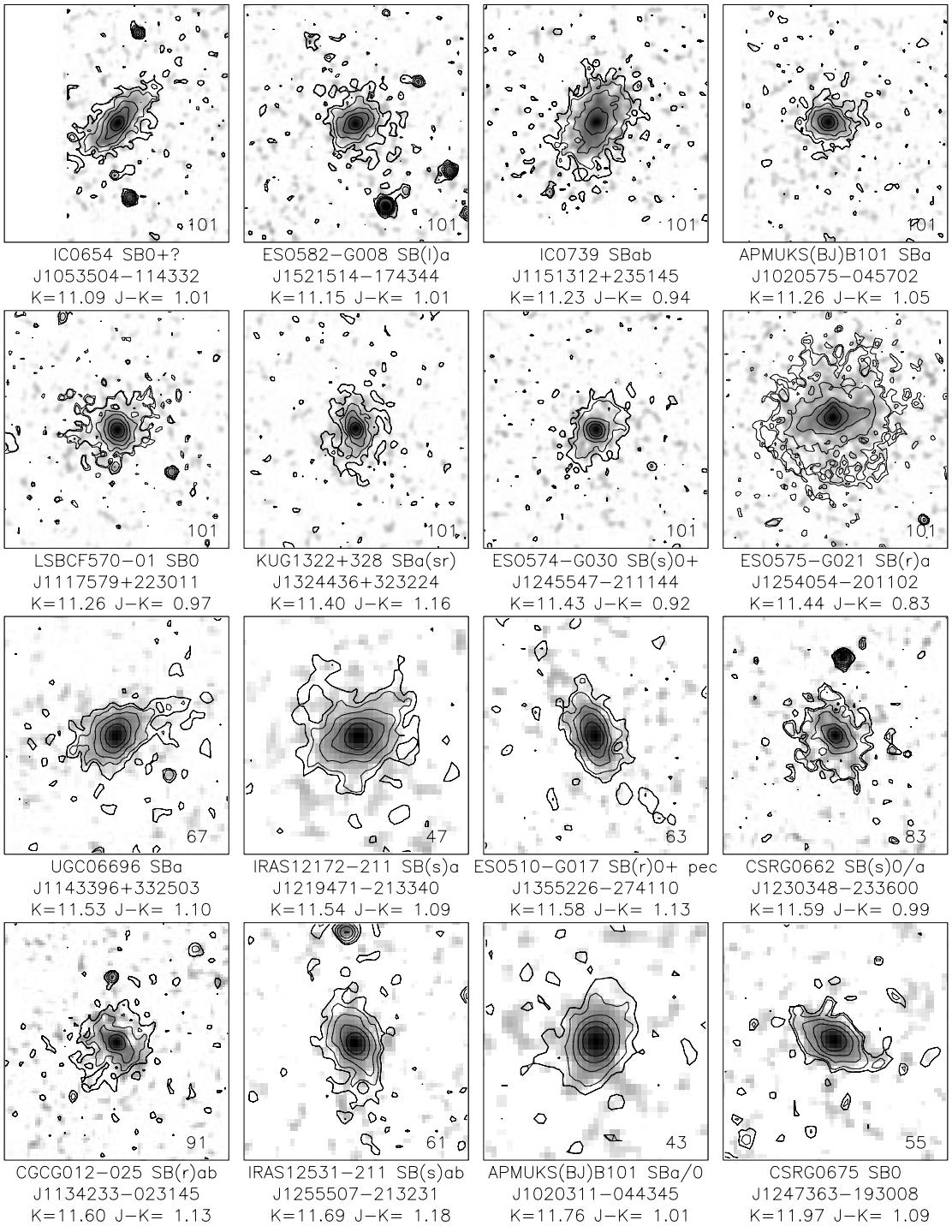
101
IC0654 SB0+?
J1053504−114332
K=11.09 J−K= 1.01
101
ESO582−G008 SB(l)a
J1521514−174344
K=11.15 J−K= 1.01
101
IC0739 SBab
J1151312+235145
K=11.23 J−K= 0.94
101
APMUKS(BJ)B101 SBa
J1020575−045702
K=11.26 J−K= 1.05
101
LSBCF570−01 SB0
J1117579+223011
K=11.26 J−K= 0.97
101
KUG1322+328 SBa(sr)
J1324436+323224
K=11.40 J−K= 1.16
101
ESO574−G030 SB(s)0+
J1245547−211144
K=11.43 J−K= 0.92
101
ESO575−G021 SB(r)a
J1254054−201102
K=11.44 J−K= 0.83
67
UGC06696 SBa
J1143396+332503
K=11.53 J−K= 1.10
47
IRAS12172−211 SB(s)a
J1219471−213340
K=11.54 J−K= 1.09
63
ESO510−G017 SB(r)0+ pec
J1355226−274110
K=11.58 J−K= 1.13
83
CSRG0662 SB(s)0/a
J1230348−233600
K=11.59 J−K= 0.99
91
CGCG012−025 SB(r)ab
J1134233−023145
K=11.60 J−K= 1.13
61
IRAS12531−211 SB(s)ab
J1255507−213231
K=11.69 J−K= 1.18
43
APMUKS(BJ)B101 SBa/0
J1020311−044345
K=11.76 J−K= 1.01
55
CSRG0675 SB0
J1247363−193008
K=11.97 J−K= 1.09

FIG. 20*af*

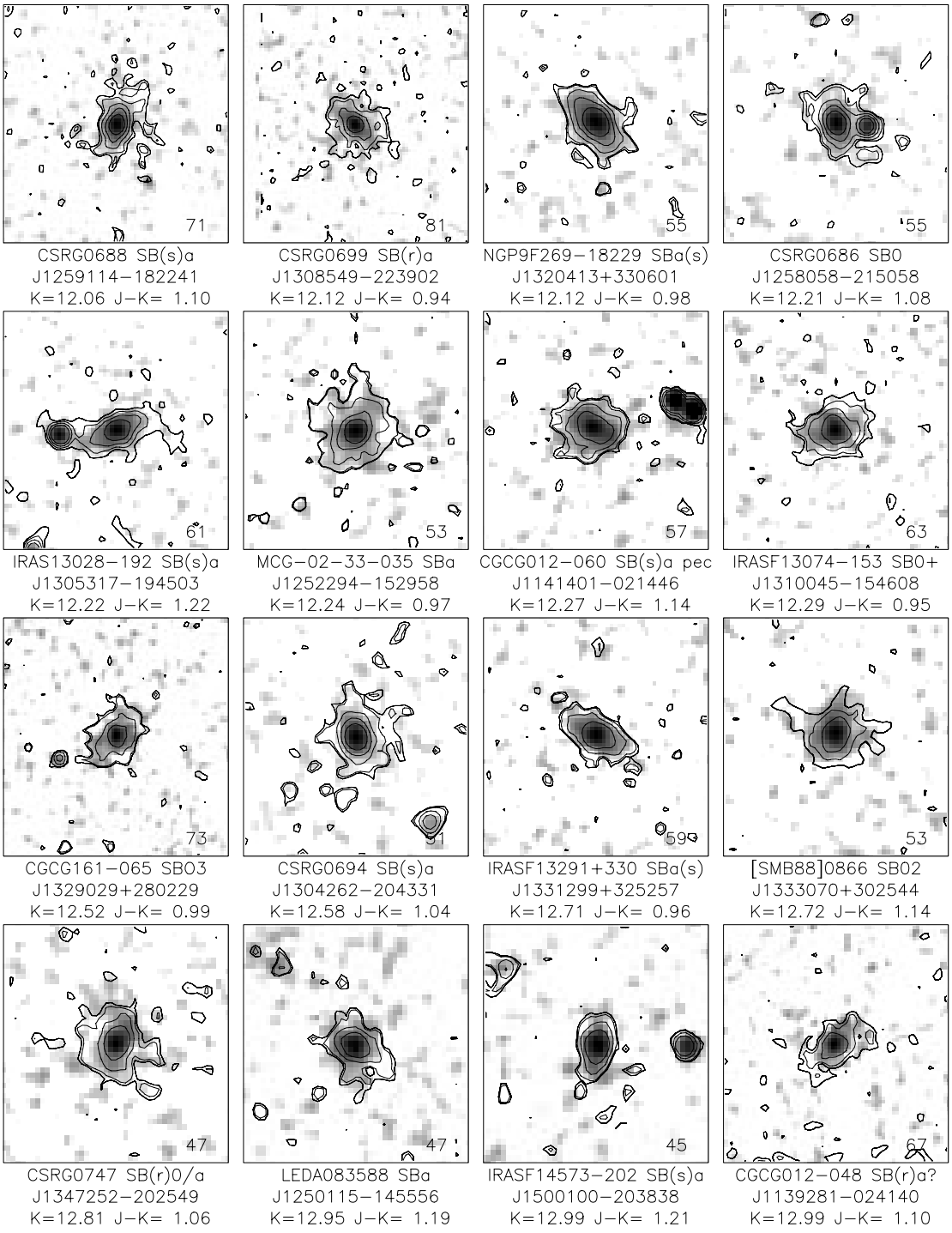
71
CSRG0688 SB(s)a
J1259114−182241
K=12.06 J−K= 1.10
81
CSRG0699 SB(r)a
J1308549−223902
K=12.12 J−K= 0.94
55
NGP9F269−18229 SBa(s)
J1320413+330601
K=12.12 J−K= 0.98
55
CSRG0686 SB0
J1258058−215058
K=12.21 J−K= 1.08
61
IRAS13028−192 SB(s)a
J1305317−194503
K=12.22 J−K= 1.22
53
MCG−02−33−035 SBa
J1252294−152958
K=12.24 J−K= 0.97
57
CGCG012−060 SB(s)a pec
J1141401−021446
K=12.27 J−K= 1.14
63
IRASF13074−153 SB0+
J1310045−154608
K=12.29 J−K= 0.95
73
CGCG161−065 SB03
J1329029+280229
K=12.52 J−K= 0.99
51
CSRG0694 SB(s)a
J1304262−204331
K=12.58 J−K= 1.04
59
IRASF13291+330 SBa(s)
J1331299+325257
K=12.71 J−K= 0.96
53
[SMB88]0866 SB02
J1333070+302544
K=12.72 J−K= 1.14
47
CSRG0747 SB(r)0/a
J1347252−202549
K=12.81 J−K= 1.06
47
LEDA083588 SBa
J1250115−145556
K=12.95 J−K= 1.19
45
IRASF14573−202 SB(s)a
J1500100−203838
K=12.99 J−K= 1.21
67
CGCG012−048 SB(r)a?
J1139281−024140
K=12.99 J−K= 1.10

FIG. 20*ag*

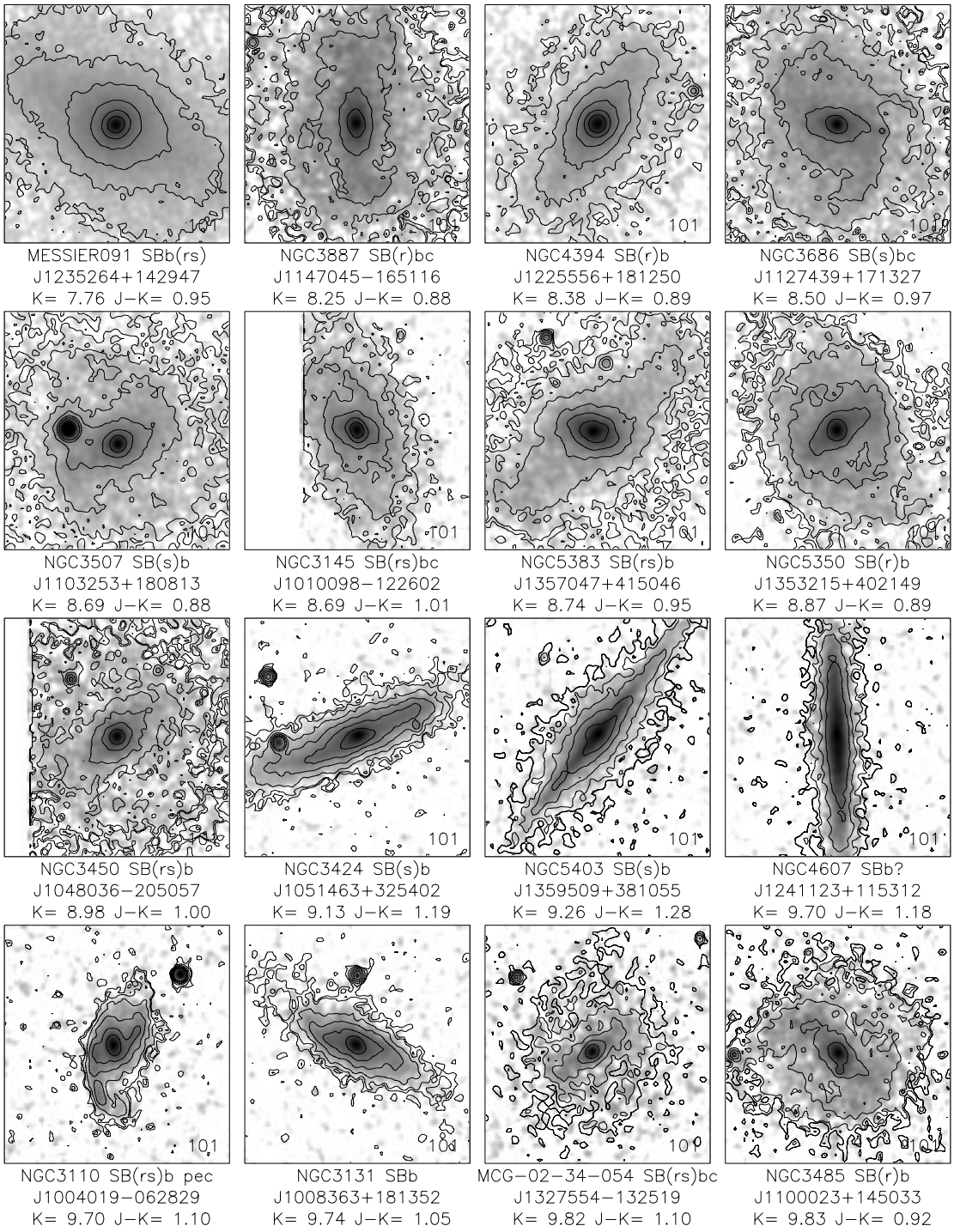
MESSIER091 SBb(rs)
J1235264+142947
K= 7.76 J−K= 0.95
NGC3887 SB(r)bc
J1147045−165116
K= 8.25 J−K= 0.88
NGC4394 SB(r)b
J1225556+181250
K= 8.38 J−K= 0.89
NGC3686 SB(s)bc
J1127439+171327
K= 8.50 J−K= 0.97
NGC3507 SB(s)b
J1103253+180813
K= 8.69 J−K= 0.88
NGC3145 SB(rs)bc
J1010098−122602
K= 8.69 J−K= 1.01
NGC5383 SB(rs)b
J1357047+415046
K= 8.74 J−K= 0.95
NGC5350 SB(r)b
J1353215+402149
K= 8.87 J−K= 0.89
NGC3450 SB(rs)b
J1048036−205057
K= 8.98 J−K= 1.00
NGC3424 SB(s)b
J1051463+325402
K= 9.13 J−K= 1.19
NGC5403 SB(s)b
J1359509+381055
K= 9.26 J−K= 1.28
NGC4607 SBb?
J1241123+115312
K= 9.70 J−K= 1.18
NGC3110 SB(rs)b pec
J1004019−062829
K= 9.70 J−K= 1.10
NGC3131 SBb
J1008363+181352
K= 9.74 J−K= 1.05
MCG−02−34−054 SB(rs)bc
J1327554−132519
K= 9.82 J−K= 1.10
NGC3485 SB(r)b
J1100023+145033
K= 9.83 J−K= 0.92

FIG. 20*ah*

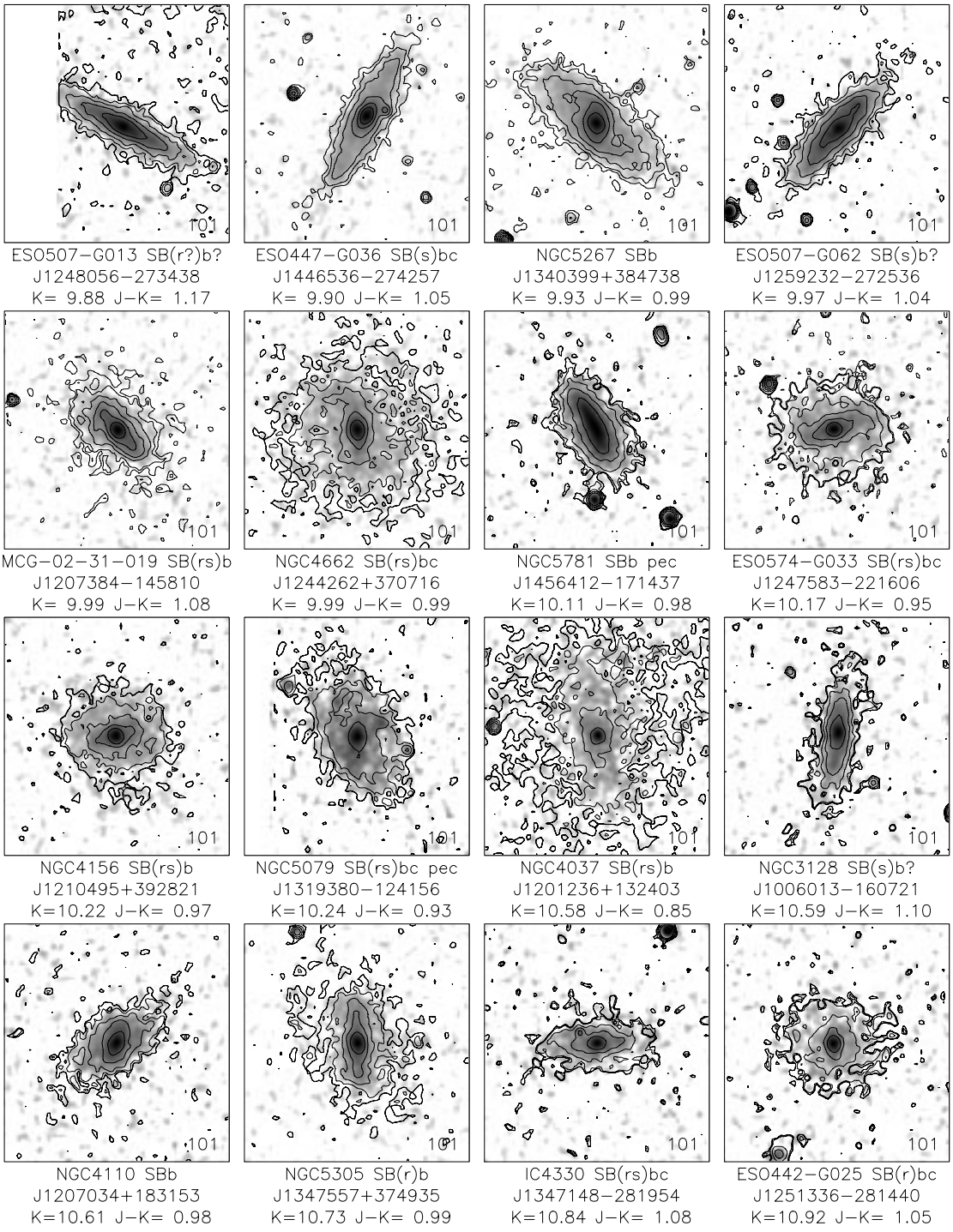
ESO507−G013 SB(r?)b?
J1248056−273438
K= 9.88 J−K= 1.17
ESO447−G036 SB(s)bc
J1446536−274257
K= 9.90 J−K= 1.05
NGC5267 SBb
J1340399+384738
K= 9.93 J−K= 0.99
ESO507−G062 SB(s)b?
J1259232−272536
K= 9.97 J−K= 1.04
MCG−02−31−019 SB(rs)b
J1207384−145810
K= 9.99 J−K= 1.08
NGC4662 SB(rs)bc
J1244262+370716
K= 9.99 J−K= 0.99
NGC5781 SBb pec
J1456412−171437
K=10.11 J−K= 0.98
ESO574−G033 SB(rs)bc
J1247583−221606
K=10.17 J−K= 0.95
NGC4156 SB(rs)b
J1210495+392821
K=10.22 J−K= 0.97
NGC5079 SB(rs)bc pec
J1319380−124156
K=10.24 J−K= 0.93
NGC4037 SB(rs)b
J1201236+132403
K=10.58 J−K= 0.85
NGC3128 SB(s)b?
J1006013−160721
K=10.59 J−K= 1.10
NGC4110 SBb
J1207034+183153
K=10.61 J−K= 0.98
NGC5305 SB(r)b
J1347557+374935
K=10.73 J−K= 0.99
IC4330 SB(rs)bc
J1347148−281954
K=10.84 J−K= 1.08
ESO442−G025 SB(r)bc
J1251336−281440
K=10.92 J−K= 1.05

FIG. 20*ai*

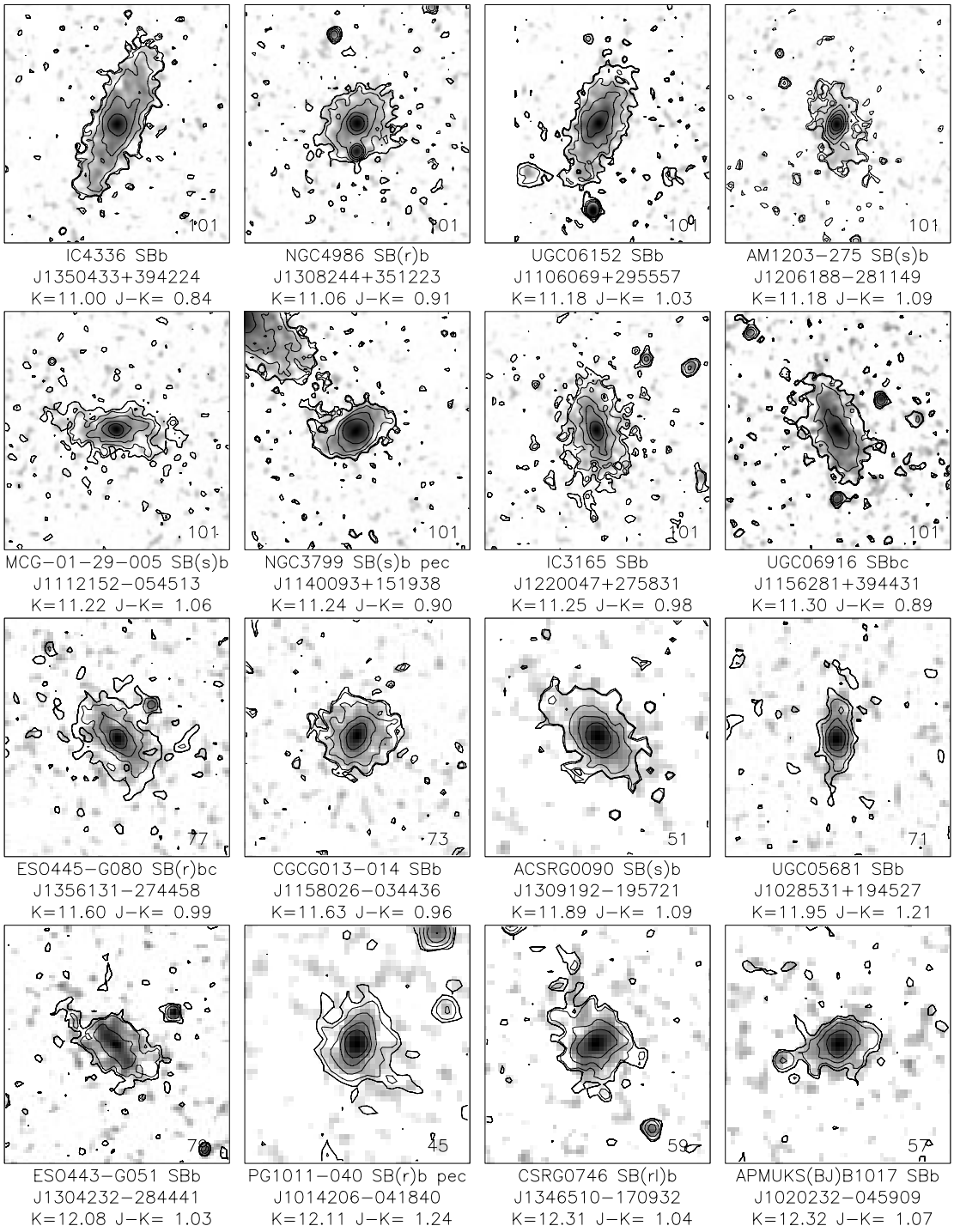
IC4336 SBb
J1350433+394224
K=11.00 J−K= 0.84
NGC4986 SB(r)b
J1308244+351223
K=11.06 J−K= 0.91
UGC06152 SBb
J1106069+295557
K=11.18 J−K= 1.03
AM1203−275 SB(s)b
J1206188−281149
K=11.18 J−K= 1.09
MCG−01−29−005 SB(s)b
J1112152−054513
K=11.22 J−K= 1.06
NGC3799 SB(s)b pec
J1140093+151938
K=11.24 J−K= 0.90
IC3165 SBb
J1220047+275831
K=11.25 J−K= 0.98
UGC06916 SBbc
J1156281+394431
K=11.30 J−K= 0.89
ESO445−G080 SB(r)bc
J1356131−274458
K=11.60 J−K= 0.99
CGCG013−014 SBb
J1158026−034436
K=11.63 J−K= 0.96
ACSRG0090 SB(s)b
J1309192−195721
K=11.89 J−K= 1.09
UGC05681 SBb
J1028531+194527
K=11.95 J−K= 1.21
ESO443−G051 SBb
J1304232−284441
K=12.08 J−K= 1.03
PG1011−040 SB(r)b pec
J1014206−041840
K=12.11 J−K= 1.24
CSRG0746 SB(rl)b
J1346510−170932
K=12.31 J−K= 1.04
APMUKS(BJ)B1017 SBb
J1020232−045909
K=12.32 J−K= 1.07

FIG. 20*aj*

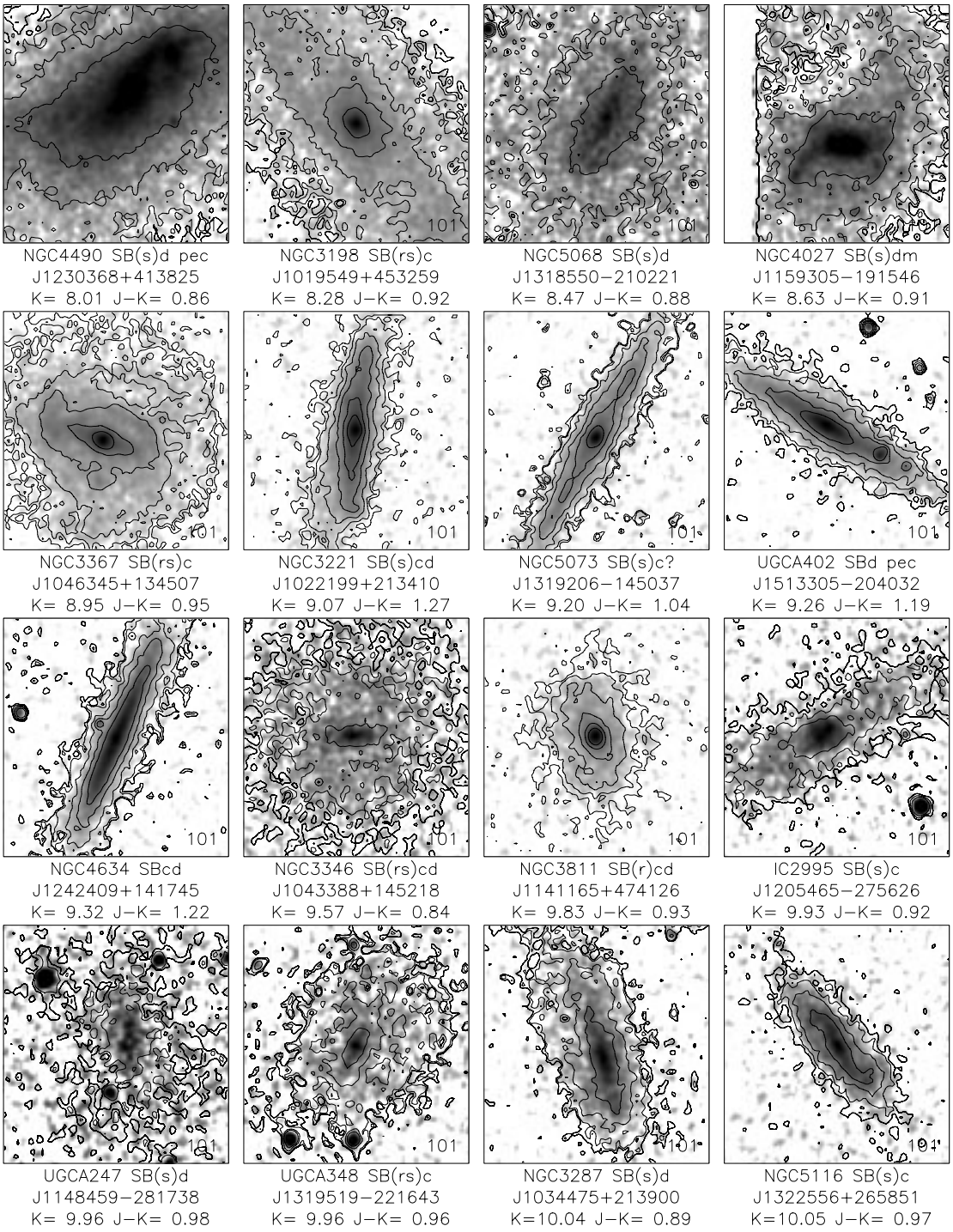
NGC4490 SB(s)d pec
J1230368+413825
K= 8.01 J−K= 0.86
NGC3198 SB(rs)c
J1019549+453259
K= 8.28 J−K= 0.92
NGC5068 SB(s)d
J1318550−210221
K= 8.47 J−K= 0.88
NGC4027 SB(s)dm
J1159305−191546
K= 8.63 J−K= 0.91
NGC3367 SB(rs)c
J1046345+134507
K= 8.95 J−K= 0.95
NGC3221 SB(s)cd
J1022199+213410
K= 9.07 J−K= 1.27
NGC5073 SB(s)c?
J1319206−145037
K= 9.20 J−K= 1.04
UGCA402 SBd pec
J1513305−204032
K= 9.26 J−K= 1.19
NGC4634 SBcd
J1242409+141745
K= 9.32 J−K= 1.22
NGC3346 SB(rs)cd
J1043388+145218
K= 9.57 J−K= 0.84
NGC3811 SB(r)cd
J1141165+474126
K= 9.83 J−K= 0.93
IC2995 SB(s)c
J1205465−275626
K= 9.93 J−K= 0.92
UGCA247 SB(s)d
J1148459−281738
K= 9.96 J−K= 0.98
UGCA348 SB(rs)c
J1319519−221643
K= 9.96 J−K= 0.96
NGC3287 SB(s)d
J1034475+213900
K=10.04 J−K= 0.89
NGC5116 SB(s)c
J1322556+265851
K=10.05 J−K= 0.97

FIG. 20*ak*

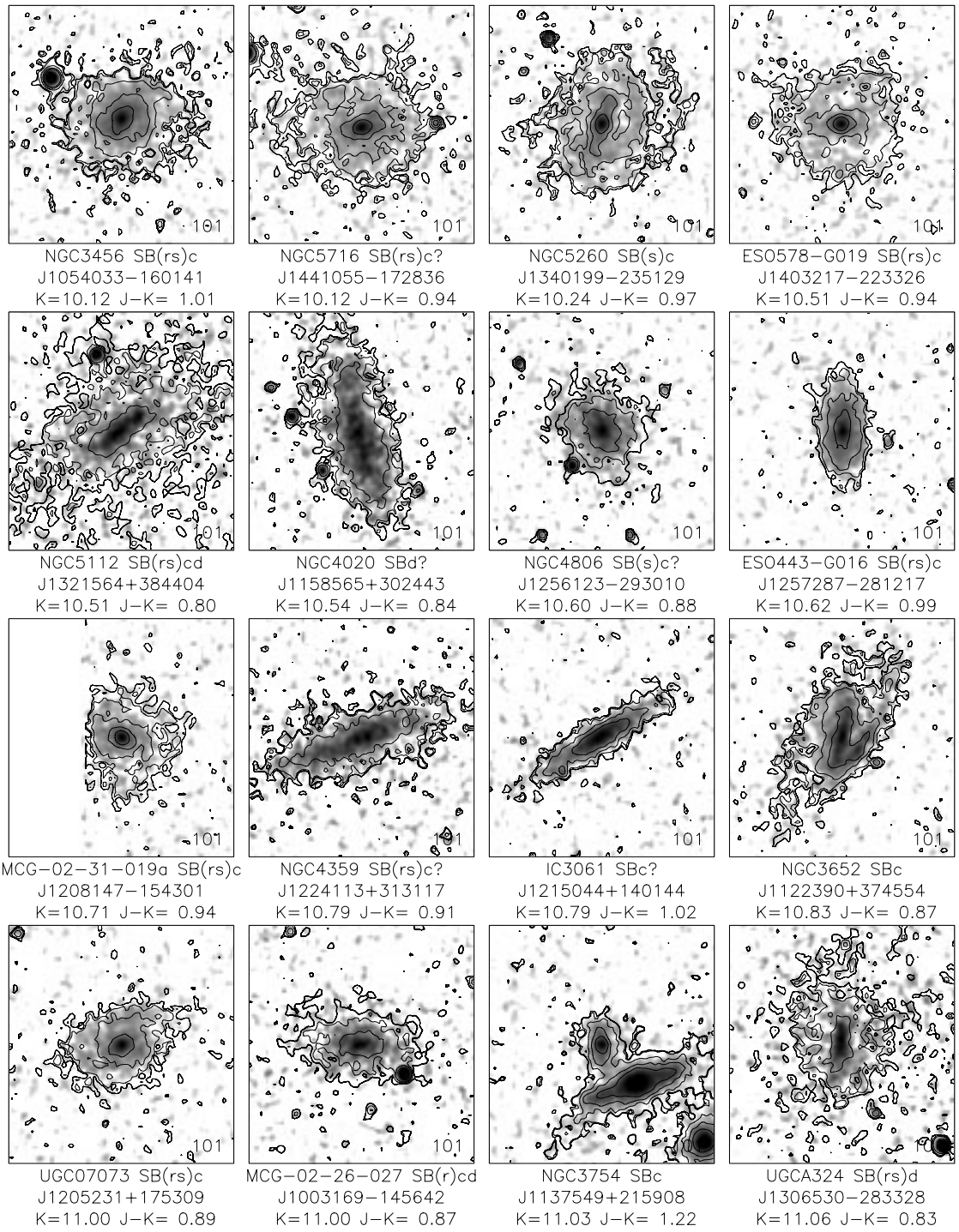
NGC3456 SB(rs)c
J1054033−160141
K=10.12 J−K= 1.01
NGC5716 SB(rs)c?
J1441055−172836
K=10.12 J−K= 0.94
NGC5260 SB(s)c
J1340199−235129
K=10.24 J−K= 0.97
ESO578−G019 SB(rs)c
J1403217−223326
K=10.51 J−K= 0.94
NGC5112 SB(rs)cd
J1321564+384404
K=10.51 J−K= 0.80
NGC4020 SBd?
J1158565+302443
K=10.54 J−K= 0.84
NGC4806 SB(s)c?
J1256123−293010
K=10.60 J−K= 0.88
ESO443−G016 SB(rs)c
J1257287−281217
K=10.62 J−K= 0.99
MCG−02−31−019a SB(rs)c
J1208147−154301
K=10.71 J−K= 0.94
NGC4359 SB(rs)c?
J1224113+313117
K=10.79 J−K= 0.91
IC3061 SBc?
J1215044+140144
K=10.79 J−K= 1.02
NGC3652 SBc
J1122390+374554
K=10.83 J−K= 0.87
UGC07073 SB(rs)c
J1205231+175309
K=11.00 J−K= 0.89
MCG−02−26−027 SB(r)cd
J1003169−145642
K=11.00 J−K= 0.87
NGC3754 SBc
J1137549+215908
K=11.03 J−K= 1.22
UGCA324 SB(rs)d
J1306530−283328
K=11.06 J−K= 0.83

FIG. 20*al*

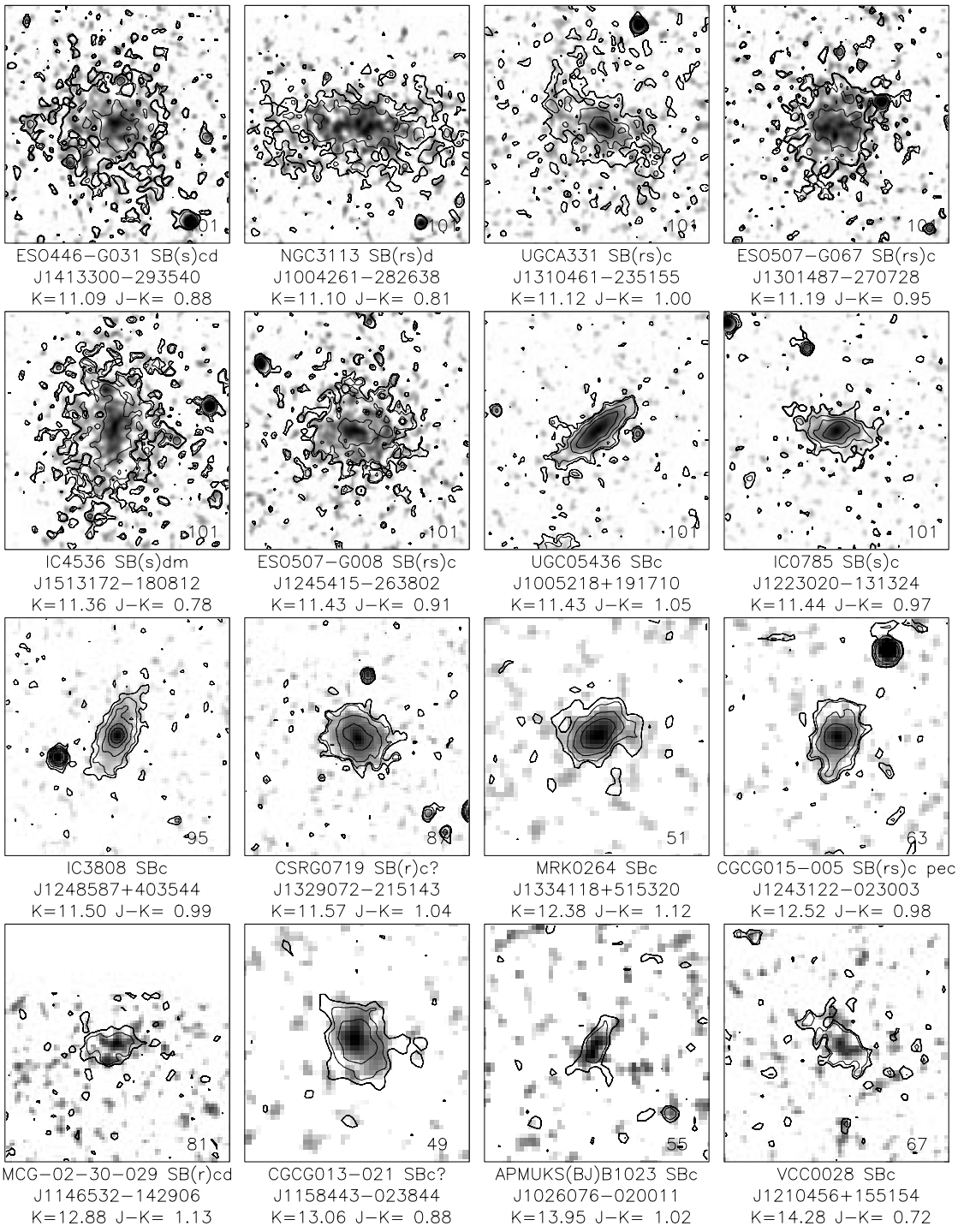
ESO446−G031 SB(s)cd
J1413300−293540
K=11.09 J−K= 0.88
NGC3113 SB(rs)d
J1004261−282638
K=11.10 J−K= 0.81
UGCA331 SB(rs)c
J1310461−235155
K=11.12 J−K= 1.00
ESO507−G067 SB(rs)c
J1301487−270728
K=11.19 J−K= 0.95
IC4536 SB(s)dm
J1513172−180812
K=11.36 J−K= 0.78
ESO507−G008 SB(rs)c
J1245415−263802
K=11.43 J−K= 0.91
UGC05436 SBc
J1005218+191710
K=11.43 J−K= 1.05
IC0785 SB(s)c
J1223020−131324
K=11.44 J−K= 0.97
IC3808 SBc
J1248587+403544
K=11.50 J−K= 0.99
CSRG0719 SB(r)c?
J1329072−215143
K=11.57 J−K= 1.04
MRK0264 SBc
J1334118+515320
K=12.38 J−K= 1.12
CGCG015−005 SB(rs)c pec
J1243122−023003
K=12.52 J−K= 0.98
MCG−02−30−029 SB(r)cd
J1146532−142906
K=12.88 J−K= 1.13
CGCG013−021 SBc?
J1158443−023844
K=13.06 J−K= 0.88
APMUKS(BJ)B1023 SBc
J1026076−020011
K=13.95 J−K= 1.02
VCC0028 SBc
J1210456+155154
K=14.28 J−K= 0.72

FIG. 20*am*

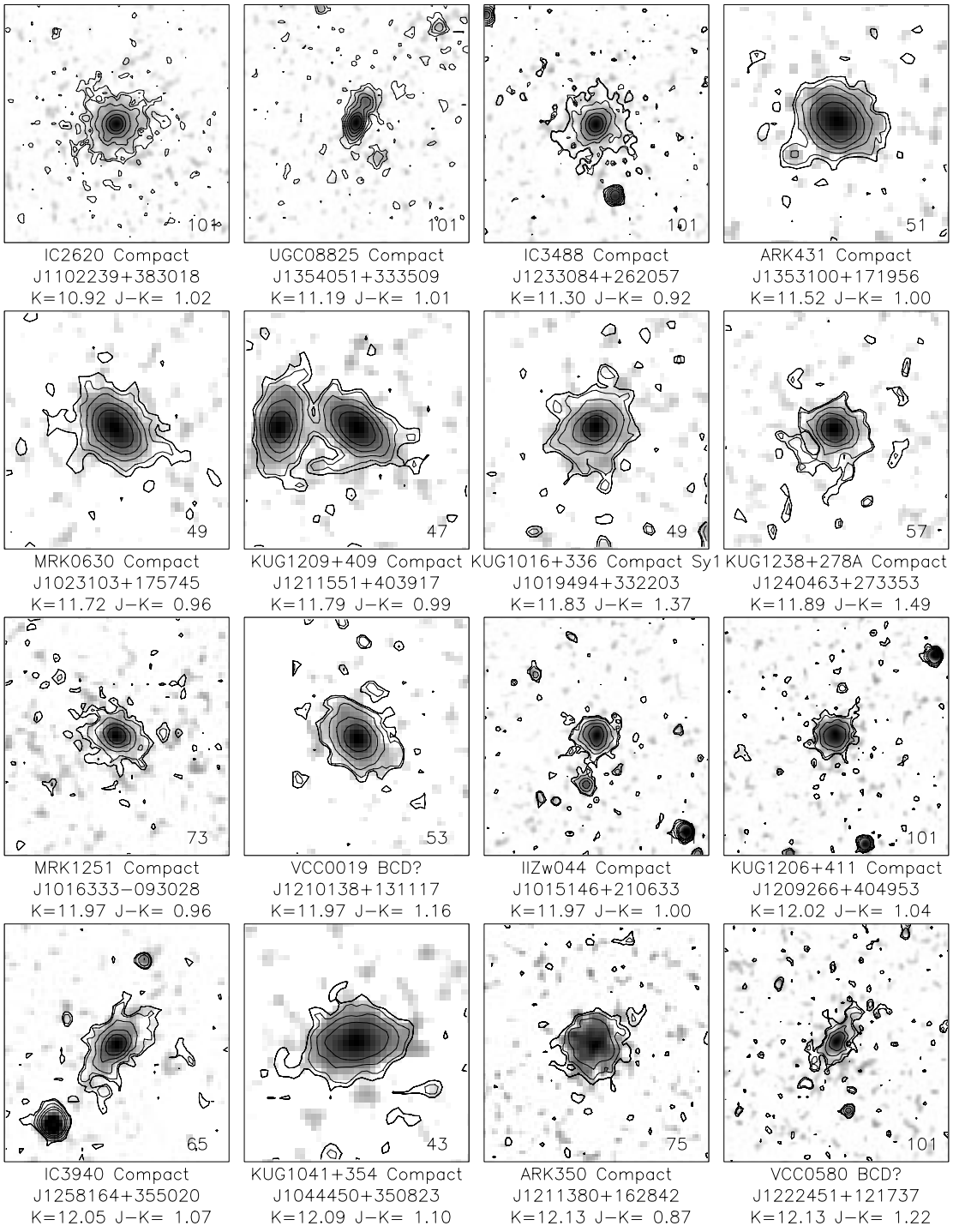
IC2620 Compact
J1102239+383018
K=10.92 J−K= 1.02
UGC08825 Compact
J1354051+333509
K=11.19 J−K= 1.01
IC3488 Compact
J1233084+262057
K=11.30 J−K= 0.92
ARK431 Compact
J1353100+171956
K=11.52 J−K= 1.00
MRK0630 Compact
J1023103+175745
K=11.72 J−K= 0.96
KUG1209+409 Compact
J1211551+403917
K=11.79 J−K= 0.99
KUG1016+336 Compact Sy1
J1019494+332203
K=11.83 J−K= 1.37
KUG1238+278A Compact
J1240463+273353
K=11.89 J−K= 1.49
MRK1251 Compact
J1016333−093028
K=11.97 J−K= 0.96
VCC0019 BCD?
J1210138+131117
K=11.97 J−K= 1.16
IIZw044 Compact
J1015146+210633
K=11.97 J−K= 1.00
KUG1206+411 Compact
J1209266+404953
K=12.02 J−K= 1.04
IC3940 Compact
J1258164+355020
K=12.05 J−K= 1.07
KUG1041+354 Compact
J1044450+350823
K=12.09 J−K= 1.10
ARK350 Compact
J1211380+162842
K=12.13 J−K= 0.87
VCC0580 BCD?
J1222451+121737
K=12.13 J−K= 1.22

FIG. 20*an*

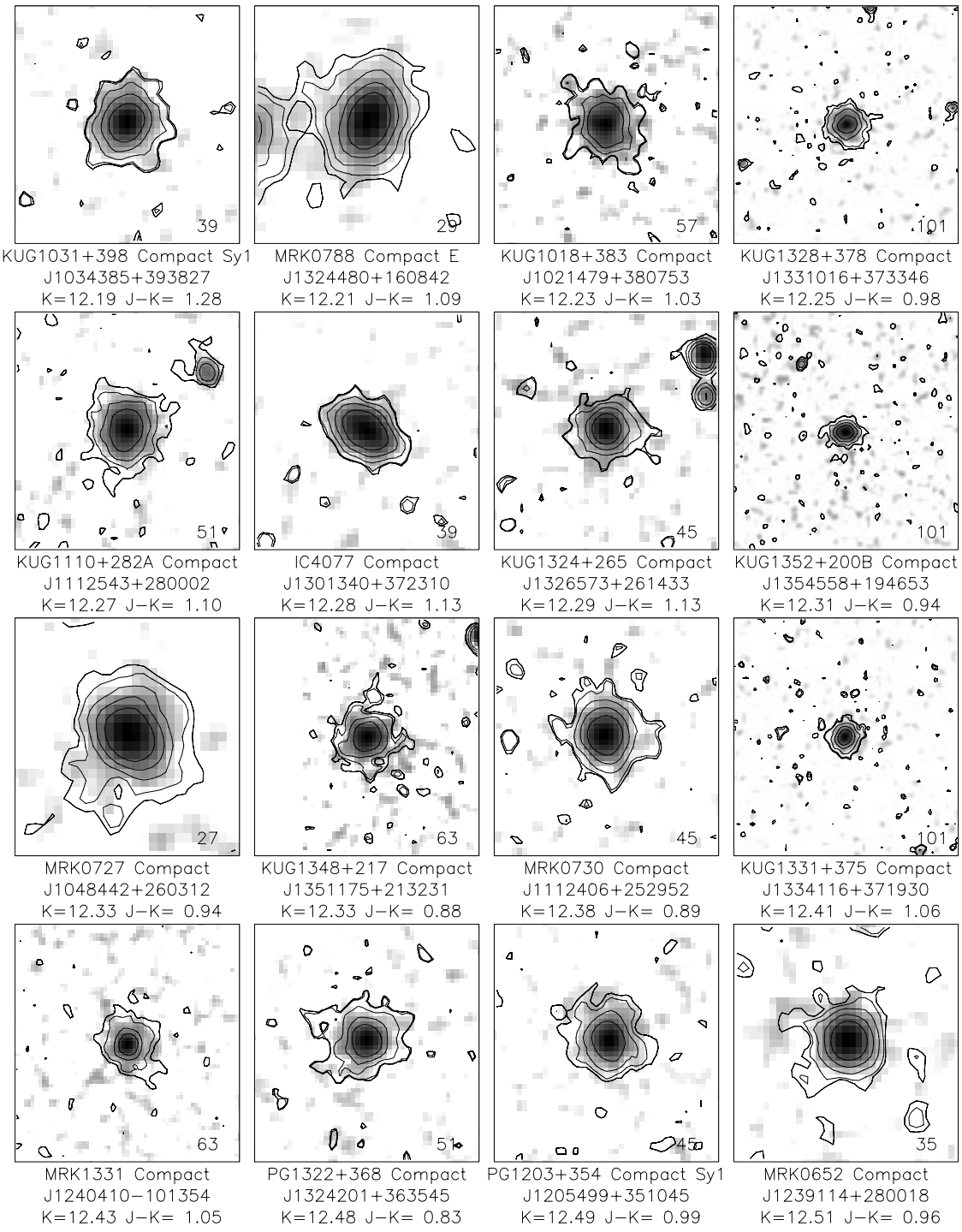
39
KUG1031+398 Compact Sy1
J1034385+393827
K=12.19 J−K= 1.28
29
MRK0788 Compact E
J1324480+160842
K=12.21 J−K= 1.09
57
KUG1018+383 Compact
J1021479+380753
K=12.23 J−K= 1.03
101
KUG1328+378 Compact
J1331016+373346
K=12.25 J−K= 0.98
51
KUG1110+282A Compact
J1112543+280002
K=12.27 J−K= 1.10
39
IC4077 Compact
J1301340+372310
K=12.28 J−K= 1.13
45
KUG1324+265 Compact
J1326573+261433
K=12.29 J−K= 1.13
101
KUG1352+200B Compact
J1354558+194653
K=12.31 J−K= 0.94
27
MRK0727 Compact
J1048442+260312
K=12.33 J−K= 0.94
63
KUG1348+217 Compact
J1351175+213231
K=12.33 J−K= 0.88
45
MRK0730 Compact
J1112406+252952
K=12.38 J−K= 0.89
101
KUG1331+375 Compact
J1334116+371930
K=12.41 J−K= 1.06
63
MRK1331 Compact
J1240410−101354
K=12.43 J−K= 1.05
51
PG1322+368 Compact
J1324201+363545
K=12.48 J−K= 0.83
45
PG1203+354 Compact Sy1
J1205499+351045
K=12.49 J−K= 0.99
35
MRK0652 Compact
J1239114+280018
K=12.51 J−K= 0.96

FIG. 20*ao*

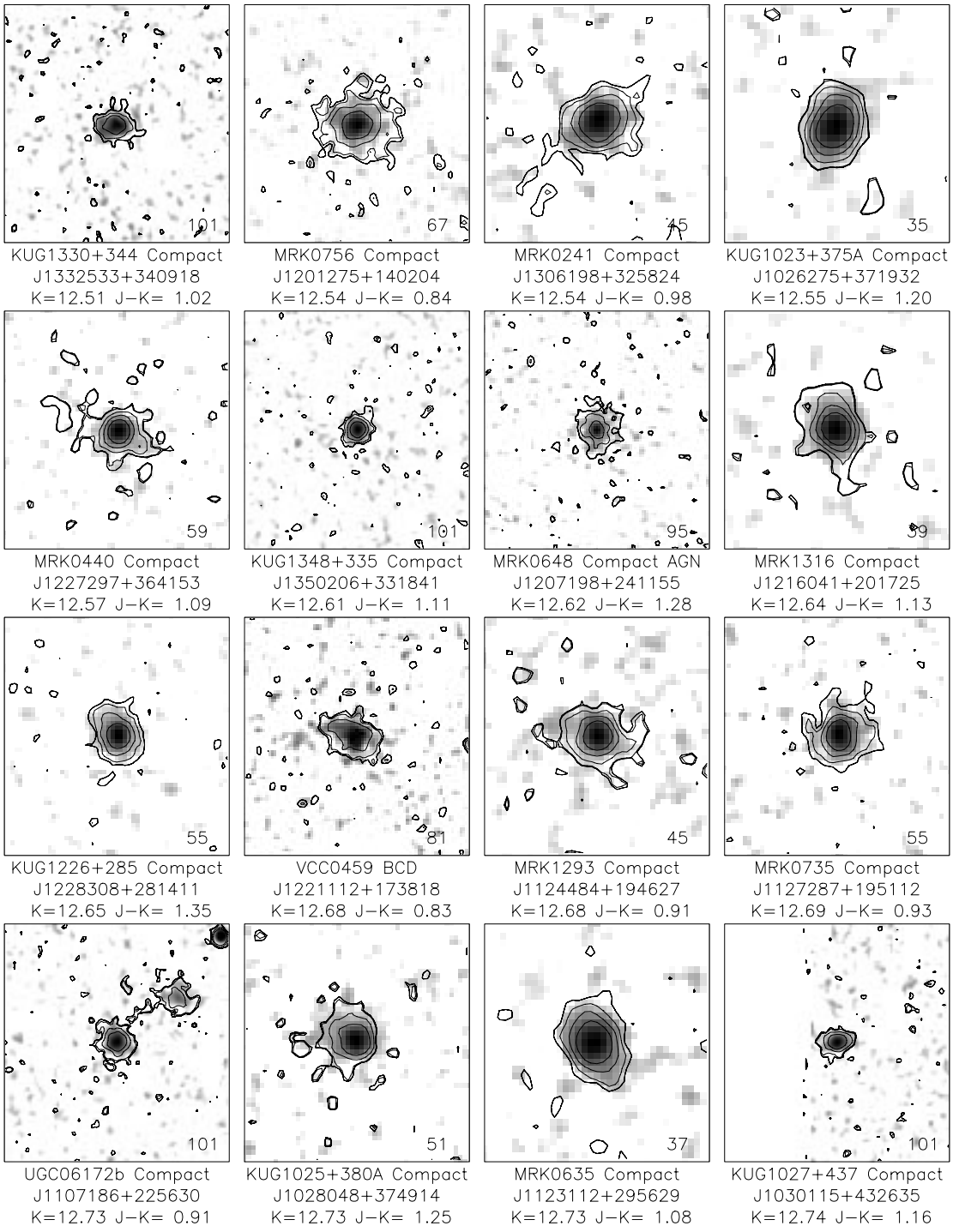
101
KUG1330+344 Compact
J1332533+340918
K=12.51 J−K= 1.02
67
MRK0756 Compact
J1201275+140204
K=12.54 J−K= 0.84
45
MRK0241 Compact
J1306198+325824
K=12.54 J−K= 0.98
35
KUG1023+375A Compact
J1026275+371932
K=12.55 J−K= 1.20
59
MRK0440 Compact
J1227297+364153
K=12.57 J−K= 1.09
101
KUG1348+335 Compact
J1350206+331841
K=12.61 J−K= 1.11
95
MRK0648 Compact AGN
J1207198+241155
K=12.62 J−K= 1.28
39
MRK1316 Compact
J1216041+201725
K=12.64 J−K= 1.13
55
KUG1226+285 Compact
J1228308+281411
K=12.65 J−K= 1.35
81
VCC0459 BCD
J1221112+173818
K=12.68 J−K= 0.83
45
MRK1293 Compact
J1124484+194627
K=12.68 J−K= 0.91
55
MRK0735 Compact
J1127287+195112
K=12.69 J−K= 0.93
101
UGC06172b Compact
J1107186+225630
K=12.73 J−K= 0.91
51
KUG1025+380A Compact
J1028048+374914
K=12.73 J−K= 1.25
37
MRK0635 Compact
J1123112+295629
K=12.73 J−K= 1.08
101
KUG1027+437 Compact
J1030115+432635
K=12.74 J−K= 1.16

FIG. 20*ap*

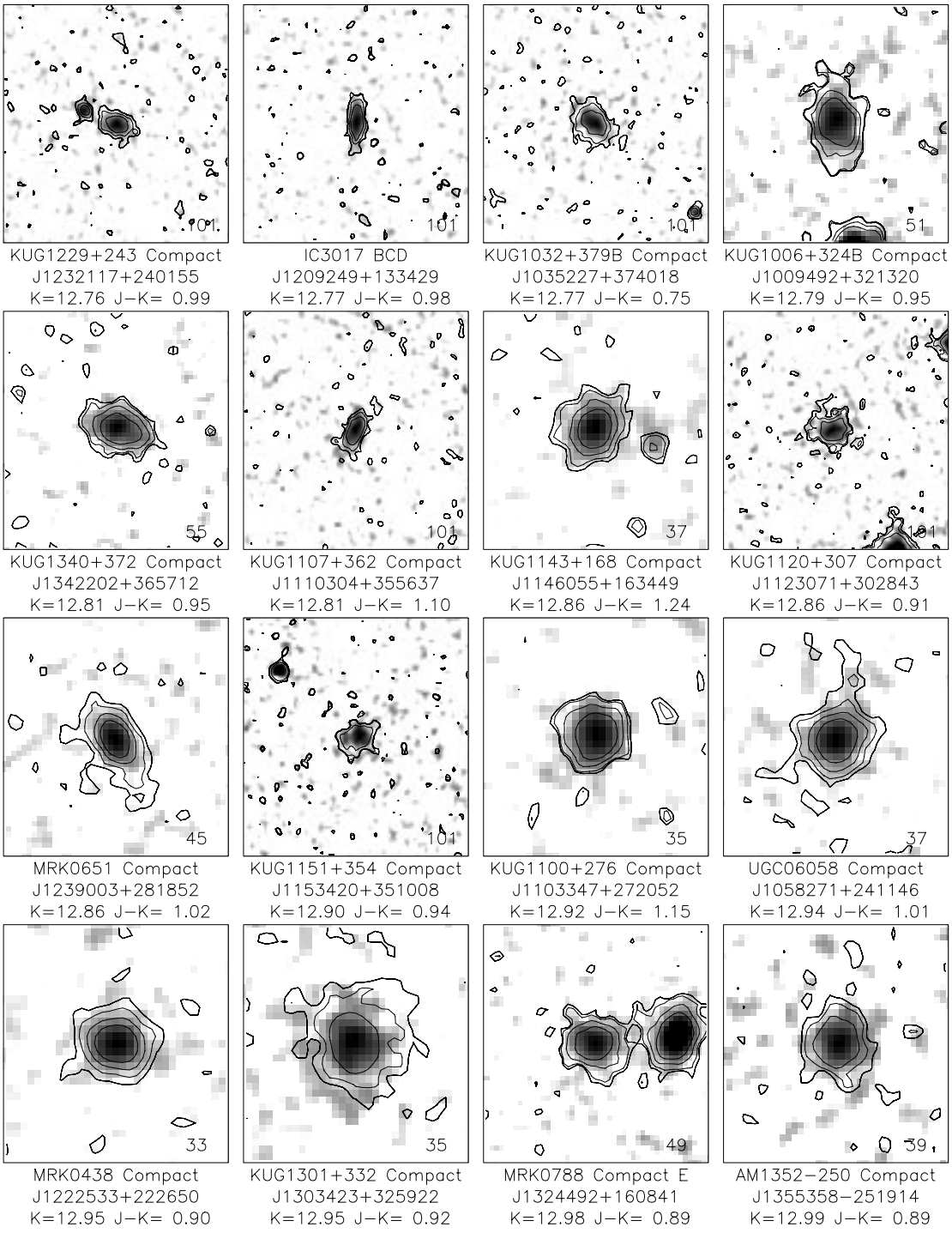
KUG1229+243 Compact
J1232117+240155
K=12.76 J−K= 0.99
IC3017 BCD
J1209249+133429
K=12.77 J−K= 0.98
KUG1032+379B Compact
J1035227+374018
K=12.77 J−K= 0.75
KUG1006+324B Compact
J1009492+321320
K=12.79 J−K= 0.95
KUG1340+372 Compact
J1342202+365712
K=12.81 J−K= 0.95
KUG1107+362 Compact
J1110304+355637
K=12.81 J−K= 1.10
KUG1143+168 Compact
J1146055+163449
K=12.86 J−K= 1.24
KUG1120+307 Compact
J1123071+302843
K=12.86 J−K= 0.91
MRK0651 Compact
J1239003+281852
K=12.86 J−K= 1.02
KUG1151+354 Compact
J1153420+351008
K=12.90 J−K= 0.94
KUG1100+276 Compact
J1103347+272052
K=12.92 J−K= 1.15
UGC06058 Compact
J1058271+241146
K=12.94 J−K= 1.01
MRK0438 Compact
J1222533+222650
K=12.95 J−K= 0.90
KUG1301+332 Compact
J1303423+325922
K=12.95 J−K= 0.92
MRK0788 Compact E
J1324492+160841
K=12.98 J−K= 0.89
AM1352−250 Compact
J1355358−251914
K=12.99 J−K= 0.89

FIG. 20*aq*

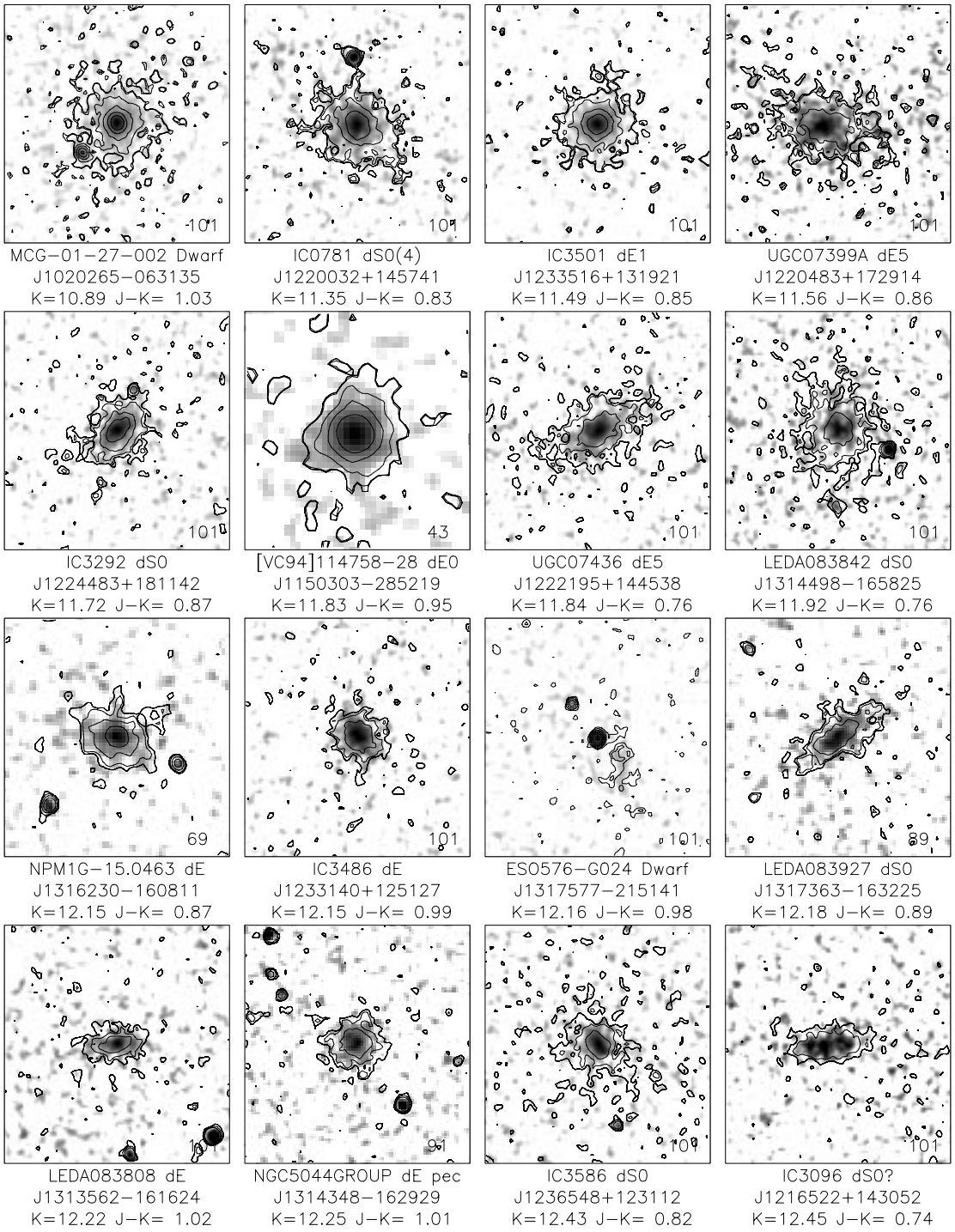
MCG−01−27−002 Dwarf
J1020265−063135
K=10.89 J−K= 1.03
IC0781 dS0(4)
J1220032+145741
K=11.35 J−K= 0.83
IC3501 dE1
J1233516+131921
K=11.49 J−K= 0.85
UGC07399A dE5
J1220483+172914
K=11.56 J−K= 0.86
IC3292 dS0
J1224483+181142
K=11.72 J−K= 0.87
[VC94]114758−28 dE0
J1150303−285219
K=11.83 J−K= 0.95
UGC07436 dE5
J1222195+144538
K=11.84 J−K= 0.76
LEDA083842 dS0
J1314498−165825
K=11.92 J−K= 0.76
NPM1G−15.0463 dE
J1316230−160811
K=12.15 J−K= 0.87
IC3486 dE
J1233140+125127
K=12.15 J−K= 0.99
ESO576−G024 Dwarf
J1317577−215141
K=12.16 J−K= 0.98
LEDA083927 dS0
J1317363−163225
K=12.18 J−K= 0.89
LEDA083808 dE
J1313562−161624
K=12.22 J−K= 1.02
NGC5044GROUP dE pec
J1314348−162929
K=12.25 J−K= 1.01
IC3586 dS0
J1236548+123112
K=12.43 J−K= 0.82
IC3096 dS0?
J1216522+143052
K=12.45 J−K= 0.74

FIG. 20*ar*

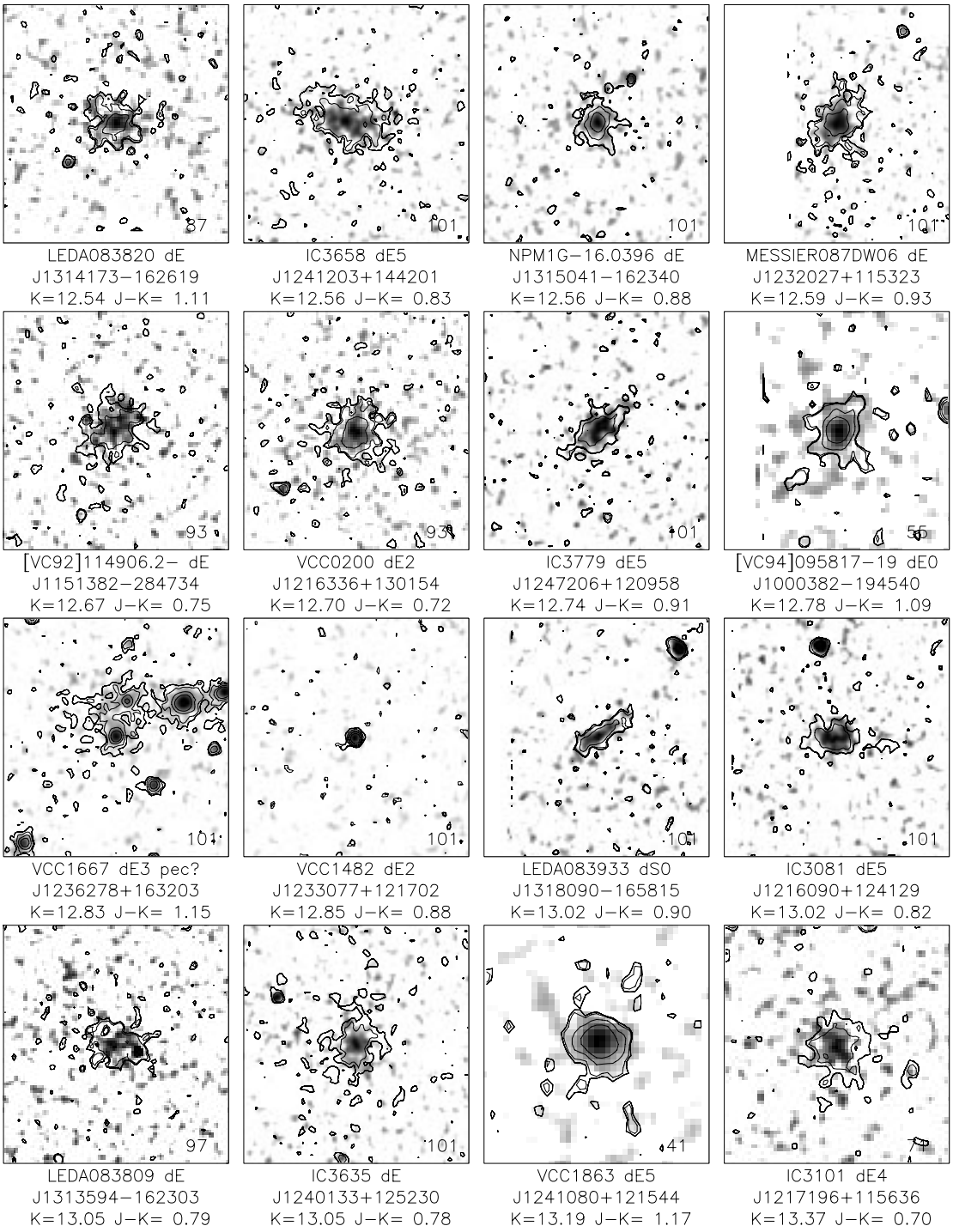
87
LEDA083820 dE
J1314173−162619
K=12.54 J−K= 1.11
101
IC3658 dE5
J1241203+144201
K=12.56 J−K= 0.83
101
NPM1G−16.0396 dE
J1315041−162340
K=12.56 J−K= 0.88
101
MESSIER087DW06 dE
J1232027+115323
K=12.59 J−K= 0.93
93
[VC92]114906.2− dE
J1151382−284734
K=12.67 J−K= 0.75
93
VCC0200 dE2
J1216336+130154
K=12.70 J−K= 0.72
101
IC3779 dE5
J1247206+120958
K=12.74 J−K= 0.91
55
[VC94]095817−19 dE0
J1000382−194540
K=12.78 J−K= 1.09
101
VCC1667 dE3 pec?
J1236278+163203
K=12.83 J−K= 1.15
101
VCC1482 dE2
J1233077+121702
K=12.85 J−K= 0.88
101
LEDA083933 dS0
J1318090−165815
K=13.02 J−K= 0.90
101
IC3081 dE5
J1216090+124129
K=13.02 J−K= 0.82
97
LEDA083809 dE
J1313594−162303
K=13.05 J−K= 0.79
101
IC3635 dE
J1240133+125230
K=13.05 J−K= 0.78
41
VCC1863 dE5
J1241080+121544
K=13.19 J−K= 1.17
IC3101 dE4
J1217196+115636
K=13.37 J−K= 0.70

FIG. 20*as*

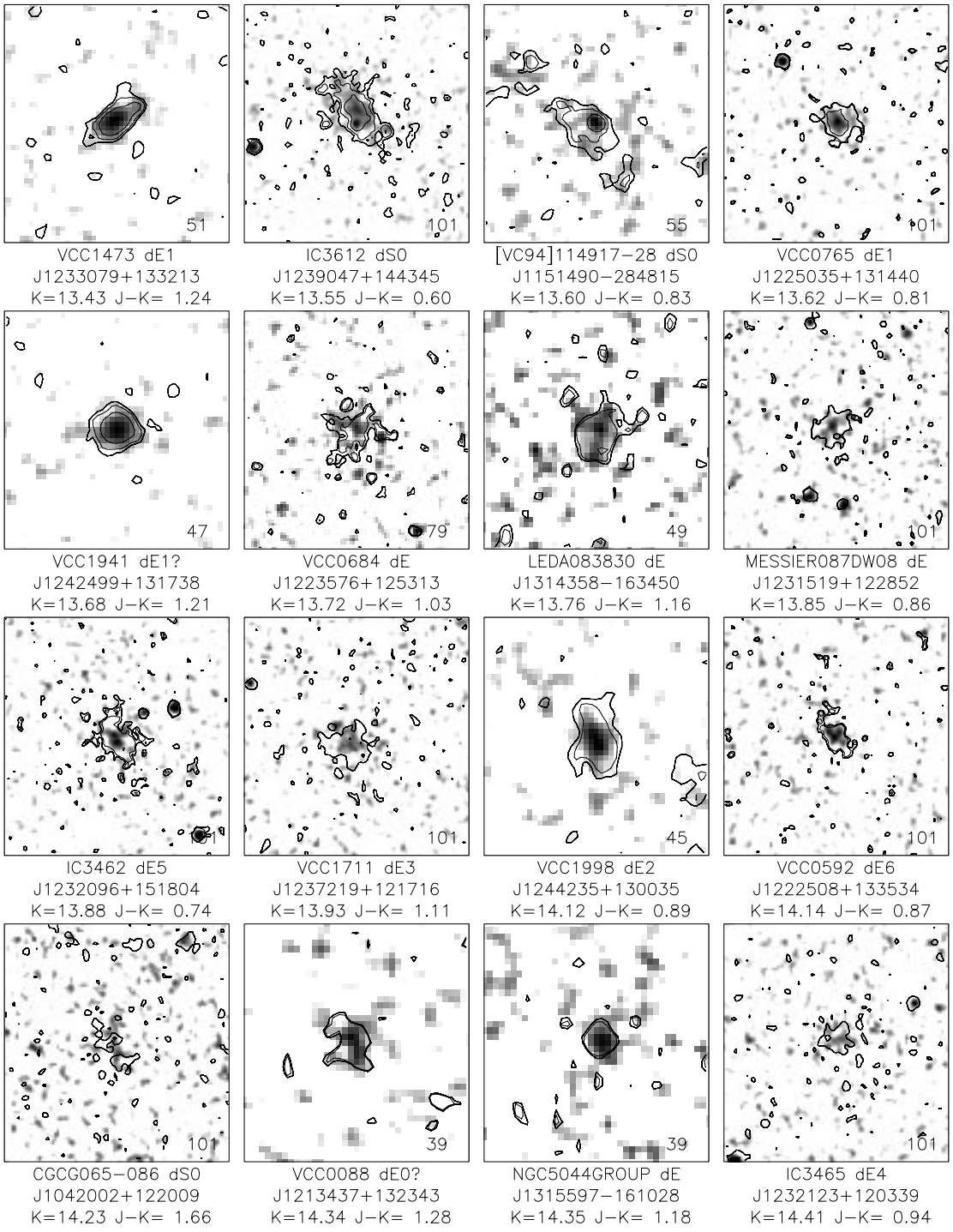
51
VCC1473 dE1
J1233079+133213
K=13.43 J−K= 1.24
101
IC3612 dS0
J1239047+144345
K=13.55 J−K= 0.60
55
[VC94]114917−28 dS0
J1151490−284815
K=13.60 J−K= 0.83
101
VCC0765 dE1
J1225035+131440
K=13.62 J−K= 0.81
47
VCC1941 dE1?
J1242499+131738
K=13.68 J−K= 1.21
79
VCC0684 dE
J1223576+125313
K=13.72 J−K= 1.03
49
LEDA083830 dE
J1314358−163450
K=13.76 J−K= 1.16
101
MESSIER087DW08 dE
J1231519+122852
K=13.85 J−K= 0.86
IC3462 dE5
J1232096+151804
K=13.88 J−K= 0.74
101
VCC1711 dE3
J1237219+121716
K=13.93 J−K= 1.11
45
VCC1998 dE2
J1244235+130035
K=14.12 J−K= 0.89
101
VCC0592 dE6
J1222508+133534
K=14.14 J−K= 0.87
101
CGCG065−086 dS0
J1042002+122009
K=14.23 J−K= 1.66
39
VCC0088 dE0?
J1213437+132343
K=14.34 J−K= 1.28
39
NGC5044GROUP dE
J1315597−161028
K=14.35 J−K= 1.18
101
IC3465 dE4
J1232123+120339
K=14.41 J−K= 0.94

FIG. 20*at*

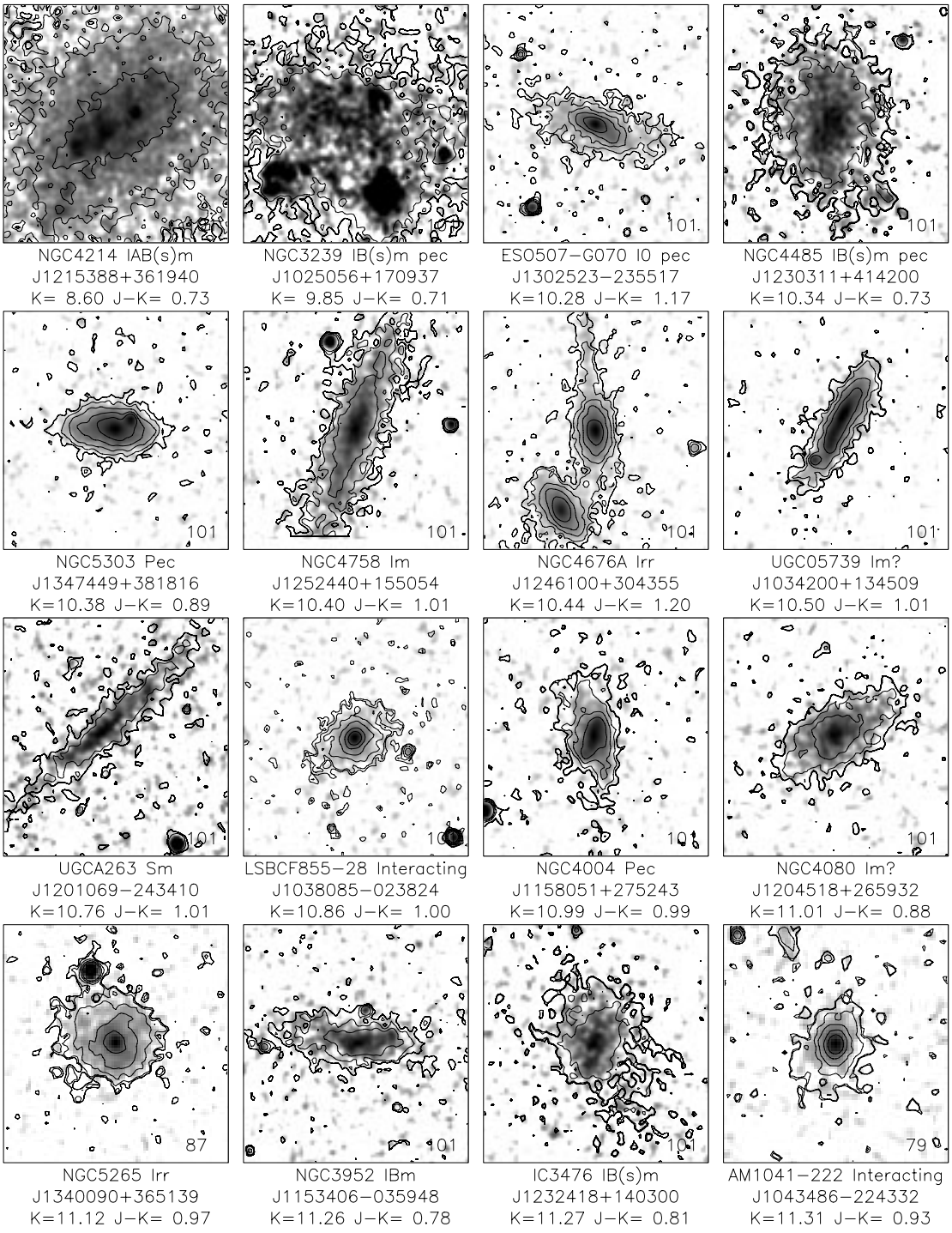
NGC4214 IAB(s)m
J1215388+361940
K= 8.60 J−K= 0.73
NGC3239 IB(s)m pec
J1025056+170937
K= 9.85 J−K= 0.71
ESO507−G070 I0 pec
J1302523−235517
K=10.28 J−K= 1.17
NGC4485 IB(s)m pec
J1230311+414200
K=10.34 J−K= 0.73
NGC5303 Pec
J1347449+381816
K=10.38 J−K= 0.89
NGC4758 Im
J1252440+155054
K=10.40 J−K= 1.01
NGC4676A Irr
J1246100+304355
K=10.44 J−K= 1.20
UGC05739 Im?
J1034200+134509
K=10.50 J−K= 1.01
UGCA263 Sm
J1201069−243410
K=10.76 J−K= 1.01
LSBCF855−28 Interacting
J1038085−023824
K=10.86 J−K= 1.00
NGC4004 Pec
J1158051+275243
K=10.99 J−K= 0.99
NGC4080 Im?
J1204518+265932
K=11.01 J−K= 0.88
NGC5265 Irr
J1340090+365139
K=11.12 J−K= 0.97
NGC3952 IBm
J1153406−035948
K=11.26 J−K= 0.78
IC3476 IB(s)m
J1232418+140300
K=11.27 J−K= 0.81
AM1041−222 Interacting
J1043486−224332
K=11.31 J−K= 0.93

FIG. 20*au*

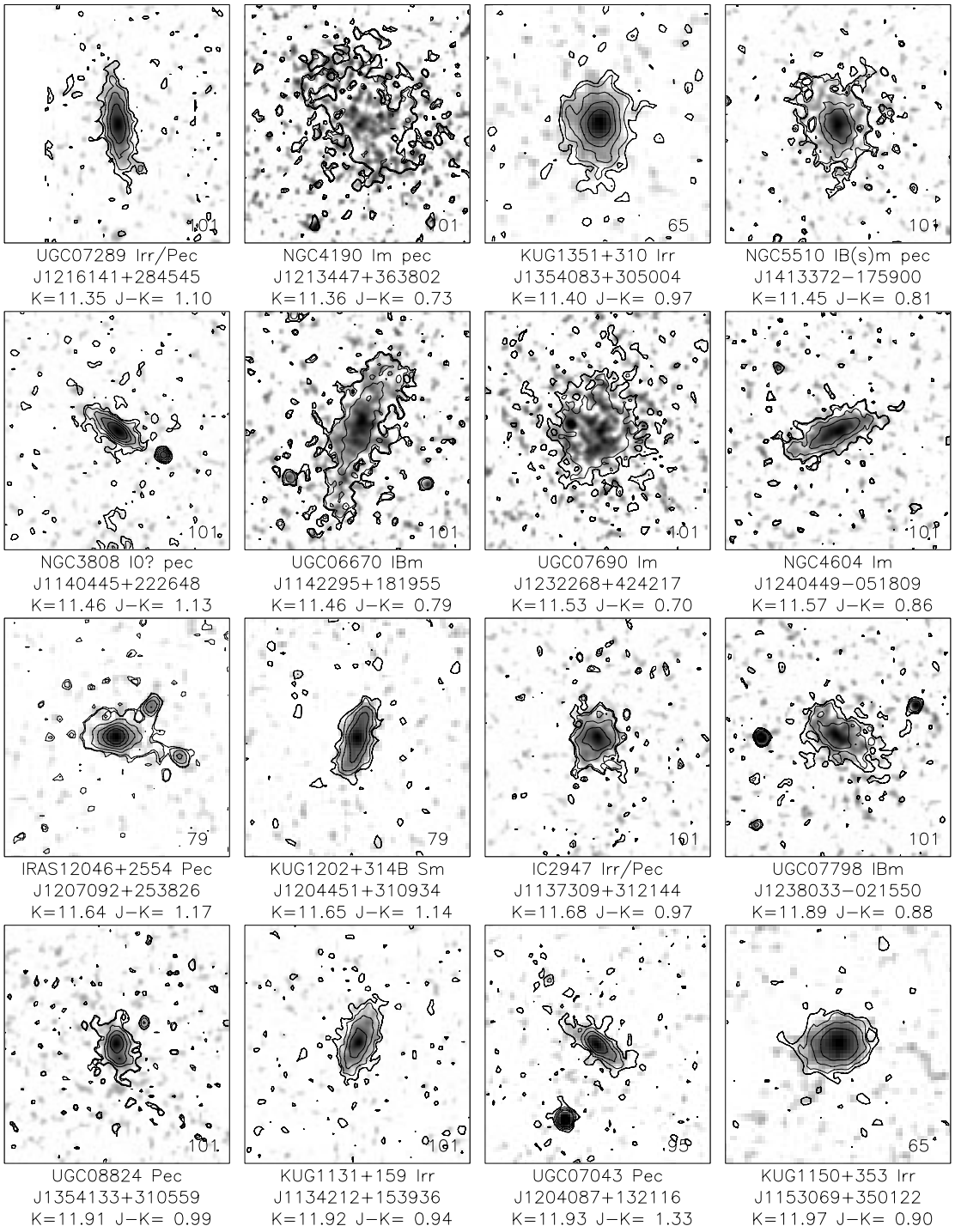
101
UGC07289 Irr/Pec
J1216141+284545
K=11.35 J−K= 1.10
101
NGC4190 Im pec
J1213447+363802
K=11.36 J−K= 0.73
65
KUG1351+310 Irr
J1354083+305004
K=11.40 J−K= 0.97
101
NGC5510 IB(s)m pec
J1413372−175900
K=11.45 J−K= 0.81
101
NGC3808 I0? pec
J1140445+222648
K=11.46 J−K= 1.13
101
UGC06670 IBm
J1142295+181955
K=11.46 J−K= 0.79
101
UGC07690 Im
J1232268+424217
K=11.53 J−K= 0.70
101
NGC4604 Im
J1240449−051809
K=11.57 J−K= 0.86
79
IRAS12046+2554 Pec
J1207092+253826
K=11.64 J−K= 1.17
79
KUG1202+314B Sm
J1204451+310934
K=11.65 J−K= 1.14
101
IC2947 Irr/Pec
J1137309+312144
K=11.68 J−K= 0.97
101
UGC07798 IBm
J1238033−021550
K=11.89 J−K= 0.88
101
UGC08824 Pec
J1354133+310559
K=11.91 J−K= 0.99
101
KUG1131+159 Irr
J1134212+153936
K=11.92 J−K= 0.94
99
UGC07043 Pec
J1204087+132116
K=11.93 J−K= 1.33
65
KUG1150+353 Irr
J1153069+350122
K=11.97 J−K= 0.90

FIG. 20*av*

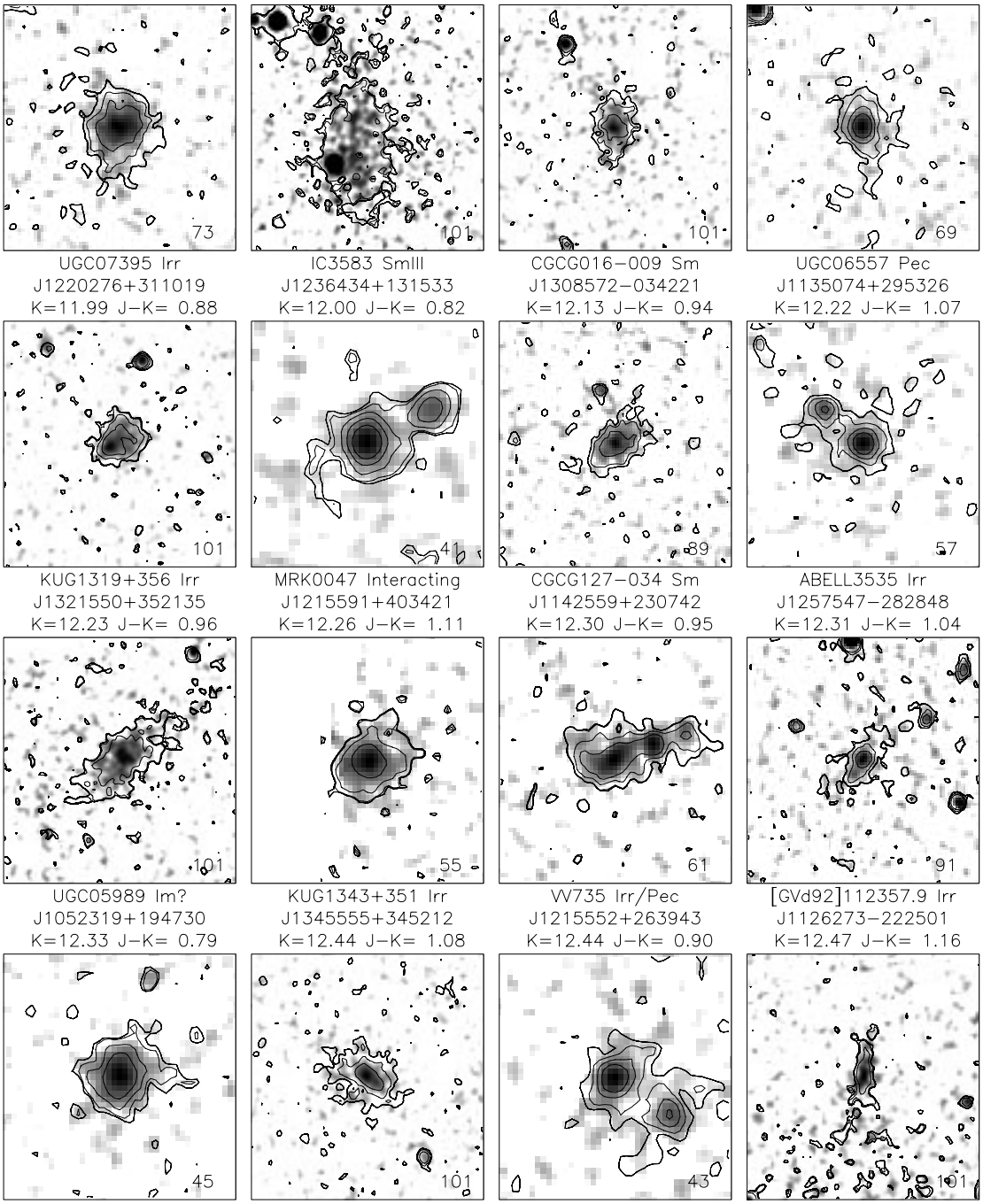
73
UGC07395 Irr
J1220276+311019
K=11.99 J−K= 0.88
101
IC3583 SmIII
J1236434+131533
K=12.00 J−K= 0.82
101
CGCG016−009 Sm
J1308572−034221
K=12.13 J−K= 0.94
69
UGC06557 Pec
J1135074+295326
K=12.22 J−K= 1.07
101
KUG1319+356 Irr
J1321550+352135
K=12.23 J−K= 0.96
41
MRK0047 Interacting
J1215591+403421
K=12.26 J−K= 1.11
89
CGCG127−034 Sm
J1142559+230742
K=12.30 J−K= 0.95
57
ABELL3535 Irr
J1257547−282848
K=12.31 J−K= 1.04
101
UGC05989 Im?
J1052319+194730
K=12.33 J−K= 0.79
55
KUG1343+351 Irr
J1345555+345212
K=12.44 J−K= 1.08
61
W735 Irr/Pec
J1215552+263943
K=12.44 J−K= 0.90
91
[GVd92]112357.9 Irr
J1126273−222501
K=12.47 J−K= 1.16
45
MRK1319 Im
J1219246+180414
K=12.51 J−K= 1.10
101
KUG1318+318 Irr
J1321196+313308
K=12.52 J−K= 0.83
43
PRCD−17 I
J1125588−234220
K=12.62 J−K= 1.19
101
MCG−03−34−040 Sm
J1316562−163534
K=12.62 J−K= 1.06

FIG. 20*aw*

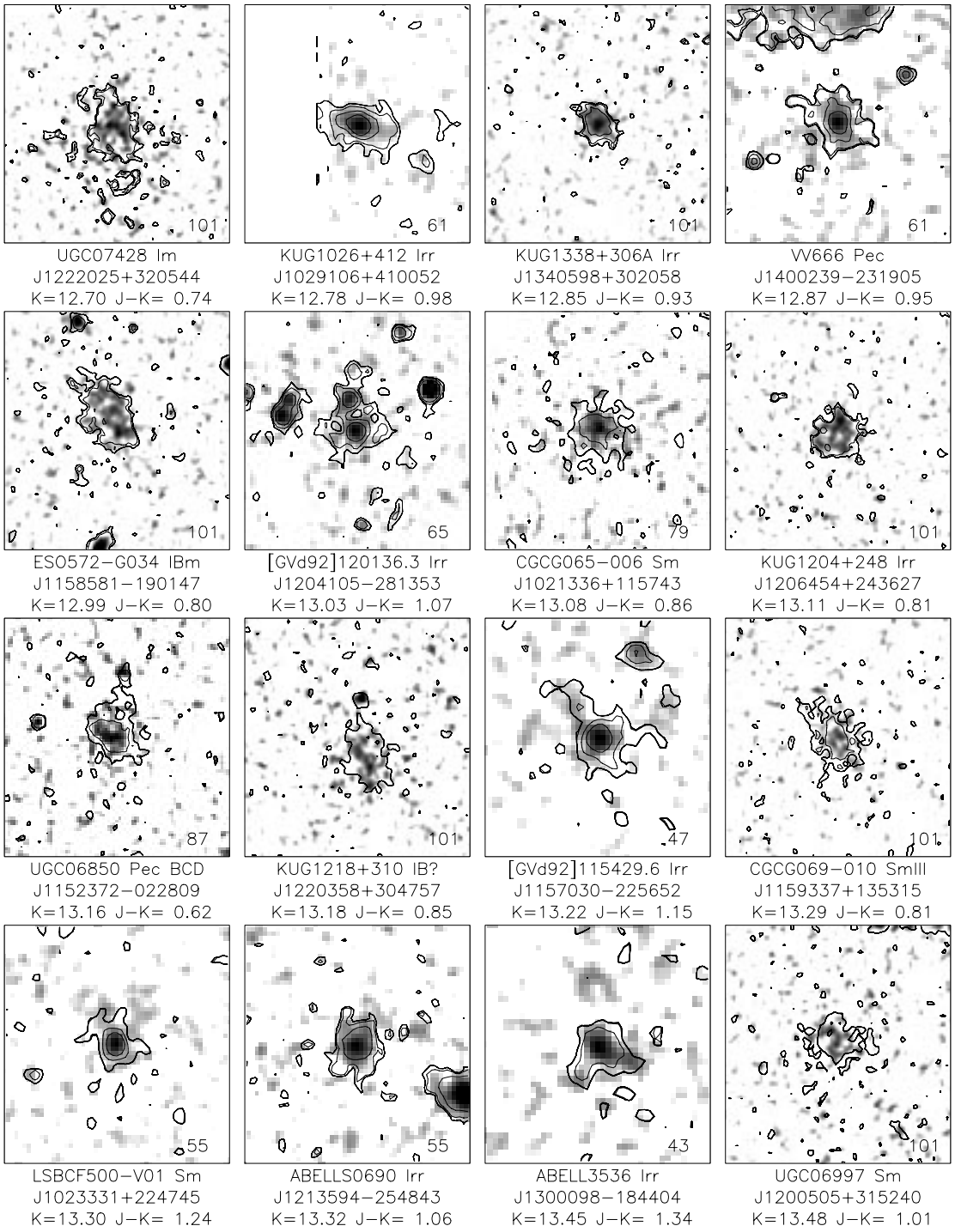
101
UGC07428 Im
J1222025+320544
K=12.70 J−K= 0.74
61
KUG1026+412 Irr
J1029106+410052
K=12.78 J−K= 0.98
101
KUG1338+306A Irr
J1340598+302058
K=12.85 J−K= 0.93
61
VV666 Pec
J1400239−231905
K=12.87 J−K= 0.95
101
ESO572−G034 IBm
J1158581−190147
K=12.99 J−K= 0.80
65
[GVd92]120136.3 Irr
J1204105−281353
K=13.03 J−K= 1.07
79
CGCG065−006 Sm
J1021336+115743
K=13.08 J−K= 0.86
101
KUG1204+248 Irr
J1206454+243627
K=13.11 J−K= 0.81
87
UGC06850 Pec BCD
J1152372−022809
K=13.16 J−K= 0.62
101
KUG1218+310 IB?
J1220358+304757
K=13.18 J−K= 0.85
47
[GVd92]115429.6 Irr
J1157030−225652
K=13.22 J−K= 1.15
101
CGCG069−010 SmIII
J1159337+135315
K=13.29 J−K= 0.81
55
LSBCF500−V01 Sm
J1023331+224745
K=13.30 J−K= 1.24
55
ABELLS0690 Irr
J1213594−254843
K=13.32 J−K= 1.06
43
ABELL3536 Irr
J1300098−184404
K=13.45 J−K= 1.34
101
UGC06997 Sm
J1200505+315240
K=13.48 J−K= 1.01

FIG. 20*ax*

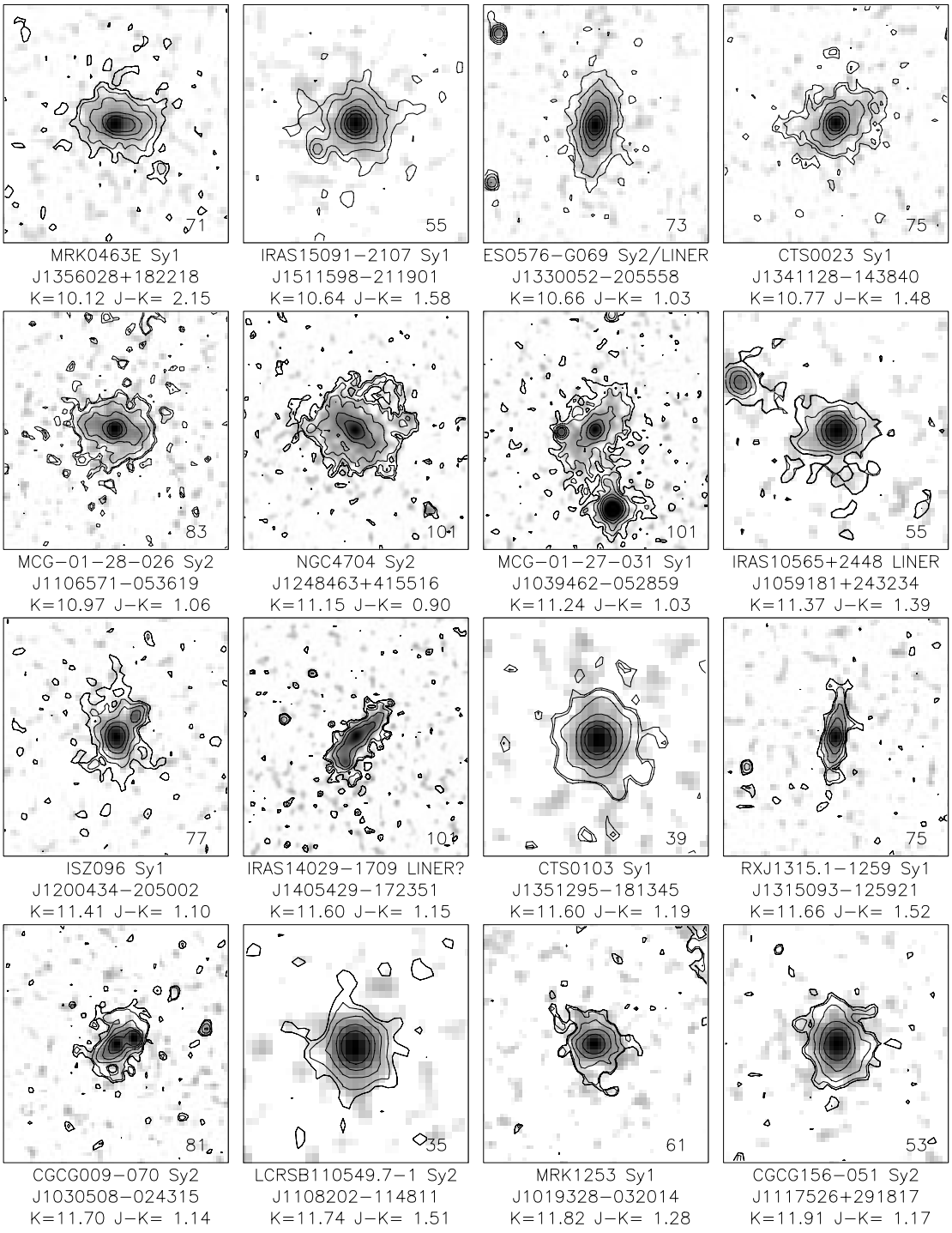
71
MRK0463E Sy1
J1356028+182218
K=10.12 J−K= 2.15
55
IRAS15091−2107 Sy1
J1511598−211901
K=10.64 J−K= 1.58
73
ESO576−G069 Sy2/LINER
J1330052−205558
K=10.66 J−K= 1.03
75
CTS0023 Sy1
J1341128−143840
K=10.77 J−K= 1.48
83
MCG−01−28−026 Sy2
J1106571−053619
K=10.97 J−K= 1.06
101
NGC4704 Sy2
J1248463+415516
K=11.15 J−K= 0.90
101
MCG−01−27−031 Sy1
J1039462−052859
K=11.24 J−K= 1.03
55
IRAS10565+2448 LINER
J1059181+243234
K=11.37 J−K= 1.39
77
ISZ096 Sy1
J1200434−205002
K=11.41 J−K= 1.10
101
IRAS14029−1709 LINER?
J1405429−172351
K=11.60 J−K= 1.15
39
CTS0103 Sy1
J1351295−181345
K=11.60 J−K= 1.19
75
RXJ1315.1−1259 Sy1
J1315093−125921
K=11.66 J−K= 1.52
81
CGCG009−070 Sy2
J1030508−024315
K=11.70 J−K= 1.14
35
LCRSB110549.7−1 Sy2
J1108202−114811
K=11.74 J−K= 1.51
61
MRK1253 Sy1
J1019328−032014
K=11.82 J−K= 1.28
53
CGCG156−051 Sy2
J1117526+291817
K=11.91 J−K= 1.17

FIG. 20*ay*

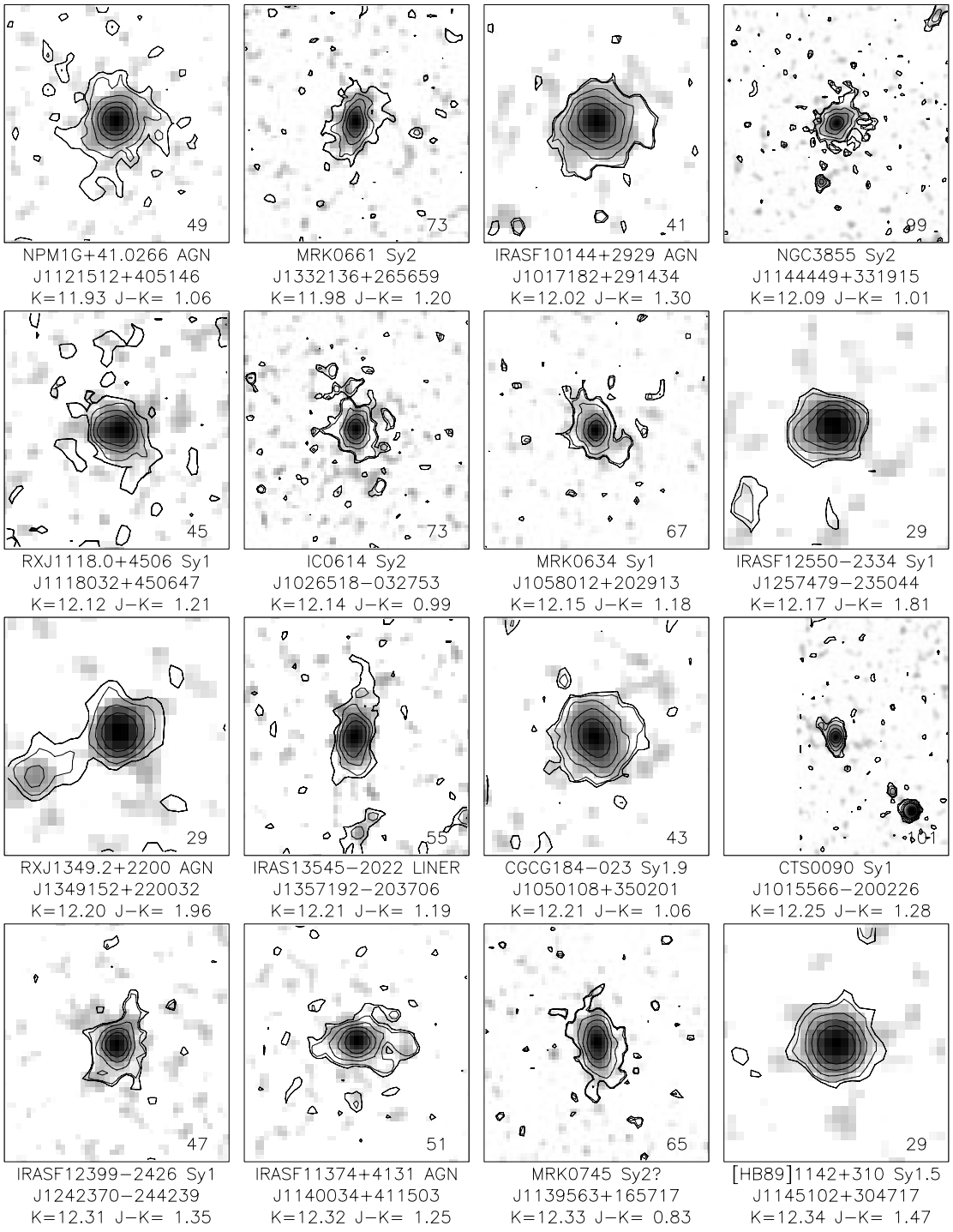
49
NPM1G+41.0266 AGN
J1121512+405146
K=11.93 J−K= 1.06
73
MRK0661 Sy2
J1332136+265659
K=11.98 J−K= 1.20
41
IRASF10144+2929 AGN
J1017182+291434
K=12.02 J−K= 1.30
99
NGC3855 Sy2
J1144449+331915
K=12.09 J−K= 1.01
45
RXJ1118.0+4506 Sy1
J1118032+450647
K=12.12 J−K= 1.21
73
IC0614 Sy2
J1026518−032753
K=12.14 J−K= 0.99
67
MRK0634 Sy1
J1058012+202913
K=12.15 J−K= 1.18
29
IRASF12550−2334 Sy1
J1257479−235044
K=12.17 J−K= 1.81
29
RXJ1349.2+2200 AGN
J1349152+220032
K=12.20 J−K= 1.96
55
IRAS13545−2022 LINER
J1357192−203706
K=12.21 J−K= 1.19
43
CGCG184−023 Sy1.9
J1050108+350201
K=12.21 J−K= 1.06
CTS0090 Sy1
J1015566−200226
K=12.25 J−K= 1.28
47
IRASF12399−2426 Sy1
J1242370−244239
K=12.31 J−K= 1.35
51
IRASF11374+4131 AGN
J1140034+411503
K=12.32 J−K= 1.25
65
MRK0745 Sy2?
J1139563+165717
K=12.33 J−K= 0.83
29
[HB89]1142+310 Sy1.5
J1145102+304717
K=12.34 J−K= 1.47

FIG. 20*az*

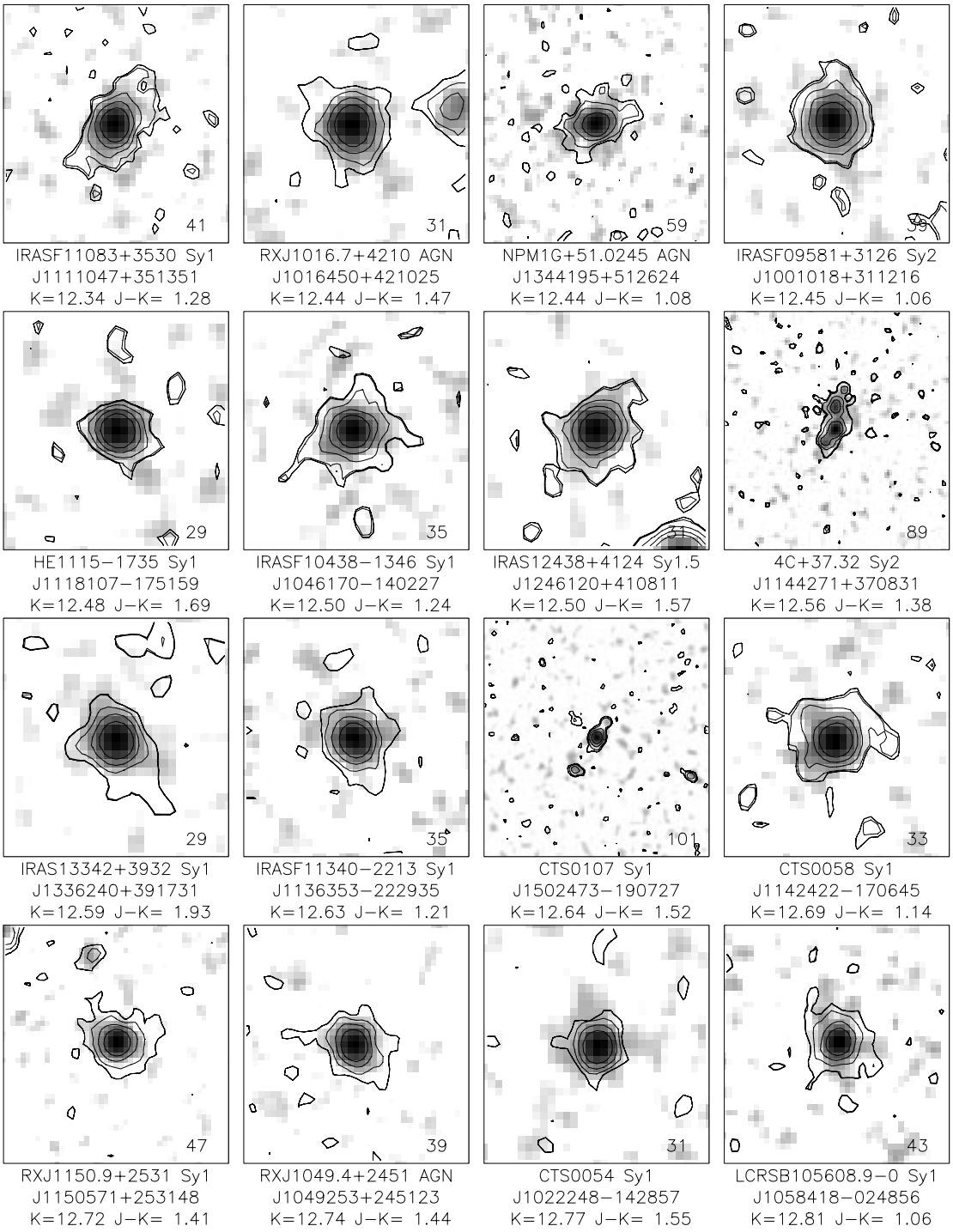
41
IRASF11083+3530 Sy1
J1111047+351351
K=12.34 J−K= 1.28
31
RXJ1016.7+4210 AGN
J1016450+421025
K=12.44 J−K= 1.47
59
NPM1G+51.0245 AGN
J1344195+512624
K=12.44 J−K= 1.08
39
IRASF09581+3126 Sy2
J1001018+311216
K=12.45 J−K= 1.06
29
HE1115−1735 Sy1
J1118107−175159
K=12.48 J−K= 1.69
35
IRASF10438−1346 Sy1
J1046170−140227
K=12.50 J−K= 1.24
51
IRAS12438+4124 Sy1.5
J1246120+410811
K=12.50 J−K= 1.57
89
4C+37.32 Sy2
J1144271+370831
K=12.56 J−K= 1.38
29
IRAS13342+3932 Sy1
J1336240+391731
K=12.59 J−K= 1.93
35
IRASF11340−2213 Sy1
J1136353−222935
K=12.63 J−K= 1.21
101
CTS0107 Sy1
J1502473−190727
K=12.64 J−K= 1.52
33
CTS0058 Sy1
J1142422−170645
K=12.69 J−K= 1.14
47
RXJ1150.9+2531 Sy1
J1150571+253148
K=12.72 J−K= 1.41
39
RXJ1049.4+2451 AGN
J1049253+245123
K=12.74 J−K= 1.44
31
CTS0054 Sy1
J1022248−142857
K=12.77 J−K= 1.55
43
LCRSB105608.9−0 Sy1
J1058418−024856
K=12.81 J−K= 1.06

FIG. 20*ba*

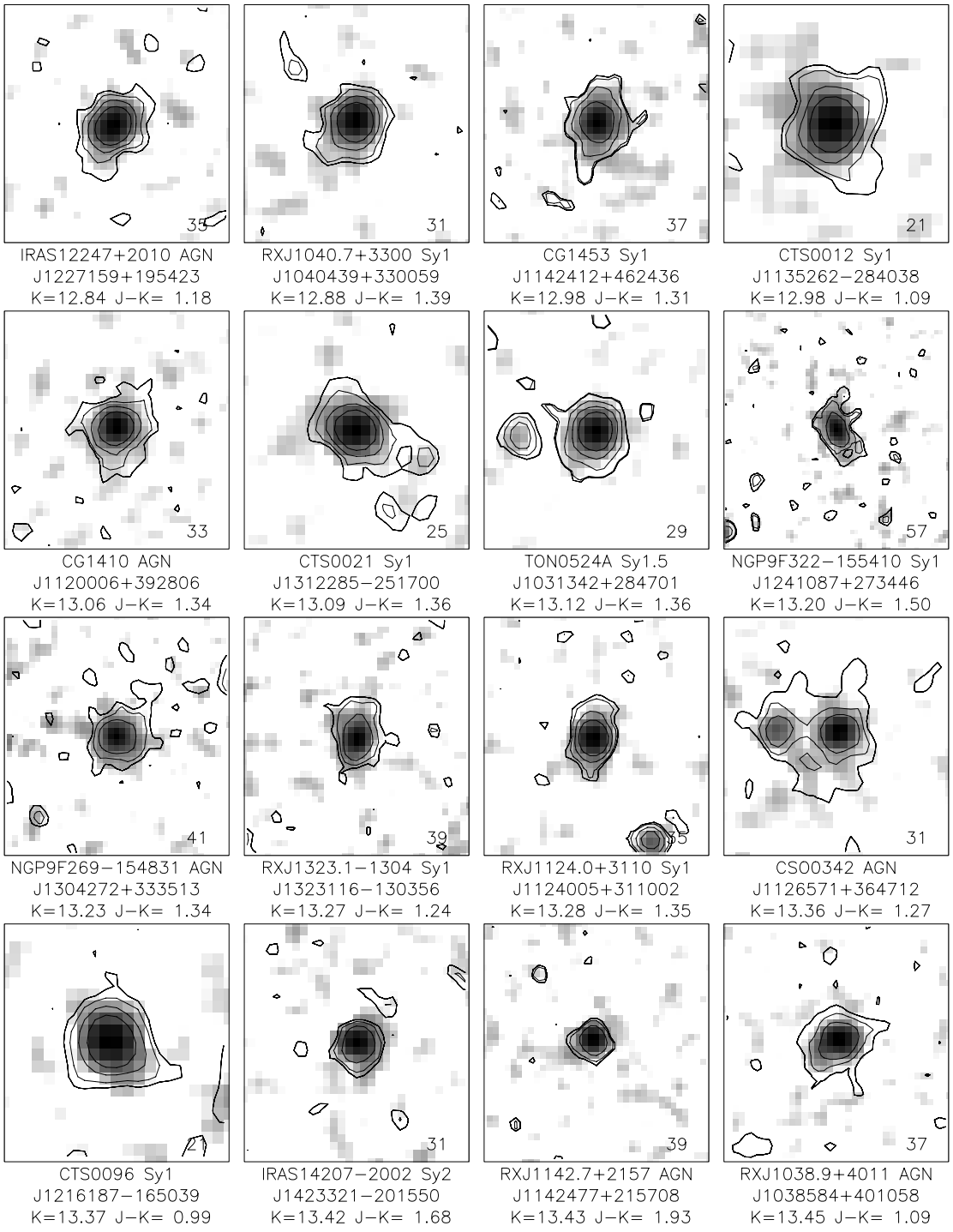
35
IRAS12247+2010 AGN
J1227159+195423
K=12.84 J−K= 1.18
31
RXJ1040.7+3300 Sy1
J1040439+330059
K=12.88 J−K= 1.39
37
CG1453 Sy1
J1142412+462436
K=12.98 J−K= 1.31
21
CTS0012 Sy1
J1135262−284038
K=12.98 J−K= 1.09
33
CG1410 AGN
J1120006+392806
K=13.06 J−K= 1.34
25
CTS0021 Sy1
J1312285−251700
K=13.09 J−K= 1.36
29
TON0524A Sy1.5
J1031342+284701
K=13.12 J−K= 1.36
57
NGP9F322−155410 Sy1
J1241087+273446
K=13.20 J−K= 1.50
41
NGP9F269−154831 AGN
J1304272+333513
K=13.23 J−K= 1.34
39
RXJ1323.1−1304 Sy1
J1323116−130356
K=13.27 J−K= 1.24
RXJ1124.0+3110 Sy1
J1124005+311002
K=13.28 J−K= 1.35
31
CSO0342 AGN
J1126571+364712
K=13.36 J−K= 1.27
CTS0096 Sy1
J1216187−165039
K=13.37 J−K= 0.99
31
IRAS14207−2002 Sy2
J1423321−201550
K=13.42 J−K= 1.68
39
RXJ1142.7+2157 AGN
J1142477+215708
K=13.43 J−K= 1.93
37
RXJ1038.9+4011 AGN
J1038584+401058
K=13.45 J−K= 1.09

FIG. 20*bb*